# Green Nanofabrication
# @
# Leidenfrost Condition

**Dissertation**

zur Erlangung des akademischen Grades

**Doktor der Ingenieurwissenschaften**
(Dr.- Ing.)

**der Technischen Fakultät**
**der Christian-Albrechts-Universität zu Kiel**

**Ramzy Abdelaziz**

**Kiel**

**2015**

1. Gutachter: Prof. Dr. Mady Elbahri
2. Gutachter: Prof. Dr. Franz Faupel
3. Gutachter: Prof. Dr. Rainer Adelung
Datum der mündlichen Prüfung: 25.03.2015

**Dedicated to My Beloved**
**Kids, Wife and Parents**

# Publications, Patents, Awards and Presentation

## Publications

- **R. Abdelaziz**, D. Disci-Zayed, M. K. Hedayati, J. Pöhls, A. U. Zillohu, B. Erkartal, V. S. K. Chakravadhanula, V. Duppel, L. Kienle, M. Elbahri, Green chemistry and nanofabrication in a levitated Leidenfrost drop, **Nature Communications 2013**, 4, doi:10.1038/ncomms3400.

    - Press release: Nature Publishing Group Asia-Pacific
    - Press release: New scientist
    - Press release: Chemistry World
    - Press release: Physics.org
    - Press release: Chemical and Engineering News (C & EN)
    - Press release: Spiegel Online (in German)
    - Press release: University of Kiel (in German)
    - Press release: Guardian
    - Press release: MRS Bulletin (News & Analysis)

- H. Papavlassopoulos, Y. K. Mishra, S. Kaps, I. Paulowicz, **R. Abdelaziz**, M. Elbahri, E. Maser, R. Adelung, C. Roehl, Toxicity of Functional Nano-Micro Zinc Oxide Tetrapods: Impact of Cell Culture Conditions, Cellular Age and Material Properties, **PLOS one 2014**, 9, e84983.

- A. U. Zillohu, N. Alissawi, **R. Abdelaziz**, M. Elbahri, Thermo-Plasmonics for Localized Graphitization and Welding of Polymeric Nanofibers, **Materials 2014**, 7, 323-332.

- A. U. Zillohu, **R. Abdelaziz,** M. K. Hedayati, T. Emmler, S. Homaeigohar, M. Elbahri, Plasmon-mediated embedding of nanoparticles in a polymer matrix: nanocomposites patterning, writing and defect healing, **The Journal of Physical Chemistry C 2012**, 116, 17204-17209.

- M. Jamali, M. K. Hedayati, B. Mozooni, M. Javaherirahim, **R. Abdelaziz**, A. U. Zillohu, M. Elbahri, Photoresponsive Transparent Conductive Metal with a Photobleaching Nose, **Advanced Materials 2011,** 23, 4243-4247.

- M. Elbahri, S. S. Homaeigohar, T. Dai, **R. Abdelaziz**, R. Khalil, A. U. Zillohu, Smart Metal–Polymer Bionanocomposites as Omnidirectional Plasmonic Black Absorber Formed by Nanofluid Filtration, **Advanced Functional Materials 2012**, 22, 4771-4777.

- M. Elbahri, S. S. Homaeigohar, T. Dai, **R. Abdelaziz**, R. Khalil, A. U. Zillohu, Bionanocompsite: Smart Metal–Polymer Bionanocomposites as Omnidirectional Plasmonic Black Absorber Formed by Nanofluid Filtration, **Advanced Functional Materials 2012** (Inside Front Cover), 22, 4626.

- A. U. Zillohu, **R. Abdelaziz**, S. S. Homaeigohar, I. Krasnov, M. Müller, T. Strunskus, Mady Elbahri, Biomimetic Transferable Surface for a Real Time Control over Wettability and Photoerasable Writing with Water Drop Lens, **Scientific Reports 2014**, 4, doi:10.1038/srep07407.

- M. Elbahri*, A. U. Zillohu, B. Gothe, M. K. Hedayati, **R. Abdelaziz**, H. J. El-Khozondar, M. Bawa'aneh, M. Abdelaziz, A. Lavrinenko, S. Zhukovsky, S. Homaeigohar, Specular Reflection by Oscillating Photochromic Molecules with Tailored Photoswitchable Brewster Wavelength and Molecular Photonic Coupling **Light: Science & Applications 2015** (Accepted).

## Patents

- M. Elbahri, S. S. Homaeigohar, T. Dai, **R. Abdelaziz**, Biofunctionalized microfiltration or ultrafiltration membrane, US20120318731 A1, 2012.

## Awards

- Young scientist award, European Materials Research Society (E-MRS), Spring Meeting, May 2014, Lille, France.

- A special prize for the best presentation in "Nano erleben" competition, Nanofabrication @ Leidenfrost condition, March 2014, Germany.

- Doctoral scholarship from Kiel University, Institute of Materials Science, Faculty of Engineering, August 2009, Germany.

## Conferences: Presentations and Posters

- **Invited talk** in the area of Nanoscience education, Nanofabrication @ Leidenfrost condition, Fortbildungs und Vortragstagung der Fachgruppe Chemieunterricht (FGCU), September 2014, Kiel, Germany

- **R. Abdelaziz** and M. Elbahri, Green Nanolab in a Leidenfrost Drop, (E-MRS), Spring Meeting, May 2014, Lille, France.

- **R. Abdelaziz**, J. Worley, D. Disci , R. Podschun, C. Röhl , M. Elbahri, Biomedical Applications of Zinc Peroxide Nanoparticles Fabricated by Shock Synthesis Using the Leidenfrost Phenomenon, BioMat 2011, Jena, Germany.

# Contents

# Abstract

Nanotechnology applications revolutionize our daily life in the new millennium. It has enormous promising applications that considerably influences the whole world. Things like consumer goods, nanofiltration, nanoelectronics, nanomedicine, aerospace, defense, energy, environment, and all fields of economy are deeply affected by nanotechnology. Thus, there should be some innovative methods to meet the growing requirement of nanobased products. These methods need to be simple to handle, environmental-friendly, energy efficient, and low cost. Leidenfrost effect can be reflected in our daily life. In our home kitchen, while cooking for example, if a drop of water touches a hot surface which is at a temperature much higher than the boiling point of water, the lower part of the drop is evaporated and the water levitates on its own vapor film. In this thesis, the Leidenfrost drop has been introduced as a water-based green chemical reactor for simultaneous synthesis and self-organization of nanostructures. An important contribution of this work is in exploring the origin and mechanism of the nanofabrication at Leidenfrost condition. It turns out that these conditions are based upon overheated and charged nature of the droplet.

Moreover, this thesis demonstrates the synthesis of structured nanoparticles, their assembly in the form of 3D nanocoating on complex objects, the design and development of nanoporous metal suspension and the foam structures. Through the nanofabrication process, some exemplar applications are represented such as plasmonic wideband superabsorber, which could be a good candidate for solar energy harvesting as well as a superhydrophilic and thermal resistive metal-polymer hybrid foam. Furthermore, it turns out that this new green strategy provides the possibility to produce nanopowder with customized morphology thereby affecting the thermal emissivity in addition to many other functions. This water-based, one step, cost effective and eco-friendly approach does not contain any hazardous organics, capping agents or coordination compounds that can contaminate the product and consequently complicate its application. The synthesized nanomaterials are characterized by scanning electron microscopy (SEM), transmission electron microscopy (TEM), infrared (IR) thermography, X-ray diffraction (XRD) and ultraviolet-visible spectroscopy (UV-Vis).

# Chapter 1

# Introduction

## 1.1 Background

The colorful windows of a cathedral show that nanoparticles have been synthesized and used by mankind for ages. However, a new era of scientific progress known as "nano-revolution" started after the historical lecture of Feynman in 1959. The fascinating aspect of this field is the ability to manipulate material structures and its properties down to a few atoms.[1] Such structures show some properties which are not present in their bulk counterparts because of high surface to volume ratio and quantum effects.[2] Thus, the scientific progress in nanotechnology has started to change our daily life. In this regard, more than 1628 nano-based products have been introduced to the consumers since 2005. This amount has increased 24 percent since 2010.[3] Nanomaterials are now used, on a large scale, in industrial applications such as catalysts, sensors, coatings, sport goods, filtration, textiles, cosmetics, electronics, medical tools, fuel cells, batteries and solar cells.[4] On the other hand, the last updated BCC Research report shows that:

- "The global market for nanotechnology was valued at nearly $20.1 billion in 2011 and should reach $20.7 billion in 2012. Total sales are expected to reach $48.9 billion in 2017 after increasing at a five-year compound annual growth rate (CAGR) of 18.7%.
- Nanomaterials are expected to have sales worth $15.9 billion in 2012 and $37.3 billion in 2017, a CAGR of 18.6%
- Nanotools should total nearly $4.8 billion in 2012 and $11.4 billion in 2017, a CAGR of 19.1%."[5]

The potential of manipulating material properties at nanoscale brings it to the forefront of the current scientific research. Hsinchun Chen *et al.*[6] reported that in global nanotechnology development: "Patents and papers increased in (2001–2010) as compared to (1991–2000) by 4.31 and 4.99 times, respectively, while in the two year interval (2011–2012) as compared to (2001–2010) increases are 2.34 and 1.91." So, one could conclude that the coming nano-revolution would have a mega-effect.

Thus, it is obvious that novel methods have to be introduced for handling the ever increasing demand of nano-based consumer products that should be simple to handle, environmental-friendly, energy efficient, and low cost. The fabrication of nanoparticles with controlled size, morphology and structural properties can be achieved through a lot of various techniques. Many synthetic approaches for nanostructures have already been reported that mainly involve nucleation, either as homogeneous or heterogeneous in solid, liquid and

gaseous media.[7-9] These synthetic approaches can be generally sub-divided into two different categories: chemical and physical.

The physical techniques of preparing nanoparticles such as laser ablation,[10] flame pyrolysis,[11] electric arc discharge,[12] ball miling,[13] ion sputtering[14] and thermal evaporation[15] introduce high potential routes for preparing nanoparticles free from undesirable chemical toxicity. However, these techniques have some drawbacks such as low rate of production, high temperature and pressure requirements which leads to a high energy consumption and ultimately high price.[16-18]

On the other side, there are different chemical methods to synthesize nanomaterials with desired size, morphology and surface properties by adjusting the solution parameters including temperature, solvents, surfactants, templates and micelles. The nanochemistry approaches are used to synthesize various interesting nanostructures with special properties such as Au, Ag, Pt, ZnO, MnO, CuO, $CuO_2$, $TiO_2$, $Fe_2O_3$, $Fe_3O_4$, $SnO_2$, InAs, CdS, ZnS, MnS, $Co_3O_4$, $Gd_2O_3$, $In_2O_3$, etc.[19-22] These approaches include sol-gel methods, co-precipitation process, microemulsion techniques, hydrothermal and solvothermal methods.[23-24] Chemical methods of nanosynthesis generally involve wet chemistry, i.e., reducing the metal complexes, thus, forming colloidal dispersions of metal nanoparticles. To prevent coagulation of nanopartilces, a stabilizer or a capping agent is often added. Chemical methods have already proved their unprecedented success in producing novel nanoparticles in an easy and efficient way that it cannot be achieved by other methods of nanosynthesis. But, the problem remains with the inherent use of hazardous chemicals. The use of harmful reducing agents, organic surfactants, solvents and capping agents can easily contaminate the food chain. Another problem is the contamination of nanoparticles themselves by adsorbing toxic byproducts on their surface, thus, negating their biocompatibility. Green chemistry seeks the solutions to these problems through the design and implementation of chemical processes with limited use or generation of substances harmful to the environment.[17,25]

## 1.2 Green chemistry and nanosynthesis

### 1.2.1 Green chemistry

Green chemistry is a sustainable concept, which includes two main approaches. First, it improves the efficiency of resources utilization associated with minimization of the waste. Second, it minimizes or eliminates the utilization and generation of toxic substances by the design, development and application of innovative chemical processes.[26-27] The definition of "green chemistry" coined by Paul T. Anatas and John C. Warner: "It is indeed the utilization

of a set of principles that reduces or eliminates the use or generation of hazardous substances in the design, manufacture and application of chemical products." The meaning of the term can be also clarified and summarized by the following "twelve principles."[28]

1. "**Prevention:** It is better to prevent waste than to treat or clean up waste after it has been created.
2. **Atom Economy:** Synthetic methods should be designed to maximize the incorporation of all materials used in the process into the final product.
3. **Less Hazardous Chemical Syntheses:** Wherever practicable, synthetic methods should be designed to use and generate substances that possess little or no toxicity to human health and the environment.
4. **Designing Safer Chemicals:** Chemical products should be designed to affect their desired function while minimizing their toxicity.
5. **Safer Solvents and Auxiliaries:** The use of auxiliary substances (e.g., solvents, separation agents, etc.) should be made unnecessary wherever possible and innocuous when used.
6. **Design for Energy Efficiency:** Energy requirements of chemical processes should be recognized for their environmental and economic impacts and should be minimized. If possible, synthetic methods should be conducted at ambient temperature and pressure.
7. **Use of Renewable Feedstocks:** A raw material or feedstock should be renewable rather than depleting whenever technically and economically practicable.
8. **Reduce Derivatives:** Unnecessary derivatization (use of blocking groups, protection/deprotection, temporary modification of physical/chemical processes) should be minimized or avoided if possible, because such steps require additional reagents and can generate waste.
9. **Catalysis:** Catalytic reagents (as selective as possible) are superior to stoichiometric reagents.
10. **Design for Degradation:** Chemical products should be designed so that at the end of their function they break down into innocuous degradation products and do not persist in the environment.
11. **Real-time analysis for Pollution Prevention:** Analytical methodologies need to be further developed to allow for real-time, in-process monitoring and control prior to the formation of hazardous substances.

12. **Inherently Safer Chemistry for Accident Prevention:** Substances and the form of a substance used in a chemical process should be chosen to minimize the potential for chemical accidents, including releases, explosions, and fires."

The twelve principles of green chemistry have become an ideal guide for chemists and chemical engineers all over the world to develop less toxic and environmental-friendly chemical syntheses. In the last two years, a lot of 'green chemistry' books described and discussed green methods in general[29-32] and their specialized aspects, including several methods in synthesis, green engineering and manufacturing, hydrogen and syngas production and uses, wastewater treatment, green tribology, textiles, food, biomass and bio-composites, and particle technology.[33]

The core of green chemistry is simplified in the word of "REDUCE." It could summarize the reduction of waste, risk, cost, hazard, materials, derivatives and energy. The strategy of green chemistry has already been applied to all the branches of chemistry such as analytical chemistry, inorganic chemistry, organic chemistry, biochemistry, physical chemistry and nanochemistry. It exactly helps nanochemists to provide suitable solutions for the social problems related particularly to health, hazards and environmental damage that have originated from industrialization and the spontaneous growth of nanotechnology. For that reason, the integration of nanochemistry and green chemistry introduces a new field of science called "green nanochemistry."

## 1.2.2 Green nanochemistry

Green nanochemistry is a sustainable approach to develop nanotechnology relevant to the complete process including design, development, synthesis, characterization and application of nanoparticles. In the field of nanoscience, green nanotechnology becomes increasingly popular and is so necessary due to the worldwide problems combined with environmental pollution.[23] In other words, there is a significant interest and urgent need to find a better way for producing nanomaterials by using the basics of green nanochemistry concept. One cannot deny that, despite the intensive development of the green nanotechnology, the harmful effects of nanomaterials are still relatively unknown. Indeed, the production of nanomaterials using these nontoxic and biocompatible reagents could decrease the adverse effects of the synthesized materials and the environmental impacts of by-products and derivatives.[33-35] The methods for producing nanoparticles by using naturally occurring reagents (biogenic synthetic protocol) such as sugars, vitamins, biodegradable polymers, plant extracts, and microorganisms as capping agents and reductants can be considered as solution for the

realization of a green nanotechnology method. Nevertheless, there are some limitations such as few number of inorganic materials can be fabricated by these processes and less control over size distribution, morphology and crystal structure. Furthermore, the rate of production is slow and the produced nanoparticles are also not monodisperse.[33,36-38]

A summary of well-known green methods is presented in **Table 1.1**. According to **Table 1.1**, one can conclude that there are still several drawbacks of the available green methods for nanomaterial production and hence efforts are needed to develop novel approached or modify the currently available techniques. One of the novel and promising methods that can be used for nanosynthesis and fabrication is Leidenfrost approach. It could overcome most of the common problems (rf. **Table 1.1**) such as high cost, time consumption, sophisticated setup usage and less control over nanoparticles size and shape. Before discussing the chemistry of Leidenfrost reactor and for better understanding, an introduction including the Leidenfrost phenomena, heat transfer, self-ionization of water and its boiling will be presented in the next sections.

***Table 1.1: Green methods for fabrication of nanomaterials including advantages and disadvantages.***[17,33,36-39]

| **Methods of synthesis** | **The commonly synthesized nanoparticles** | **Green context** | **Advantages** | **Disadvantages** |
|---|---|---|---|---|
| (1) Reduction method by citrate | Au and Ag | Atom economy | Mild reagents are used in these methods | Surface chemistry of nanoparticles is not controlled |
| (2) Laser ablation technique | Au and Ag | - Solvent free<br>- Eco-friendly | Nanoparticles in high purity with controlled size and morphology | - Laser maintenance is costly.<br>- Expensive equipment is required |
| (3) Sonochemical method | Au | Safer solvent | Particle size is Controlled with reasonable stability of the nanoparticles | - Less widely studied method.<br>- Sophisticated equipment is required. |
| (4) Ligand stabilized method | Au, Ag, Pt and Pd | Less toxic reagent are required | Greater control on shape | Ligands overlap with functionalization steps |
| (5) Electrochemical method | Au, ZnO and other metal oxide nanoparticles | - Minimal production of waste<br>- Energy efficient and atom economy<br>- Catalyst free | - Easy control.<br>- A uniform functional surface with considerable particle size distributions | - High cost.<br>- Specific expertise is required.<br>- Scale-up is limited |
| (6) Ionic liquids mediated method | Au, Pt, Pd, Pb, ZnO and PbO | Reusability of non-inflammable solvent and ability to dissolve different materials | - Stability is increased.<br>- Narrowed size distribution and lower average size of produced metal nanoparticles | Potential harmful to aquatic ecosystem due to high water solubility of ionic liquids |
| (7) Microwave method | ZnO, TiO2 and semiconductor nanoparticles | Less reaction time and energy consumption | - Fast and clean and without refluxing system.<br>- NaOH Free | Relatively less control over size and morphology of nanoparticles |
| (8) Supercritical fluids using method | Au, Ag, Co, Ni, and semiconductor materials | Nonflammable, non-toxic, and safer solvent | - Eco-friendly<br>- Less hazardous | - The availability of supercritical fluids are Limited.<br>- Sophisticated setup is required.<br>- Costly |
| (9) Biological methods | Mainly metal nanoparticles as Au and Ag | - Cost-effective<br>- Environmentally friendly | - Safe and eco-friendly<br>- Cost-effective | - Not easy to have large quantity<br>- Time-consuming<br>- Control over size distribution, shape and crystallinity is difficult<br>- Limited number of metal oxide nanoparticles is prepared |

## 1.3 Leidenfrost phenomenon

When water drop touches the hot surface which is much hotter than the boiling point of water, the bottom surface of the drop in contact with the hot surface immediately vaporizes. The gas pressure from this vapor film is insulating the rest of the drop from boiling rapidly and thereby longer time is taken by the liquid drop to evaporate.[40-41]

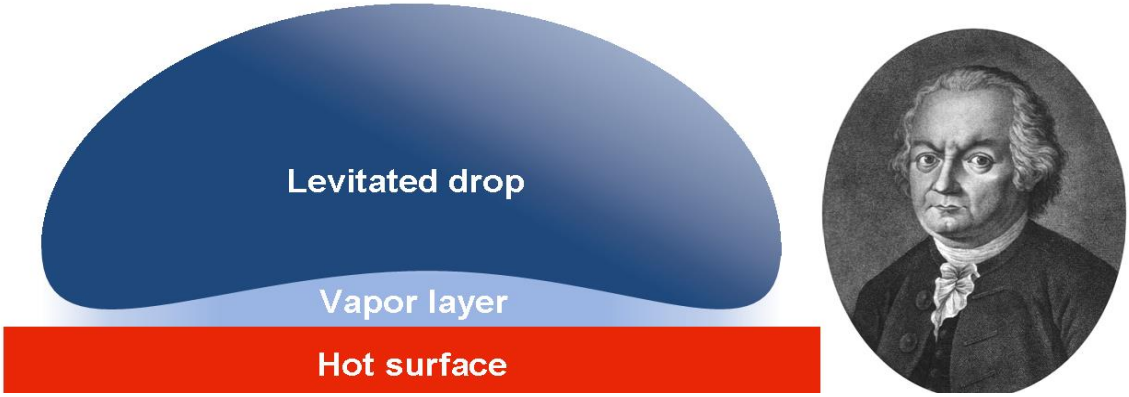


***Figure 1.1: (left) Drop of liquid levitates on its vapor film on heated surface at Leidenfrost temperature. (right) an image of Prof. Dr. J. G. Leidenfrost[42] (1715-1794).***

The phenomenon i.e., levitation and dancing of the liquid drop on its own vapor film (**Figure 1.1**) is named after Johann Gottlob Leidenfrost,[42] who documented the phenomenon in 1756. This study demonstrated that the Leidenfrost drop can be used as water based green chemical reactor for nanofabrication.[43] There are some basics which may be useful for better understanding of the Leidenfrost effect and its utilization for nanofabrication such as the heat transfer, the nature of water and its boiling regimes which are presented in the coming sub-sections.

### 1.3.1 Heat transfer

Heat transfer is a field of science that is concerned with the study of energy transfer between physical systems due to temperature difference. Heat transfer includes three fundamental methods or mechanisms: conduction, thermal radiation, convection.[44-46]

- **Conduction or diffusion**

It is type of heat transfer that takes place between bodies that are in physical contact. In this case, the heat is transferred from the hotter object to the lower one because of random molecular diffusion. The hot, fast vibrating or moving atoms and molecules transfer some of

their energy to the neighboring atoms and molecules. That happens when a Leidenfrost drop touches a very hot surface. This kind of momentary thermal conduction causes the vapor formation.

- **Thermal radiation**

Thermal radiation takes place through a vacuum of space or any other transparent medium (liquid or solid). It is the transfer of heat by means of emission or absorption of electromagnetic radiation which propagates because of a temperature difference.

- **Convection**

Convective heat transfer is the transfer of energy from one region to another by random molecular motion (diffusion) and bulk or macroscopic movement of the fluid. Convective heat or cooling may be expressed by Newton's law of cooling.[45] The rate of heat loss of a body is proportional according to the difference in temperatures between the body and its surroundings:

$$q = hA\left(T_w - T_\infty\right) \tag{1.1}$$

where $q$ is the thermal energy, $h$ is convection heat transfer coefficient ($W/m^2K$), $A$ is surface area, $T_w$ is wall (surface) temperature and $T_\infty$ is fluid temperature. In general, there are two types of convection: forced convection and natural convection.

### Forced convection

Forced convection occurs under the influence of an external source such as fans, pumps or stirring.

### Natural (or free) convection

Natural convection occurs when fluid motion is induced by buoyancy forces that arise from the density variations caused by variations of the temperature in the fluid. Without any external source, when a liquid is in contact with a hot surface, it becomes less dense because of separation and scattering of its molecules. As a result, the liquid is displaced while the cooler liquid gets denser and the liquid sinks. For that reason, the hotter part transfers heat in the direction of the cooler part of that liquid.[2] The levitated Leidenfrost droplet is an example showing the convective flow and circulation of the water at Leidenfrost temperature. The convective flows of the levitated water droplet could be also affected by shear drag produced

by the escape of water vapor and variations of the surface tension as well as temperatures inside the drop.[47-48]

### 1.3.2 Self-ionization of water and steam electricity

Self-ionization of water is proposed due to the collision of water molecules with each other. The hydronium ion ($H_3O^+$) and hydroxide ion ($OH^-$) are formed consequently due to the following chemical reaction:[49]

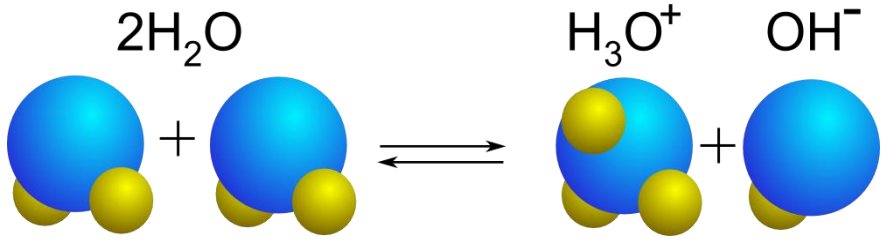


(1.2)

This reversible reaction has chemical equilibrium constant, $K_{eq}$ of:

$$K_{eq} = \frac{[H_3O^+][OH^-]}{[H_2O]^2} \quad (1.3)$$

and acid dissociation constant, $K_a$ is:

$$K_a = K_{eq} * [H_2O] = \frac{[H_3O^+][OH^-]}{[H_2O]} \quad (1.4)$$

For a diluted aqueous solution, which is the case in this work, molarity of water [50] is considered as constant. It is ignored from the acidity expression by convection. So the thermodynamic equilibrium constant, ionic product, dissociation constant or self-ionization constant for the water shown by $K_w$ can be calculated by the following equality:

$$K_w = K_a * [H_2O] = [H_3O^+][OH^-] \quad (1.5)$$

Accordingly, at standard temperature (25 °C) and pressure (STP), one would end up with $K_w = 1.0\times10^{-14}$. At STP conditions, the self-ionization of water is quite slow but it accelerates with increasing the temperature up to $10^{-12}$ at 300 °C. The dependence of the self-ionization constant on the temperature,[51-52] pressure and ionic strength are shown in **Figure 1.2**.

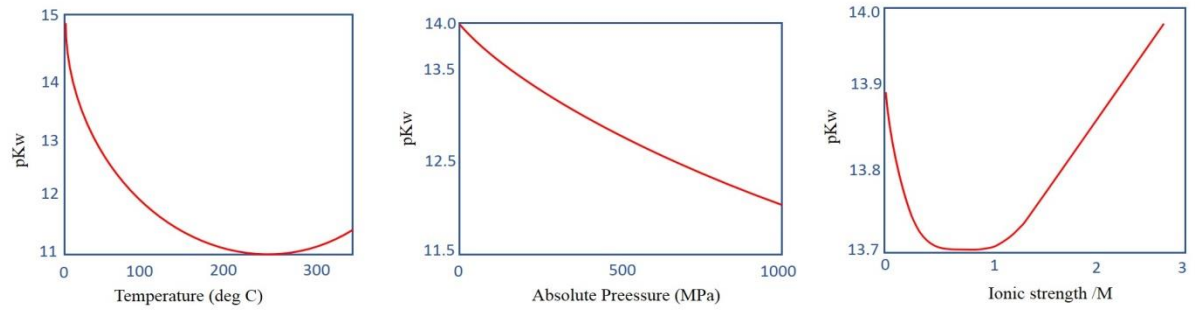


***Figure 1.2: Variation in $K_w$ values with temperature (left), pressure (middle) in case of water and ionic strength in case of NaCl solutions at 25 °C. [These data based on International Association for the Properties of Water and Steam[50] (IAPWS)].***

Where $pK_w = Log_{10}(1/K_w) = -Log_{10}(K_w)$

In this work, Leidenfrost temperature is above 250 °C and hence the water evaporates fast at that degree. By using IR thermography, the temperature at the base (liquid\vapor interface) of the Leidenfrost drop is between 100 and 105 °C. Nevertheless, the values of $[H_3O^+]$ and $[OH^-]$ are always equal at all different temperatures. This occurs because of the shift in equilibrium of **Equation 1.1** in forward direction (Le Chatelie's Principle).

Self-ionization of water is essential for producing nanoparticles in the Leidenfrost chemical reactor as the hydroxide ions stay inside the drop while hydronium ion becomes vapor. Furthermore, adding NaOH or $NH_4OH$ to the medium generates more hyrdroxide by self-ionization[53-54]. Indeed, the Leidenfrost phenomenon represents water drop electrification stimulated by levitation of the drop on its own vapor film caused by the hot surface[55-56]. This steam electrification caused by the charge separation of the hydroxyl and hydronium ions enhances the self-ionization resulting in the required conditions for nanofabrication. The average charge produced at these conditions depends on the concentrations of hydroxyl and hydronium ions. The charge probability[57] ($P^+$ ,$P^-$) could be expressed by:

$$P^+ = \frac{\left[H_3O^+\right]_b}{\left[H_3O^+\right]_b \left[OH^-\right]_b} \qquad (1.6)$$

and

$$P^- = \frac{\left[OH^-\right]_b}{\left[H_3O^+\right]_b \left[OH^-\right]_b} \qquad (1.7)$$

In 1980, Pounder studied the Leidenfrost phenomenon by using 1 mL drop of 3.5 % NaCl aqueous solution at 610 °C and discovered charged micrometer particles. He documented

that electricity can be produced form the Leidenfrost boiling of saline solution. The emitted particles have an average charge of $10^{-14}$ C and there is an increase in their charges by rising their radius.[58-59]

### 1.3.3 Water boiling and Leidenfrost point

By placing an amount of liquid on a hot surface, the liquid starts to evaporate in different rates based on its boiling point relative to the surface temperature. Generally, there are three modes of boiling,[40,60] as illustrated in **Figure 1.3**.

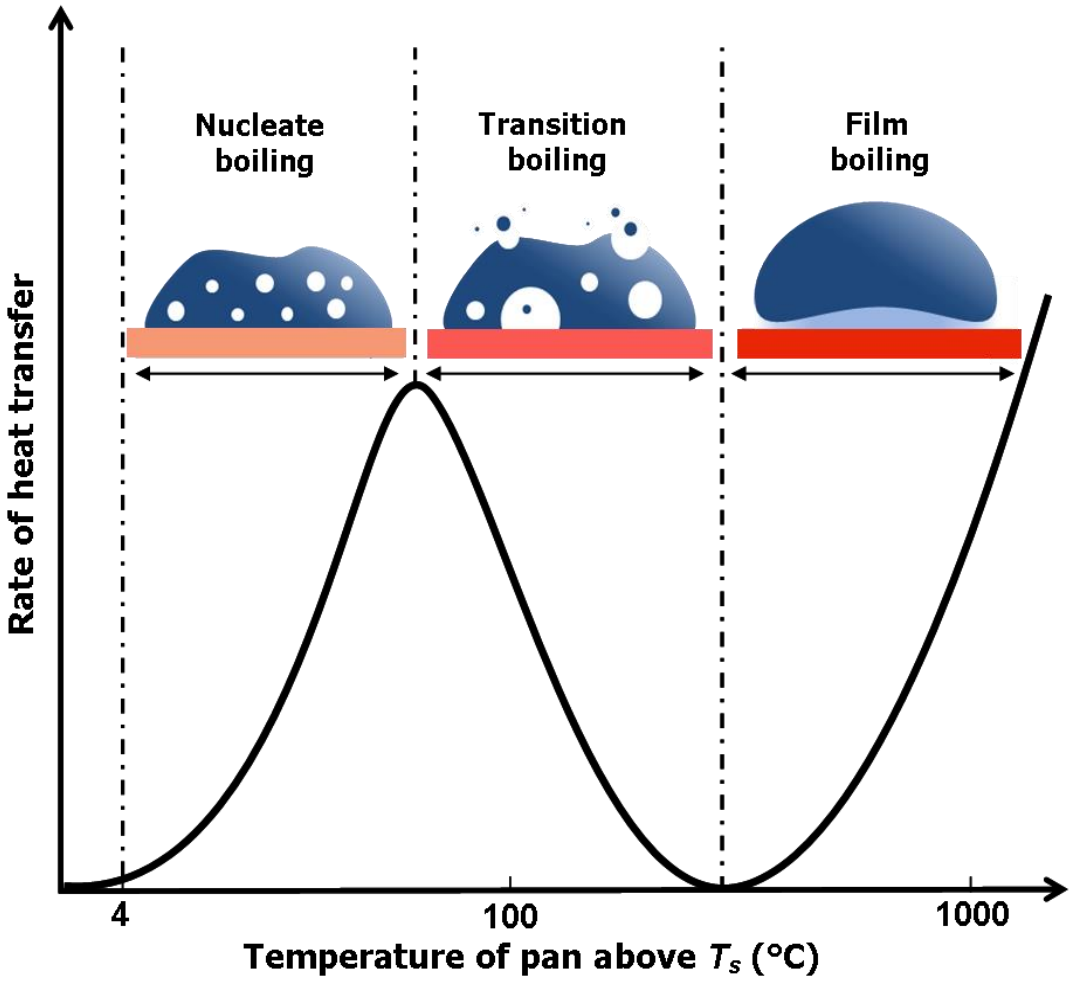


***Figure 1.3: The curve of water boiling at different temperatures (at 1 atm) shows that, by increasing the pan temperature above the normal boiling temperature ($T_s$), the rate of heat transfer from the pan to water initially increases. However, the rate of transfer almost vanishes above certain temperature. Then the transfer reappears again at higher temperatures.***

1. Nucleate boiling begins above the boiling point characterized by the growth of bubbles or pockets of gas which develop from discrete points along the heated surface of the liquid. Also, the nucleation points are generally increased with an increasing in the surface temperature.

2. Transition boiling: By increasing the temperature above the nucleate temperature, the boiling becomes strong for including more rapid and larger gas pockets. This unstable physical process which frequently encompasses acoustic effect is called transition boiling.
3. Film boiling: When a surface is significantly hotter than the liquid boiling point, the liquid initially will contact the surface and then the evaporation occurs, where a thin layer of vapor insulates the surface from the liquid. This condition is considered as film boiling regime or Leidenfrost phenomenon.

The Leidenfrost temperature can be determined commonly by measuring the droplet evaporation life time for its known initial size over a range of surface temperatures. The curve of the drop evaporation time versus the temperature of the surface which is called droplet evaporation curve,[60] is shown in **Figure 1.4**. The curve represents the distinct heat transfer regimes of water boiling.

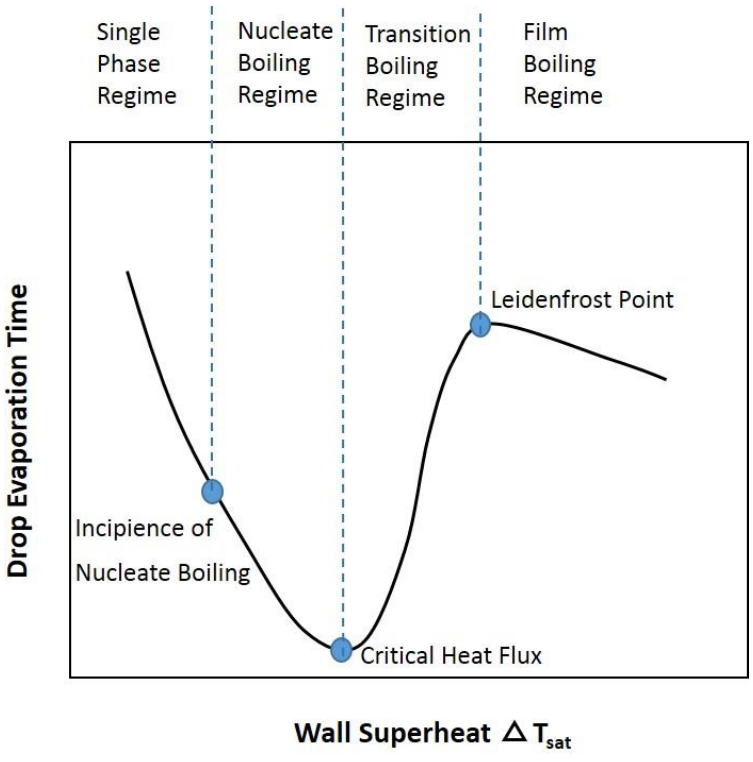


***Figure 1.4: The curve of the drop evaporation.***

## 1.3.4 Leidenfrost drops and its levitated pattern

Several values of Leidenfrost temperature of water have been reported in the literature.[60] The variations in the Leidenfrost point is due to a lot of parameters affecting it.

These parameters includes surface material, the volume of the liquid, droplet impact velocity, the surface morphology, pressure and presence of additives or impurities. In 1966, Baumeister *et al.* showed the Leidenfrost states of the liquid in different volumes[61] (**Figure 1.5)**.

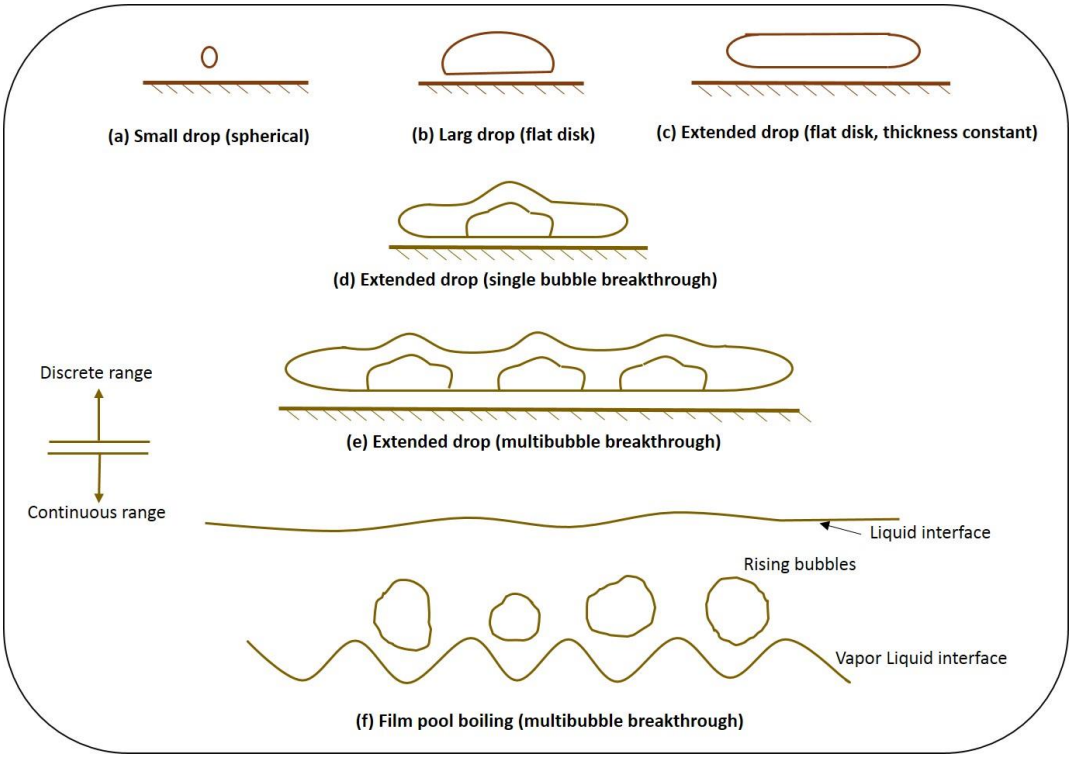


***Figure 1.5: Schematic diagram showing the film boiling states of different liquid volumes[61].***

In a recent work, Paul *et al.* has studied the pattern and oscillations in the Leidenfrost droplets of different volumes by using a high-speed camera (**Figure 1.6**), to show the gradual progress of the drop size and shape with time.[62] Actually, there are several models[60] discussing the commonly postulated mechanisms for the Leidenfrost point based on the hydrodynamic instability, thermo-mechanical effects, the surface wettability, or metastability of the liquid.[60]

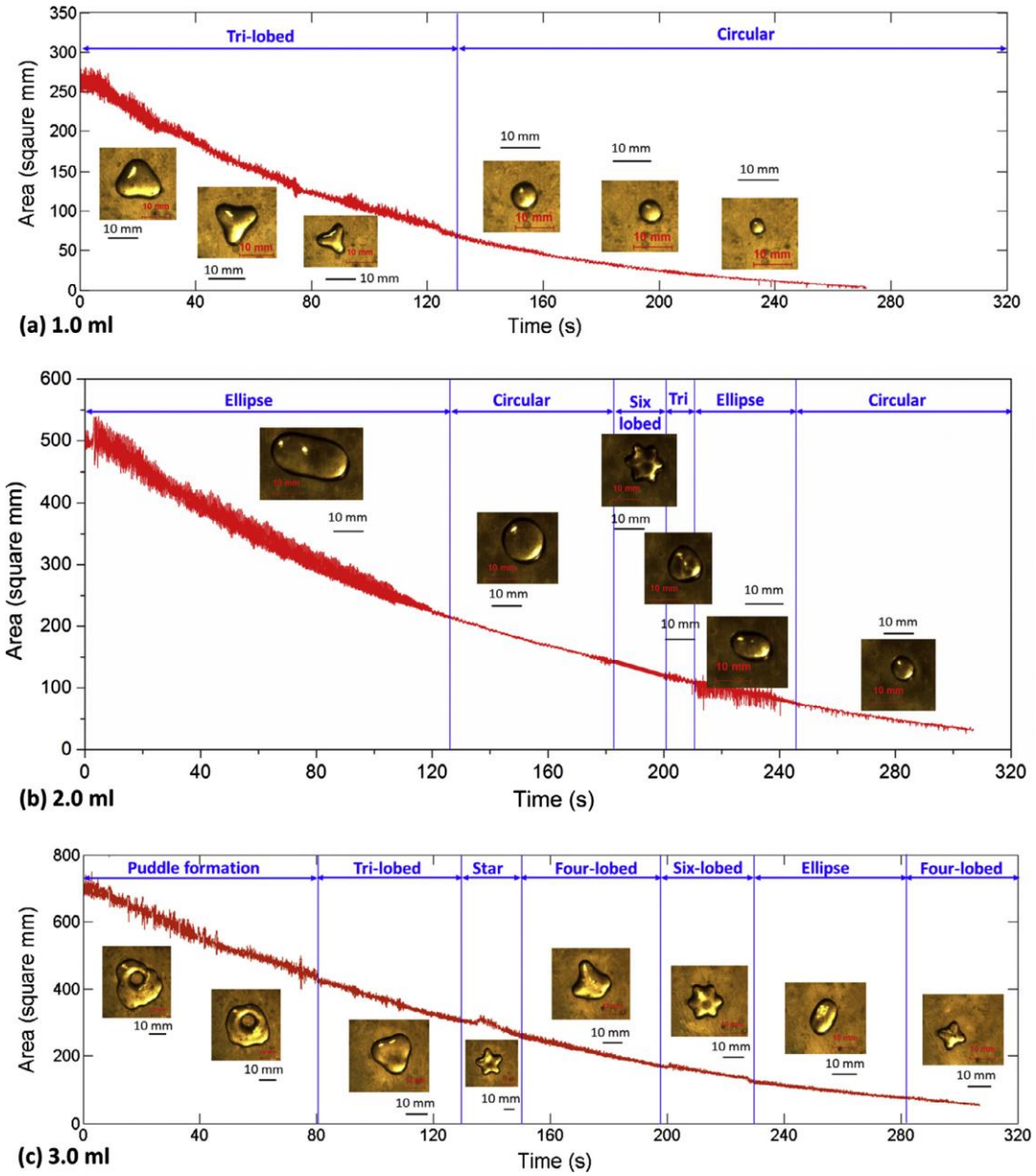


***Figure 1.6: Shape and size evolution of Leidenfrost drops with time for a substrate temperature of 400 °C having initial volume (a) 1.0 ml, (b) 2.0 ml and (c) 3.0 ml. [Reprinted with permission from ref. [62] (Copyright 2014, Elsevier Inc.)]***

## 1.3.5 Leidenfrost nanochemistry

The first demonstration of Leidenfrost drops for the green nanofabrication was done by Elbahri *et al.* in 2007. Elbahri and co-workers showed that nanostructure could not be only formed but could be simultaneously organized and deposited on various substrates, too. In that work, the deposition of Ag and ZnO nanoparticles on a preheated silicon substrate (230 °C) was demonstrated by using a Leidenfrost water droplet loaded with the particles. This kind of pattering of nanostructure can be called anti-Lotus effect. Also, the direct production of ZnO and Ag nanoparticles and its deposition in the form of rings and wires on a surface is shown by using the droplet which contains an aqueous precursor solution[63] (**Figure 1.7)**.

Prof. Dr. Rainer Adelung, who was a junior researcher at that time in the Department of Multicomponent Materials at the University of Kiel, and the supervisor of Elbahri, named it as the "Elbahri synthesis" as a novel way for a droplet-disposition-based nanostructuring technique. "Inspired by kitchen experiments with his wife Julia, he discovered that it might be possible to ignore the typical temperature limit of 100 °C for water-based synthesis. He found that at temperatures of 250 °C, well above the boiling point, it is possible to use water droplets that contain a small amount of chemicals for nanostructuring – thanks to the Leidenfrost effect." Adelung said.[64]

This led to a new class of nanosynthesis based on a Liedenfrost droplet. This synthesis method gives the control over the design and morphology of the fabricated nanostructure to be suitable for diverse functions. Due to its simplicity, cost effectiveness, eco-friendliness and high purity of the product, it naturally attracted attention of scientific community and was covered by a great deal of scientific news, portal and blogs.[65] However, at that time, a deep understanding of the phenomenon necessary for any practical application of the process was lacking. The work presented in this thesis aims to add some more understanding about the mechanism of this phenomenon which can be ultimately used for nanostructuring, 3D coatings and self-organized nanopowders.

The thesis highlights the potential of Leidenfrost phenomenon in the synthesis and the assembly of nanoparticles which can be tailored for various functions. It also demonstrates the fabrication of IR emissive nanopowder, plasmonic super absorber based on nanoparticle hybrids for solar energy harvesting and the high thermal resistance foam.

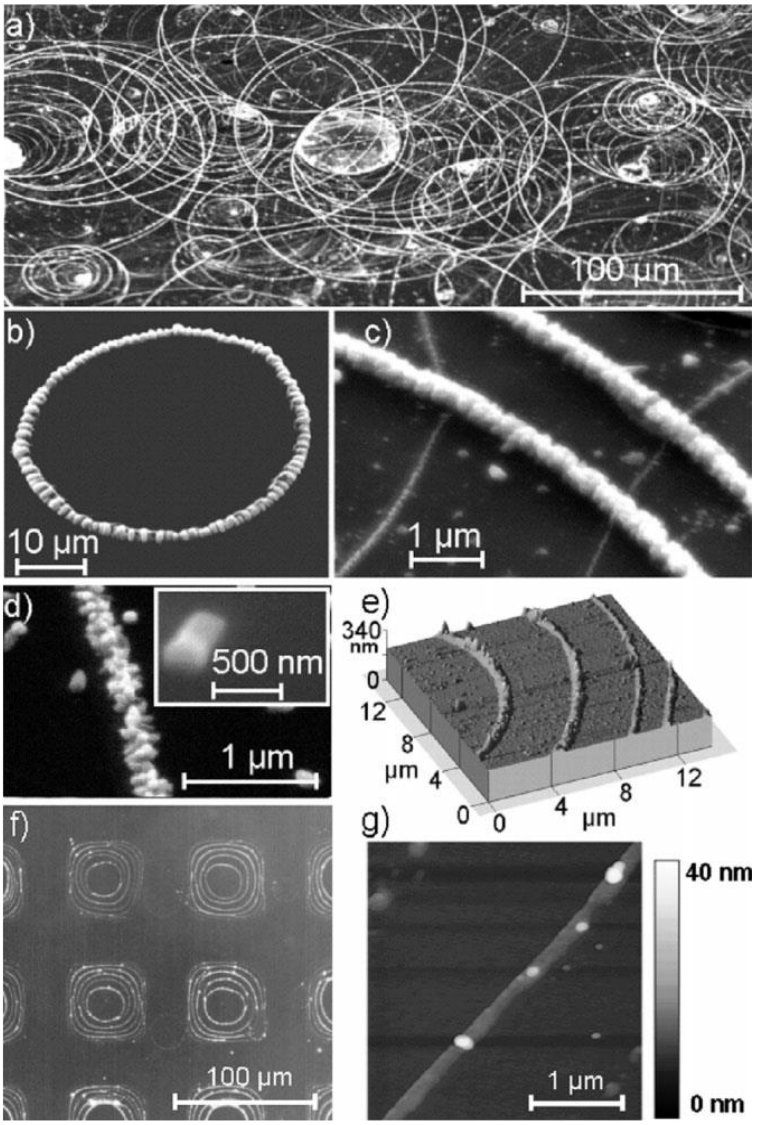


***Figure 1.7: SEM images of rings of ZnO and silver nanoparticles formed by disintegration of the droplet at the Leidenfrost temperature. (a) Overview showing intersecting ZnO rings; (b) individual ZnO circles; and (c) circles of different sizes intersecting each other. (d) A magnified image of part of a ring revealing the hexagonal crystalline character. (e) A 3D representation of an atomic force microscopy (AFM) image showing a part of a concentric silver-ring system that is aligned by using a TEM grid. (f) Dark-field optical microscopy image is showing an overview of the reproducibility of the aligned ring systems. (g) AFM image of a Ag ring in nanoscale diameters. [Reprinted with permission from ref. [63] (Copyright 2007, WILEY-VCH Verlag GmbH & Co. KGaA)]***

### 1.3.6 Applications of Leidenfrost phenomenon

It is essential to understand the Leidenfrost effect from physical and mechanical point of view not only because of solving a scientific puzzle but also for the practical application of this interesting phenomenon. It has been shown that the Leidenfrost phenomenon includes many aspects of interfacial hydrodynamics where a vapor and liquid are in motion. With the continuous flow of the vapors due to the exerted pressure of the liquid, the liquid is subjected

to self-oscillations and internal motion. Its fast displacements with tiny friction could be applied to create self-propelling devices. There are different interfaces like the solid/vapor interface at the hot solid surface which leads to a no-slip condition and can be designed and textured to induce special properties. The liquid/vapor is another interface which is sometimes unstable (e.g., chimneys formation across the liquid) and here the molecular exchange takes place. Lastly, the liquid/air interface is located at the top of the liquid where the temperature is lower than that at the bottom of drop. This produces Marangoni flows in the liquid.[66] Indeed, the study of these different interfaces, where viscous flows (in the vapor) coexist with inertial flows (in the drop), is essential towards better understanding of the Leidenfrost phenomenon.

The understanding of the hydrodynamics and different components of the drop has been utilized in different applications. The vapor layer has been shown to levitate and self-propel not only liquid[67] but also sublimating solid objects[68] on the specifically textured ratchets. This frictionless movement that requires no mechanical parts has potential in many scientific applications in case of existence of relative motion between surfaces. Vakarelski *et al.* have studied the effect of the superhydrophobic surfaces for stabilization of Leidenfrost vapor layer[69] (**Figure 1.8**). They showed that the textured superhydrophobic surface makes it possible to maintain a stable vapor layer at any temperature above the boiling point of the liquid (at all superheats) by eliminating the collapse of the vapor film. This concept may potentially be used to the design of low-drag surfaces in case of presence and stabilization of the vapor phase in the grooves of textures without heating, and to control other phase transitions, like frost or ice formation.

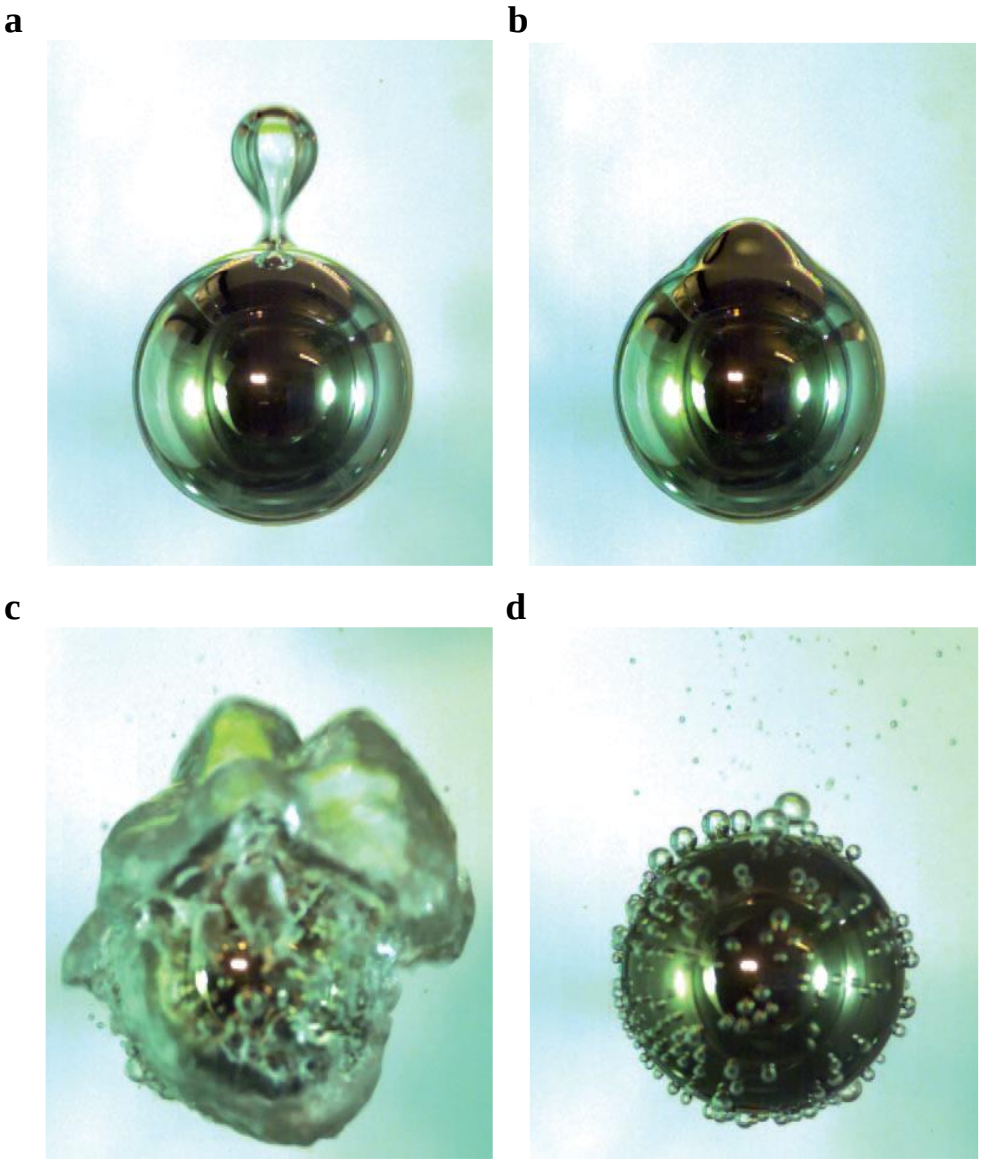


***Figure 1.8: High-speed Snapshots of 20-mm steel spheres cooling in water. (a) Bubble pinch-off from the vapour dome of a hot, superhydrophobic sphere cooling in the Leidenfrost condition. Water pool temperature is 100 °C; the temperature of the sphere is Ts = 200 °C. (b) The final state of the same superhydrophobic sphere, cooled to the pool temperature (Ts = 100 °C). (c) The hydrophilic sphere cooling in water at 100 °C, at the moment of the explosive transition from film boiling to nucleate boiling (Ts = 275 °C) and (d) during nucleate boiling where Ts = 200 °C. [Reprinted with permission from ref. [69] (Copyright 2012, Nature publishing Group).]***

In a recent study, the hydrophilic microbeads loaded within the Leidenfrost drop have shown self-organization owing to their evaporation (**Figure 1.9**). With the decreasing size of the drop, the beads gradually occupy and cover a larger proportion of the surface. With the consideration of the dynamics of evaporation, the microbeads lead to the reduction of the evaporation rate under the Leidenfrost drop, where the dewetting of the beads at the interface leads to decreasing the effective surface of evaporation.[70]

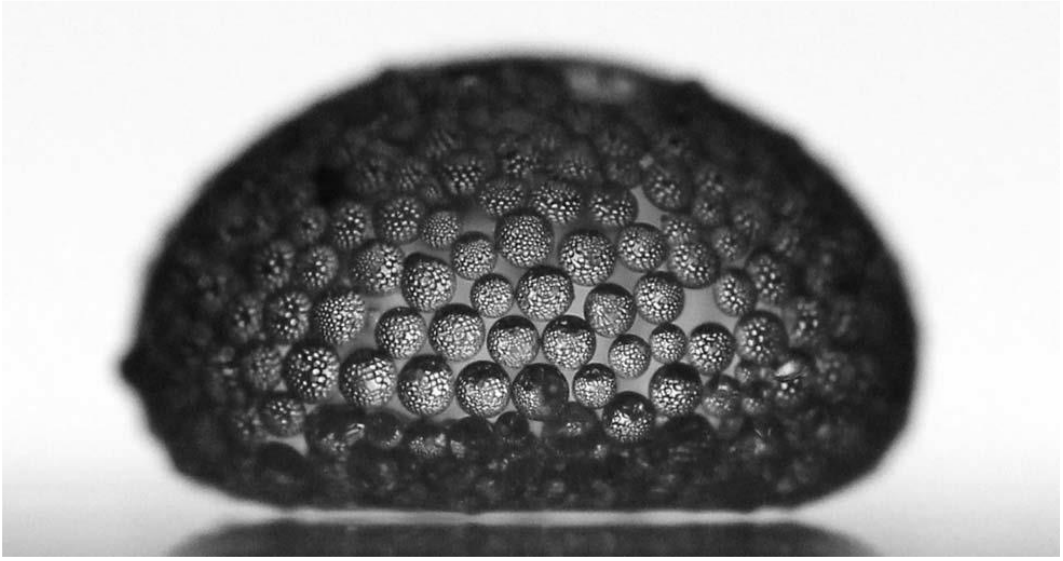

***Figure 1.9: Photograph of a centimetric Leidenfrost drop covered by glass beads of mean radius Rb = 150 µm. The dots in the beads are because of the refraction of the beads on the hidden face of the drop. [Reprinted with permission from ref. [70] (Copyright 2014, Royal Society of Chemistry).]***

In 2005, Tsapis *et al.* studied the buckling and drying dynamics of Leidenfrost droplets loaded with aqueous colloidal solution of monodispersed polystyrene particles. With drying, during the evaporation of the droplets, the particles are arranged and packed together in a form of a viscoelastic shell at its surface. With further drying, the droplet shrinks to form elastic buckles when the attractive capillary forces overcome the electrostatic forces which stabilize the poly styrene particles.[71] In a recent work, the Leidenfrost drops have been reported as a novel strategy to make colloidal assembly for creating photonic microgranules with non-iridescent structural colors and low angle-dependency.[72] In that work, the Leidenfrost drop was used as a confining geometry and a rapidly shrinking template for fast consolidation of monodispersed silica nanoparticles. In other words, the suppression of crystallization of silica nanoparticles to form amorphous structures is caused by the fast concentration of colloids under Leidenfrost conditions (**Figure 1.10**). Furthermore, carbon nanoparticles with average diameter of 23 nm are added to the ethanolic suspension of silica particles to suppress their incoherent multiple scattering, thereby improving the color contrast. In many practical coloration applications, this method may provide new opportunities as substitutes to chemical or toxic dye materials.

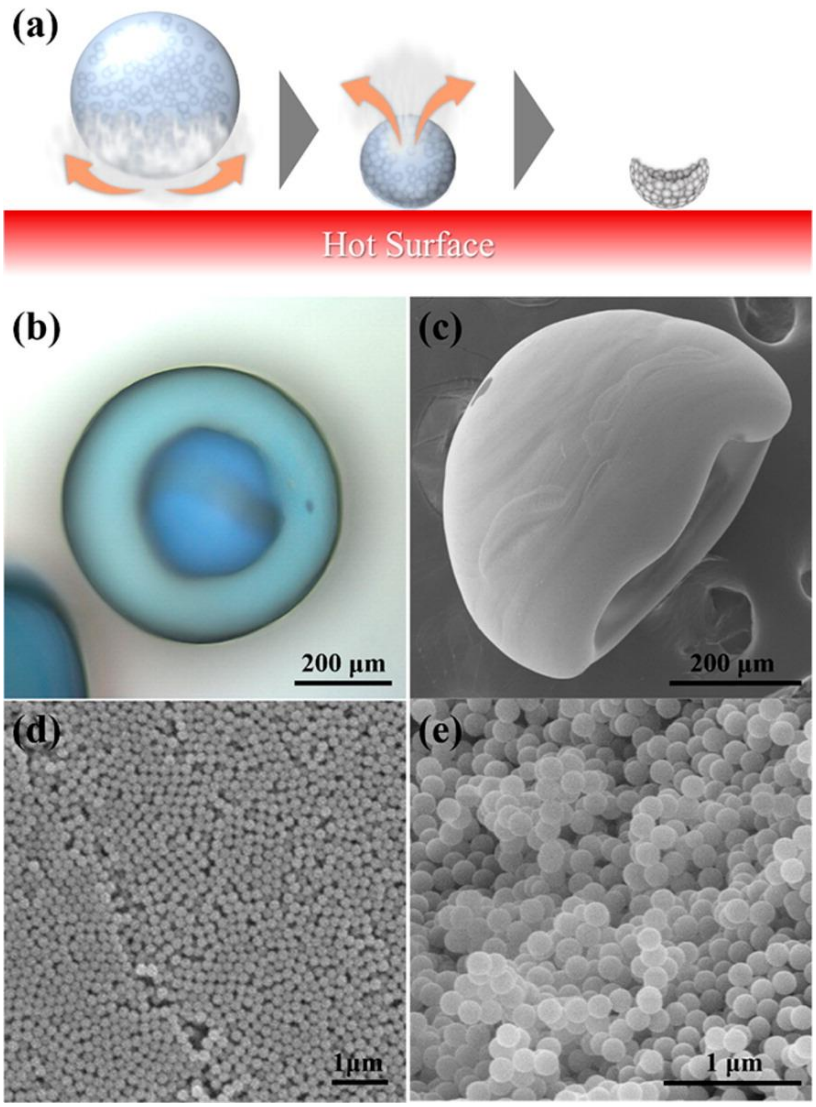


***Figure 1.10: (a) Schematic illustration presenting the formation of glass packing of colloids confined by a Leidenfrost drop. (b) An optical microscope image and (c) SEM image of a photonic microgranule composed of random packing of silica particles with diameter of 190 nm. (d) SEM image showing colloidal arrays on the microgranule surface and (d) its cross-section. [Reprinted with permission from ref. [72] (Copyright 2014, American Chemical Society).]***

Liedenfrost phenomenon does not only draw the attention of physicists and mechanical engineers but the chemical biologists as well. In a recent report, the dielectric barrier discharge ionization mass spectroscopy in open atmosphere combined with Leidenfrost phenomenon has been shown as a new strategy towards highly sensitive and direct analysis for anabolic steroids in urine.[73-74]

The present thesis also shows the efficiency of the Leidenfrost as a nanoreactor to fabricate not only plasmonic particles but also nanoporous materials. Scientific background of the functional materials produced through this process will be discussed in the following section.

- **Plasmonic nanomaterials**

There are many theories that explain the optical properties of clusters of atoms based on their size, morphology, nature, and the surrounding matrix. A plasmon in physics, can be defined as the quantum of plasma oscillation. Since a large number of atoms of the metallic nanoparticle exist at the surface, an electron cloud is developed because of the interactions of these electrons with their neighbors. Subsequently, the surface Plasmon corresponds to the overall collective excitations of the conduction electron cloud.[75] Therefore, when an electromagnetic radiation interacts with the nanoparticles, there will be excitation of the electron cloud to jump to the conduction band and these free electrons are oscillated coherently and in phase with the oscillating incident electric field, as shown in **Figure 1.11**. This kind of surface charge oscillation in case of nanoparticles is called localized surface plasmon resonance (SPR) or dipole resonance. The parameters that define and control the frequency and width of the surface plasmon absorption are the size, the morphology of metal cluster, the dielectric constant of metal, as well as the dielectric constant of the surrounding matrix.[76]

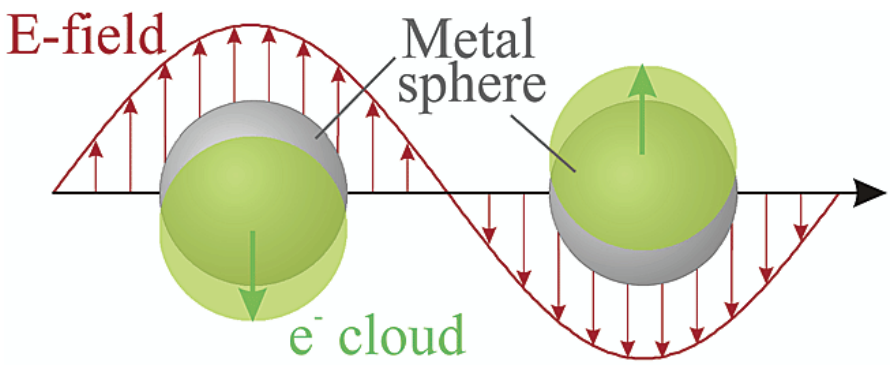


***Figure 1.11: Schematic diagram of a plasmon oscillation for a sphere, representing the displacement of the conduction electron charge cloud relative to the nuclei. [Reprinted with permission from ref. [75] (Copyright 2003, American Chemical Society).]***

Surface plasmon resonance is potentially applicable in many fields ranging from biological and chemical sensors[77] to photocatalysis,[78] genetics,[79-80] cancer therapy[81] and to energy.[82]

In this thesis, a successful synthesis of plasmonic gold nanoparticles with an average diameter of about 4 nm is demonstrated. The synthesis was carried out by using a levitated Leidenfrost reactor without using any reducing agent. By this approach, nanoparticles and plasmonic nanoporous brown gold can be designed and fabricated easily in minutes without a complicated setup.

Recently, the interest of plasmonics researchers is turning to solar cells,[83] where plasmonics can enhance the absorption[84] potentially to be close to 100%. Keeping this in view, a completely black nanoporous gold structure with almost 100% absorbance is synthesized in suspension and powder form. This kind of plasmonic wideband superabsorber can be potentially applied for the improvement of the photovoltaic devices.[84]

- ## Nanoporous materials

Nanoporous materials with a variety of pore sizes and shapes have attracted significant attention within the last two decades. Due to their unique chemical, physical and mechanical properties, they can be technologically useful for a wide spectrum of potential applications such as catalysis, separation and adsorption technologies, biological molecular isolation and purifications, drug delivery, energy conversion and storage in fuel cells, lithium ion batteries, super capacitors and hydrogen storage, chemical sensors, water purification, environmental pollution control, as well as for optical and electronic devices.[85-86]

Nanoporous metals are a subgroup of these materials, which have beneficial electrical and optical properties. Among porous metals, nanoporous gold has recently attracted interest for photonic and plasmonic applications.[87-88] Dixon *et al.* characterized the surface plasmon resonance in case of ultra-thin nanoporous gold films.[89] Maaroof *et al.* reported that the bulk and surface plasmons can be controlled in case of nanoporous gold films through controlling the porosity.[90] In 2011, Nishio *et al.* produced a nanoporous black film by the anodizing pure gold in oxalic acid solution[91] (cf. **Figure 1.12)**. In addition, the electrochemical oxidation of glucose on such fabricated black gold surfaces and its application to amperometric detection have been shown[92] by Jeong *et al*. On the other hand, the development of a suitable technique for the production of metallic nanoparticles and their colloidal self-assembly to obtain plasmonic nanoporous foam is a major challenge.[43]

This dissertation shows that the brown and black 3D nanoporous gold in suspension and in the foam form ca be designed and fabricated successfully by using the dynamics and chemistry of the Leidenfrost nanoreactor. A 3D nanoscale object can be treated by this levitated chemical reactor to produce a superhydrophilic and heat resistive metal-polymer hybrid foam. Moreover, it is shown that the fabricated black gold is a plasmonic wideband superabsorber.

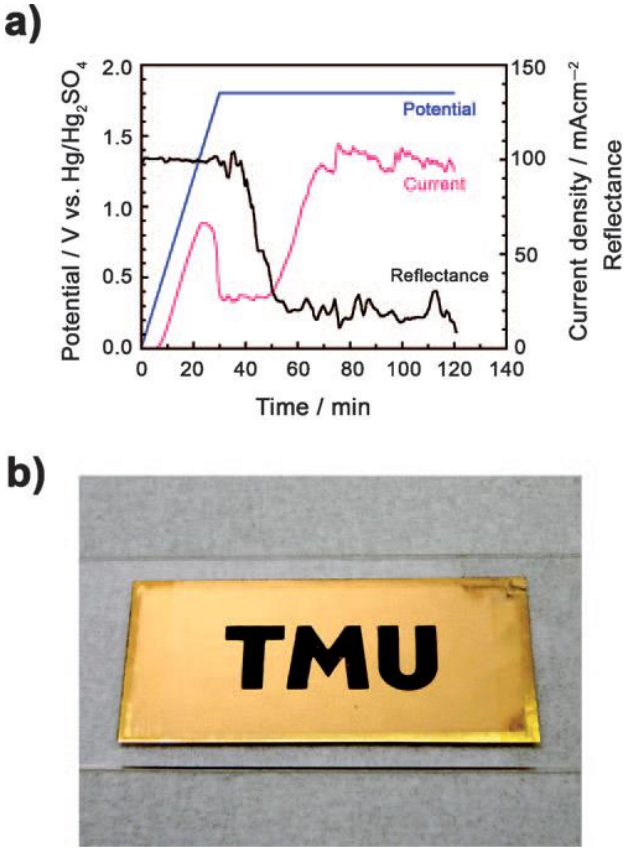


***Figure 1.12: (a) Controlled potential (blue), resulting current curve (red), and change in the reflectance at l=570 nm (black) during the anodization of pure gold in 0.3 M oxalic acid at 0 °C. (b) Photograph showing the gold foil after anodization. The size of the foil is 4.5×2.0 cm. [Reprinted with permission from ref. [91] (Copyright 2011, WILEY-VCH* Verlag GmbH & Co. KGaA*)]***

It seems that the morphology and the pore size structure in case of the black and brown gold are making a strong effect on the optical properties, and thereby change the function to be attractive candidate for certain applications. Another interesting example, Infrared emissivity can also be tuned and designed by controlling the nanoparticle shape, as would be explained in the next section.

- **High emissive nanopowder**

The electromagnetic radiation could be partially absorbed, transmitted, or reflected due to the interaction with a matter. The principle of energy conservation combines theses radiation characteristics as follows:

$$\text{Absorption}\,(A) + \text{Transmission}\,(T) + \text{Reflection}\,(R) = 1 \qquad (1.8)$$

For a system which is in a thermodynamic equilibrium at a given temperature $T$ and wavelength $\lambda$, the absorbed energy would be emitted again, such that,

$$\varepsilon(\upsilon, T, \theta) = A(\upsilon, T, \theta) \qquad (1.9)$$

This is the well-known Kirchoff's law of thermal radiation. Here, $\varepsilon$ is the emissivity, $\theta$ is the observer angle and $\nu$ is the frequency. This means that by measuring the absorbance of a body, one can easily calculate the corresponding emissivity. In the case of non-transmitting, uniform and isotropic opaque surfaces which are in thermal equilibrium, the relation among emissivity and reflection can be expressed by[93]:

$$\varepsilon(\upsilon, T, \theta) = A(\upsilon, T, \theta) = 1 - R(\upsilon, T, \theta) \qquad (1.10)$$

That is the case with many opaque objects, where a good emitter is a good absorber of energy and a poor reflector at the same time.

Emissivity ($\varepsilon$) is a term representing the ratio of thermal energy radiated by the material surface to the thermal energy radiated by a black body at the same temperature. The maximum emissivity is considered to be that of a true black body and is taken as unity at its absolute temperature, while any other object could be less than that. Indeed, the black body absorbs all the incident radiation reaching on its surface and simultaneously emits all of its thermal energy with the same spectral pattern.[93] The emissivity can be expressed by the following equation:

$$\varepsilon(T) = \frac{\int_0^{\infty} \varepsilon(\lambda) E_{\lambda} d_{\lambda}}{\sigma T^4} \qquad (1.11)$$

where $\varepsilon$ is the hemispherical emissivity of the grey body, $E$ is the heat radiated by the body to its surroundings, $T$ is the temperature (K), $\sigma$ is the Boltzman constant ($5.67 \times 10^{-8}$ W/(m$^2$×K$^4$)). A real object called the 'grey body' radiates less heat ($\varepsilon$<1) if compared to the true black body ($\varepsilon$=1). For any surface, thermal radiance depends on two parameters: (a) the temperature of the surface, which indicates the thermodynamic equilibrium state between the grey body and its surrounding, (b) the emissivity of the surface, which indicates its efficiency to radiate the energy to the surrounding.

In several high temperature applications, high emissivity coatings are widely used for effective transfer of the heat by radiation,[93-95] for example on the surface of a space vehicle. Due to the hypervelocity flight and acute friction between the vehicle surface and the surrounding atmosphere, the surface temperature exceeds 1000 °C, which can affect the performance and lifetime of the metal thermal protection systems.[96-97] However, the surface temperature can be maintained in a safe limit by coating the surface with high emissivity materials.[93]

## 1.4 Research objectives

In this thesis, a novel, simple, economic, eco-friendly and green strategy is applied for synthesis, design and fabrication of various nanostructures with a controlled size, morphology as well as crystallinity. Moreover, characterization and evaluation of the produced nanostructured materials are done by using different tools such as, SEM, TEM, XRD, UV-Vis-NIR Spectrophotometry for a better understanding of their chemical and structural properties, as well as exploring their potential functional applications.

The dance of water droplets on a hot frying pan is an everyday observation that was first explored scientifically by Leidenfrost in 1756. When a drop of water touches a hot surface whose temperature is much higher than the boiling point of water, the part of the drop which comes in contact with the hot surface vaporizes immediately and the drop levitates on its own vapor film. Using water, Leidenfrost found that the remnant solid was left on the heated surface. In a previous work, Elbahri *et al.* in 2007 demonstrated that this remnant solid takes a form of nanoclusters, wires or rings in case a small Leidenfrost drop is loaded with a precursor.[63,98] At that time, the observations raised many inquiries about the mechanism and the origin of the nanoparticles synthesis. In the last couple of years, we have intensively studied the phenomenon trying to give our interpretation for the mechanism of the chemistry inside the Leidenfrost reactor. The main aims of this dissertation can be concluded in the answer of the following questions.

1. What is the role of water in the synthesis?
2. Where and how are the nanostructures formed?
3. What is the effect of the precursor concentration and pH on the Leidenfrost chemistry?
4. Can Leidenfrost chemical reactor be used to create nanoscale coatings on complex objects and to design a 3D nanoporous metal?
5. What are the potential applications of the fabricated nanostructures?
6. Is it possible to upscale this method to produce metal oxide nanopowder with different morphology?

## 1.5 Thesis composition

This dissertation is composed of five chapters. It starts with an introduction and scientific background in Chapter 1. Chapter 2 presents the experimental details of the work. The Chapter 3 is based on an article published on the subject by the author of this thesis. The

article has been already published in Nature Communication[43] among other scientific and public journals[99] and entitled: "Green chemistry and nanofabrication in a levitated Leidenfrost drop". Moreover, the related materials (movies and supplementary documents) are also included.[43] Chapter 4 presents the metal oxide nanopowders production through Leidenfrost reactor and their infrared emissivity. This thesis ends in chapter 5 where conclusion and outlook is given.

# Chapter 2

# Experimental section

## 2.1 Materials

In the following table the materials and chemicals that are used in this thesis, are listed.

***Table 2.1: Materials and chemicals***

| Chemical name | Company | Purity |
|---|---|---|
| Zinc acetate | Sigma Aldrich | 99.99 % |
| Copper (I) acetate | Sigma Aldrich | 99.99 % |
| Copper (II) acetate | Sigma Aldrich | 99.99 % |
| Gold (III) chloride hydrate | Sigma Aldrich | 99.99 % |
| Syringaldazine | Sigma Aldrich | 99 % |
| Deionized water | Clean Room Kiel | For analysis |
| Ammonium Hydroxide | Sigma Aldrich | 28.0 - 30.0 % NH3 basis |
| Sodium hydroxide | Sigma Aldrich | ≥ 98 % |

In this work, silicon substrates are used as purchased from 'Si-Mat'. Silicon and glass substrates of different sizes used for deposition of nanostructures are bath sonicated in isopropanol (5 min) and water (5 min), and air dried.

## 2.2 Nanofabrication by Leidenfrost drop

The set up and methods used in this section of nanosynthesis are mentioned in details in Chapter 3.

### 2.2.1 Nanopowder synthesis by Leidenfrost puddle

The materials (**Table 2.1**) used for nanopowder synthesis includes a precursor in aqueous solution of the desired material, a hotplate at Leidenfrost temperature (~ 300 °C), and 50 mL burette.


***Figure 2.1: (a) hot plate used for nanopowder synthesis by using levitated Leidenfrost puddle on heated aluminum substrate, the solution is introduced to the hotplate by using the (b) 50 mL burette.***

A glass burette was filled with a 50 mL of 10 mM zinc acetate aqueous solution and placed at a distance of ~ 0.6 cm from a preheated (300 °C) aluminum substrate. The feed rate of the solution from the burette was adjusted by the valve to 1 mL/25 Sec. The nanopowders produced out of the Leidenfrost puddle were centrifuged, washed with $dH_2O$ two times and deposited on a glass substrate by drop casting for IR emissivity. Sample for SEM characterization were produced by simply dipping a piece of silicon wafer into the solution of nanoparticle. A copper grid which was dipped in the nanoparticles solution was used for investigation of ZnO nanoparticles by TEM. The IR emissivity samples were prepared by drop casting the colloidal suspensions of ZnO nanoparticles, which were subsequently dried in ambient atmosphere. These samples were then compared with ZnO (spherical nanoparticles) from Sigma-Aldrich, as well as, with a commercially available, high efficiency black coating for infrared emissivity. The latter was supplied by 'Senotherm' (no. 17-1644-702.338).

## 2.3 Characterization techniques

### 2.3.1 Scanning Electron Microscopy (SEM)

SEM is used to image the conductive material surfaces through a highly focused and energetic electron beam. Once the beam hits the sample surface, it generates signals routed from the surface-electron interaction, thus providing a high depth of focus when compared to light microcopy, such as a large amount of the sample could be focused at a time, since the primary electrons are accelerated at voltages ranging from 2 to 30 KV.

The primary electron beam is emitted either by thermionic emission or field electron emission. In case of thermionic emission, a cathode is heated up to a high temperature allowing the electrons to overcome the energy barrier of the material work function, leaving thus the cathode, and accelerated towards the anode by a potential difference $U_o$. When the emitted electrons traverse the condenser lens, they will be subjected to the Lorentz force making them move in a radial helical movement. Therefore, the condenser and the probe forming lenses focus and collect the electron beam. Then, the resulting beam will be scanned over the sample through the deflection coils. Imaging could be performed either with secondary electrons (SE) or backscattered electrons (BSE). When the primary electrons interact with the specimen, there will be either elastic or inelastic collisions. Elastic collisions between the primary electrons and the positive nucleus lead to backscattering of electrons because of the strong Coulomb repulsion. The BSE has enough energy (higher than 50 eV), allowing depth profiling of the sample surface.[100] On the other hand, a multitude of inelastic collisions between the primary electrons and electrons of the specimen lead to emission of SE with the lowest kinetic energy. SE can only come from surface layers, while BSE can escape from deeper levels of the specimen.

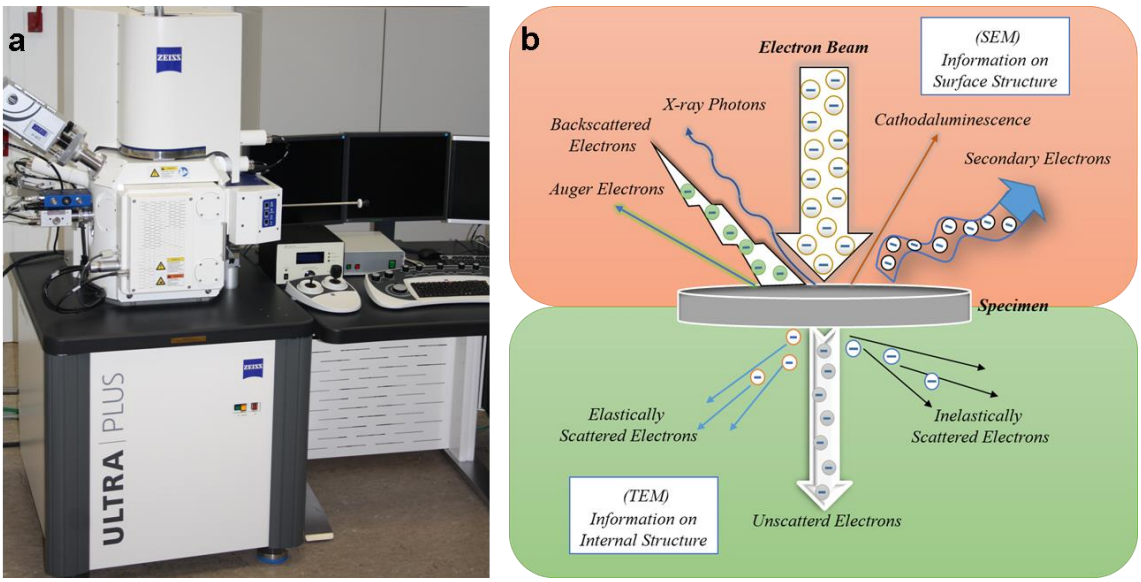


***Figure 2.2: (a) Image of Field Emission SEM, ZEISS ULTRA plus connected with Oxford Instruments INCA-X-act EDS. (b) Diagram of the interaction between electrons and matter.***

There are other types of signals produced from the interaction between the primary electron beam and the specimen such as Auger electrons, characteristic X-rays and cathodoluminescence. When the primary electron displaces an electron from an inner atomic shell by collision, a vacancy in that electron shell is produced. In order to re-establish the proper

balance in the orbitals, an electron from outer shell of the atom fills the vacancy. The difference between the higher energy shell and the low-energy shell in energy could be released in the form of X-rays. These characteristic X-rays are usually used for energy-dispersive X-ray analysis (EDX). This analysis can be used to perform simultaneous, nondestructive and specific elemental analysis along a specific line with a resolution down to10 nm. The SEM images of the nanofabricated structures in this thesis are performed by using Phillips XL 30 and Field Emission SEM ZEISS ULTRA connected with Oxford Instruments INCA-X-act EDS (**Figure 2.2**).

### 2.3.2 X-Ray Diffraction (XRD)

The XRD measurements were carried out by a Seifert XRD 3000 and PTS XRD 3000TT (**Figure 2.3a**). XRD is a non-destructive analysis method which is generally used to investigate the crystallographic structure, as well as the chemical composition of solid materials. When an incident X-ray beam, with energy ranging from 120 eV to 120 keV, interacts with the solid, it would be diffracted or reflected by the atomic lattice planes (Bragg´s law), which act as mirror planes, quasi- transparent and reflective. A diffraction pattern is produced if the reflection at these lattice planes is constructive and in phase when the difference in the path length equals to an integer multiple of the wavelength λ, in accordance with the Bragg´s law[101] (**Figure 2.3b**):

$$n\lambda = 2d \sin\theta \qquad (2.1)$$

Where $n$ is the order of the diffraction peak, $\theta$ is the incident angle of the beam, λ is the wavelength of the incident X-ray, and $d$ is the spacing between the atom planes, which in the case of a cubic crystal can be calculated by the following equation:

$$\frac{1}{d^2} = \frac{(h^2 + k^2 + l^2)}{a^2} \qquad (2.2)$$

$h$, $k$, and $l$ are the Miller indices, and $a$ is the lattice parameter. Generally, the **Equations 2.1** and **2.2** could predict all possible lattice planes for a specific wavelength and Bragg angle.

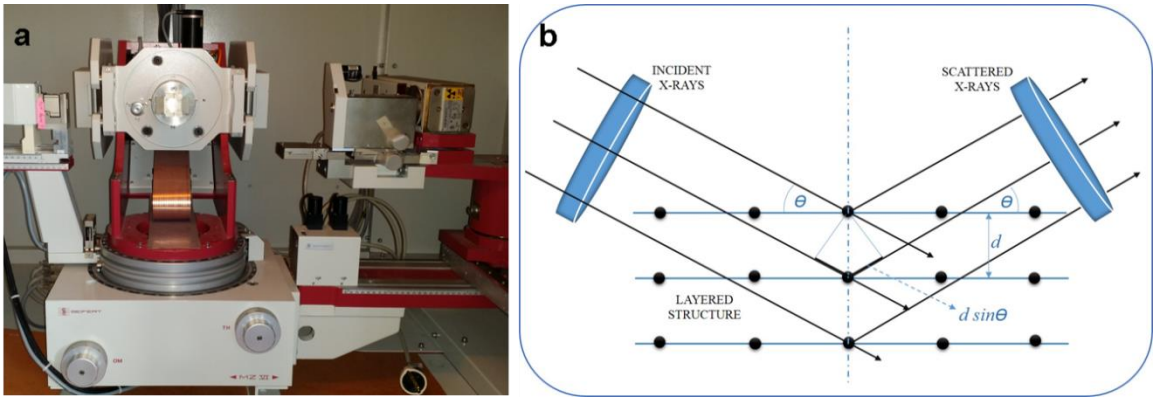


***Figure 2.3: (a) Image of X-ray diffractometer components from RICH. SEIFERT & Co GmbH (XRD 3000TT). (b)* Diagram for x-ray diffraction of Bragg equation.**

XRD is a highly versatile method providing a deep penetration depth and a good resolution because of the high energy X-ray beam produced either by the classical X-ray cathode tube (Bremmstrahlung giving a continuous spectrum), or the characteristic X-rays giving a line spectrum, or the synchrotron radiation.[100] To determine the crystallite size, the Scherrer formula is mostly used:

$$D = \frac{K\lambda}{\beta \cos\theta} \qquad (2.3)$$

where $D$ is the mean size of the ordered (crystalline) domains, $K$ is Scherrer constant of the order of unity for usual crystals, $\beta$ is the full width at half maximum (FWHM), and $\theta$ is the Bragg angle.

### 2.3.3 UV-Visible Spectroscopy (UV-Vis)

The UV-Vis spectrometer, Lambda 900 from Perkin Elmer **(Figure 2.4a**), was used for optical characterization. Aluminum mirror was used as a standard for the reflectance measurement. For solution, a standard cuvette was utilized as holder.

UV-Vis is a spectroscopic characterization technique based on absorption or fluorescence of photons, providing the measurement of parameters such as, absorption, transmission, extinction, reflection, in the UV, visible, and near infrared spectral range. The highly energetic photons in the UV or visible range of the electromagnetic radiation disturb the electronic distribution in the molecule, leading to the excitation of an electron from the ground electronic state to an excited state. Recording a portion of the UV-Vis spectrum introduces the characterization of the optical and electronic properties of a wide variety of materials, including molecules, metal-dielectric nanocomposites, organic matrices, etc. Briefly, the UV-Vis spectroscopy is based on measuring the attenuation of the incident beam of light when it hits

and penetrates the sample or when reflected from the sample surface (based on the Beer-Lambert law).

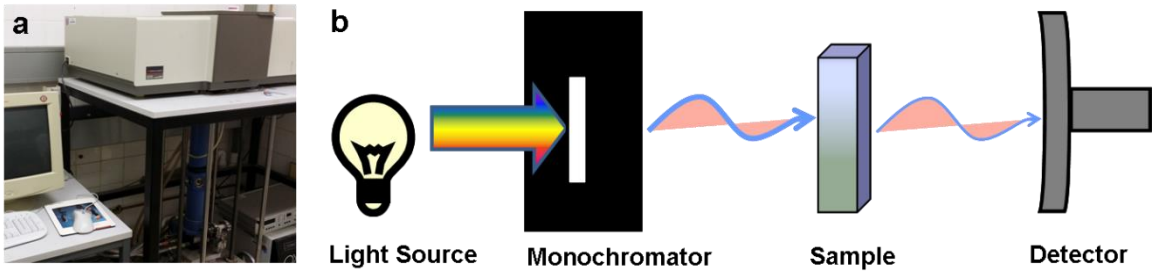


***Figure 2.4: (a) Image of the UV-Vis spectrometer Lambda 900 from PerkinElmer. (b) Illustration of a single beam UV-Vis measurement setup.***

A light beam from a visible (Tungsten Iodide) and/or UV (Deuterium) light source is separated into its component wavelengths by a diffraction grating or a prism. By a half-mirrored device, each monochromatic beam splits into two equal intensity beams. The reference beam (colored blue, **Figure 2.4b**) penetrates an identical cuvette containing only the reference specimen. The other beam is the sample beam (colored magenta) that passes through a small transparent cuvette containing the material being investigated (**Figure 2.4b**). These light beams intensities are collected and analyzed by electronic detectors. The light beam absorbance is given by:

$$\text{Absorbance} \quad A = \ln \frac{I_o}{I} \tag{2.4}$$

Where $I$ is the intensity of the light after passing through the sample, $I_o$ before passing through the sample. The ratio $I/I_o$ taken in percent is named transmittance (%$T$).

### 2.3.4 Infrared camera

Infrared thermography is an imaging technique used to receive infrared radiation (electromagnetic spectrum from 9 to 14 µm) emitted from object and converted it into temperature and hence provides an image of temperature profile. Because the quantity of radiation emitted from an object increases with temperature allows one to see the variations in temperature. The produced image out of the radiation is called thermogram. With thermography, there is possibility to see an object even in darkness. According to Kirchoff's law[102-103]as discussed before:

$$Emitted\ Energy\ (E) + Transmitted\ Energy\ (T) + Reflected\ Energy\ (R) = 1 \qquad (2.5)$$

In the most cases E+R=1 and that means, a good emitter equals poor reflector and vice versa. In other words, a good emitter is a good absorber of energy.

Emissivity (ε) is a term representing the relative ability of the material surface to emit thermal radiation. Different materials show different emissivities and it is not easy to determine the exact emissivity of an object. The emissivity of materials can vary from 0.00 (non-emissive) to 1.00 (perfect emissive). It changes with temperature. As example for complete emitting, the emissivity of the true black body equals one while emissivity of any other object is less than one.[104] Silver is a perfect example for a substance with low emissivity. Its emissivity coefficient is 0.02. An example of a substance with high emissivity would be asphalt, with an emissivity coefficient of 0.98.

In general, metals (highly polished surfaces) display low emissivity values if compared to roughened and nonmetals which tend to display higher values. Nowadays, IR thermography has wide variety of potential applications in numerous activities[102] such as: building and constructions, electronics, mechanical services, astronomy (telescope), military and police surveillance, renewable energy, medical testing for diagnosis, non-destructive testing, effluent pollution detection, research and development of new materials, etc. In this work, IR camera (**Figure 2.5**) is used for thermographic analysis of the levitated drop and the fabricated nanopowder, in addition to IR emissivity measurements of different nanoparticle morphologies.

***Figure 2.5: Image of IR camera from InfraTec PIR uc 180 with a rate of 24 Hz and a spatial resolution of 40 lm/IR pixel.***

## 2.3.5 Transmission Electron Microscope (TEM)

TEM is one of the most useful tools for nanoparticle characterization since it can provide images with a resolution of 0.1 nm (magnification factor $10^6$) and supply more information about the size and morphology of the nanostructure. In addition, the crystallinity of the specimens can easily investigated by making diffraction pattern. In this technique, the high energy electrons (50-200 keV in a vacuum around $10^{-6}$ mmHg) are transmitted through an ultra-thin sample. Due to the interaction between the transmitted electrons and the atoms of the sample **(Figure 2.2b)**, the image can be magnified and focused to form a bright-field imaging of the internal structure of the specimen on a screen or a film. The major components of TEM are shown in **Figure 2.6**.

In this work, TEM measurements were carried out using an FEI/Philips Tecnai F30 G2 TEM (FEG cathode, 300 kV, $C_s$=1.2 mm) equipped with EDX detector and Gatan imaging filter, and with a Philips CM 30ST microscope ($LaB_6$ cathode, 300 kV, $C_s$=1.15 mm). The measurements were done in the Group of Synthesis and Real Structure of Solids, faculty of engineering, Kiel.

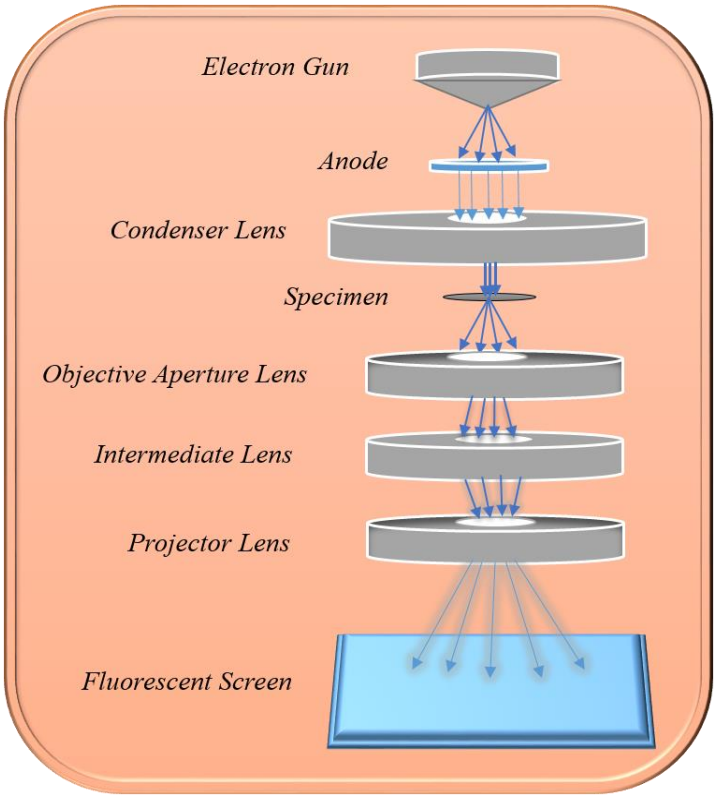


***Figure 2.6: Diagram of the basic structure of a TEM.***

# Chapter 3

# Green chemistry and nanofabrication in a levitated Leidenfrost drop

**Ramzy Abdelaziz**, Duygu Disci-Zayed, Mehdi Keshavarz Hedayati, Jan-Hendrik Pöhls, Ahnaf Usman Zillohu, Burak Erkartal, Venkata Sai Kiran Chakravadhanula, Viola Duppel, Lorenz Kienle& Mady Elbahri

Published in **Nature Communications 2013**, 4, doi:10.1038/ncomms3400.

## 3.1 Abstract

Green nanotechnology focuses on the development of new and sustainable methods of creating nanoparticles, their localized assembly and integration into useful systems and devices in a cost-effective, simple and eco-friendly manner. Here we present our experimental findings on the use of the Leidenfrost drop as an overheated and charged green chemical reactor. Employing a droplet of aqueous solution on hot substrates, this method is capable of fabricating nanoparticles, creating nanoscale coatings on complex objects and designing porous metal in suspension and foam form, all in a levitated Leidenfrost drop. As examples of the potential applications of the Leidenfrost drop, fabrication of nanoporous black gold as a plasmonic wideband superabsorber, and synthesis of superhydrophilic and thermal resistive metal–polymer hybrid foams are demonstrated. We believe that the presented nanofabrication method may be a promising strategy towards the sustainable production of functional nanomaterials.

## 3.2 Introduction

Sprinkling a drop of water onto a hot skillet is an everyday event that was first investigated by Leidenfrost.[41] When a water drop touches a hot plate whose temperature is much higher than the boiling point of water, the part of the drop which comes in contact with the hot surface vaporizes immediately and the drop levitates on its own vapors. Using water, Leidenfrost[41] found remnant solid was left on the heated surface. In our previous work, we found that this remnant solid has the form of nanoparticulate wires and rings left by a small drop loaded with a precursor, mobilized by the Leidenfrost effect.[63,98] Starting with the Leidenfrost temperature itself, which has been described by a large number of terms, including minimum film boiling, rewetting temperature, quenching temperature and others, a wide variety of investigations have been performed to explore the Leidenfrost phenomenon. The physical picture emerging from these investigations suggests that fast vaporization and expansion of the superheated part of the layer adjacent to the hot substrate provide the driving force for the observed phenomenon. It is worth noting that the Leidenfrost temperature is not a unique property of the liquid and might be changed by the properties of the surface, for example, surface roughness and wettability.[105-106]

In our previous work[98] we postulated the existence of an overheated state in the Leidenfrost droplet, which has been utilized as a chemical reactor. For example, water droplets containing dissolved zinc acetate or silver nitrate yielded zinc oxide and metallic silver nanoclusters respectively. These observations raised many questions about the phenomenon

and the origins of the nanoparticles formation. For instance, we could not prove where and how the particles were formed, nor could we explore the role of water in the synthesis.

Here we show our progress with the Leidenfrost phenomenon; trying to answer those questions, establishing the first steps towards the understanding of the 257-year-old phenomenon, demonstrating a green chemistry lab inside the levitated droplet and simultaneously implementing it in the design of functional materials. For instance, we report experimental proof of the electrostatic nature of the Leidenfrost droplet and its implementation as an overheated and charged chemical reactor inside a levitated droplet. The fabrication of nanomaterials, creation of nanoscale coatings and design of plasmonic porous metal and hybrid foam could all be realized in a levitated Leidenfrost drop.

## 3.3 Results

### 3.3.1 Thermal gradient and overheated zone in the Leidenfrost drop

With sufficiently brief contact between the cold droplet and the hot surface, impulse heating of the contact layer occurs, which leads to superheating of this layer. Following a brief incubation period, fast evaporation and expansion of the vaporized molecules near the surface forces the outer water layers to move away, resulting in the levitation of the droplet, as shown in **Figure 3.1a-c**. This method was used to determine the Leidenfrost temperature on various substrates in our experiments, including aluminum, silicon oxide and commercial silicon.

In all of our experiments, the Leidenfrost state was observed at a temperature above 230 °C, which is approximately the same as the temperature required for homogenous phase transitions of water at 1 atm.[107] At temperatures lower than that, the stable state in the Leidenfrost phenomenon was not observed.

Although the vapor layer underneath the droplet is heated by various mechanisms,[108] including induced convection to a mean temperature approximately equal to the heated substrate, the temperature of the droplet is generally assumed to be approximately at the boiling point of water, that is, 100 °C.[105] As the thermal conductivity of water is sufficiently low, and owing to the expected evaporative cooling of the levitated droplet, a temperature gradient in the droplet should be established with an overheated region at the liquid–vapor interface, a task that has not been proved so far.

Although an exact temperature determination at a multiphase interface is always a difficult task,[109] we determined a temperature gradient in a single droplet by using an infrared

thermography camera (see **Supplementary Figure S1**) as a non-contact temperature measurement tool, capable of detecting radiation in the far-infrared range.

Indeed, a vertical and horizontal temperature gradient is found inside the drop and the drop maintains a global evaporation as predicted,[110] and now ascertained by our measurement. Although the skin of the drop is much colder than the interior, the interface of the levitated drop bears an overheated zone as we postulated, which points to the existence of the two-phase regions (liquid/vapor). It should be borne in mind that there is no sharp partition at the interface between the superheated vapor/hot liquid underneath the Leidenfrost droplet, rather both regions are joined by what we called 'overheated zone', whose boundaries and temperature, which could even exceed 100 °C, are still unknown and have to be determined. Indeed, a recent report on the Leidenfrost phenomenon[111] shows that the vapor layer under a Leidenfrost drop is not uniform, which further supports our finding. There is a significant temperature difference between the base (warm) and the top surface (cool) of the levitated drop, indicating a possible thermoelectric effect and, hence, a charge separation event.[112]

### 3.3.2 Charge chemistry and green chemistry in a Leidenfrost drop

Water, which undergoes a fast phase expansion, shows different characteristics, including enhanced self-ionization and charge separation, which has been shown by Volta and George[113], and further studied by Faraday[114] and Lenard.[115] Further investigations[116-119] revealed the generation of a positively charged steam under the conditions of rapid evaporation. Although the level of understanding for the charge separation phenomenon is insufficient for its quantitative description,[120] our interest, here, is to show whether this effect appears with the Leidenfrost drop. For that purpose, a metal tungsten tip was connected to a grounded electrometer and the aluminum metal surface was preheated to 250 °C. The aluminum surface was isolated from the grounded hot plate with an insulator ceramic. The tip was placed at a distance of 300 μm from the hot surface. As shown in **Figure 3.1d** (**Supplementary Movie 1**), the Leidenfrost drop was negatively charged during the levitation. It is worth mentioning that no charges were registered with a deionized water drop at room temperature or even at boiling temperature. Two sets of experiments on an insulated preheated ceramic were carried out to eliminate any effect from the substrate and to differentiate between the charges inside the drop and vapor. The tip was set above the drop to register only the charge of the vapor phase, which resulted in only positive charges; their magnitude increased each time when a new droplet was added (**Supplementary Movie 2**). However, on placing the tip at a distance

of 1 mm from the preheated, insulated ceramic and applying small droplets of deionized water (that is, the tip enters the levitated droplet at the upper part), only negative charges were registered (**Supplementary Movie 3**).

To optimize the accuracy of the measurement, that is, to prevent the access to air or impurities, also to avoid charge leakage, the measurement of the levitated droplet was repeated in a closed lab-built apparatus controlled by the National Instruments LabView software (**Figure 3.1e**). For the charge measurement, the tip was placed at distance of 300 μm from the hot surface and a drop was injected to the hot aluminum surface, that is, $T$=250 °C. When a drop of deionized water falls on the preheated surface, it undergoes a fast evaporation followed by levitation as explained previously and showed in **Figure 3.1a-c**. In this process, charges separate during the fast evaporation. As shown in **Figure 3.1f**, transitory positive charges were registered at the beginning, followed by permanent increasing of negative charges during the levitation until the charge curves reached a negative saturated value.

Indeed, no charges were registered during the initial period, which correspond to the first contact between the cold droplet and the hot surface, indicating that the fast evaporation and steam generation caused by the fast rupture of the layer adjacent to the hot substrate are essential for the charge separation process as demonstrated by Lenard,[115] and Gilbert and Shaw.[120] Furthermore, the charge generation under the Leidenfrost condition was enhanced by an order of magnitude when a salt solution droplet was used (see **Figure 3.1f**). It already confirmed that ions at high salt concentrations can destroy the natural hydrogen-bonded network of water and thus enhance the self-ionization similar to increased temperature or pressure.[121] This effect is governed at the overheated interface by the fast phase expansion. Here the water density and the solubility of ions are considerably reduced, thus giving rise to a local increase of the ion concentration. Hence, self-ionization and, subsequently, the charge separation of the water are enhanced.

Our proof-of-concept experiments indicated that overheating, thermal gradients and charge separation are generic under Leidenfrost conditions. Although we explored the electrostatic nature of the levitated droplet, our findings are also important to enhance our comprehension of not yet fully understood phenomena of the Leidenfrost dynamics, such as deformation, vibration, internal circulation, oscillation and rotation inside the Leidenfrost drop. However, here we restrict ourselves to explore the phenomena solely for nanochemistry.

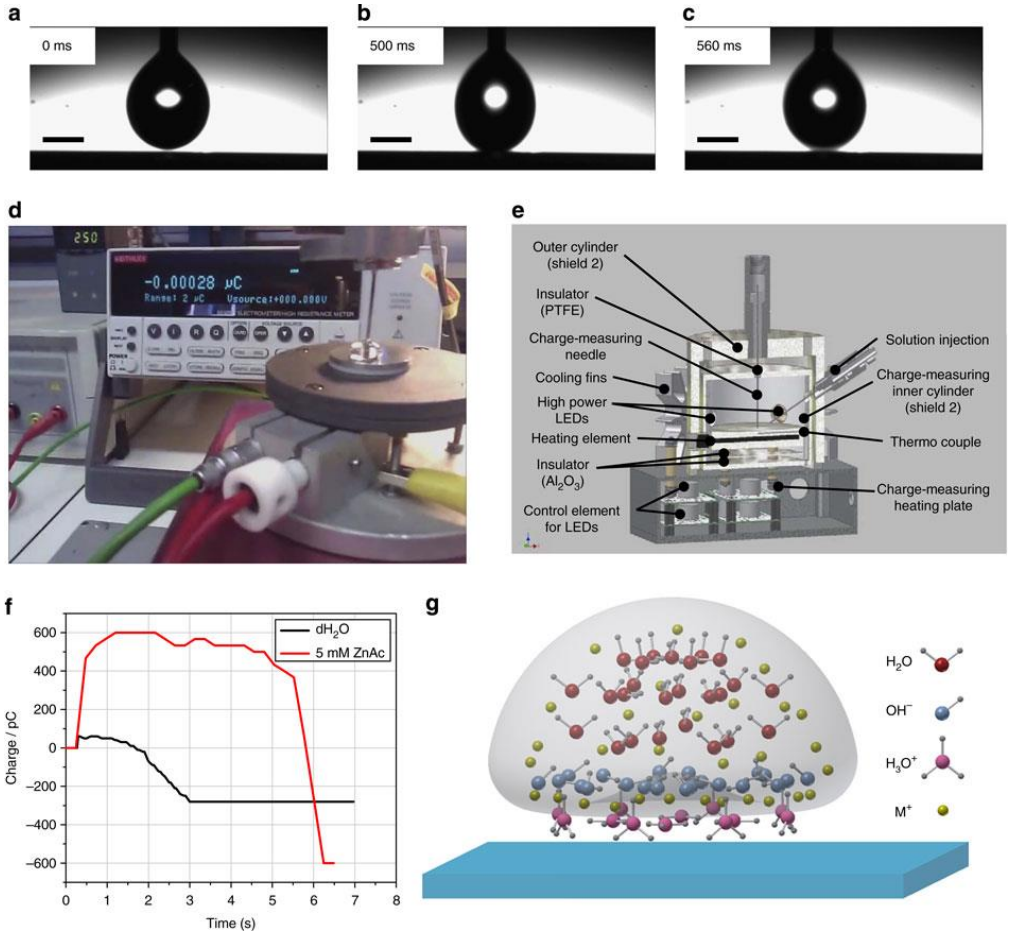


***Figure 3.1: Levitation and charge separation at Leidenfrost temperature. Steps of producing the vapor cushion (Leidenfrost effect) with a drop of water held by a needle and placed on a hot aluminum plate illustrate the approaching of the droplet to the preheated surface (a) and show a time frame of the incubation state (b), and the levitation state (c). (a–c) Scale bar, 1 mm. (d) Foreground: water drop levitating on the hot surface with the needle immersed in it, background: charge measurement output panel showing negative charge measured in the drop. (e) Lab-built set-up of the closed apparatus used for accurate measurements of the charge generation under Leidenfrost condition. Charge can be measured at the top, the bottom and on the walls of the inner cylinder. The device is controlled by the software 'National Instruments LabView'. (f) Charge curves of deionized water and 5 mM zinc acetate solution measured inside the droplet show at the initial contact no charge, followed by an increase of positive charge and finally a slow continuous increase of negative charge, whereas zinc acetate enhanced the charge separation. (g) 3D sketch of the postulated mechanism for green nanochemistry with a Leidenfrost drop: fast evaporation generates an overheated zone, which along with the self-ionization of water at the liquid-vapor interface gives rise to a local increase in metal ($M^+$) and hydroxyl ($OH^-$) ion concentrations. The increase in hydroxyl ion concentration is attributed to loss of the hydronium ions ($H_3O^+$) to the vapors; hence the basic condition is satisfied.***

For instance, the difference in measured charges in the droplet and vapor under the Leidenfrost condition manifest the earlier finding[113-115,117-119] of the charge separation and shows its occurrence with the Leidenfrost droplet. Accordingly, we postulate that the fast

evaporation and charge separation at the hot interface would serve to concentrate the precursor salt and in the same vicinity create local basic pH conditions owing to the counter hydroxide ion left behind after the loss of the hydronium ion to the vapors. The hydroxide ion would not only lead to the basic conditions required for a wide variety of nanoparticle formation[122-124] but it could also play a role as a reducing agent,[125-126] for instance, by discharging. Thus, a favorable environment for a cost-effective, efficient and green nanochemical reactor is created, as depicted in **Figure 3.1g**.

Faraday[127] was fascinated by the red color of gold nanoparticles, which were synthesized by chemical reduction of a suitable gold precursor, such as $AuCl_4^-$ ions with white phosphorus. Here we introduce the first experimental evidence of Leidenfrost chemical reactor that enables nanoparticle synthesis in a levitating drop without any additional reducing agent or sophisticated technique. For instance, a 2-ml drop of 10 mM aqueous Tetrachloroauric (III) acid solution (pH ~ 2.3) was gently placed on a preheated hot plate, which was maintained at a temperature of 270 °C. A naked eye observation of a levitating drop of gold salts that converted to plasmonic red coloured gold nanoparticles is shown in **Figure 3.2a** (**Supplementary Movie 4**). At this stage, the drop was transferred to a commercial Lacey C/Cu grid, rinsed with hot water and subsequently dried in air for transmission electron microscopy (TEM) analysis, which revealed that the plasmonic colour arose from the formation of gold nanoparticles. **Figure 3.2b** depicts a bright-field TEM image recorded on the sample, which contains randomly oriented Au nanoparticles as proven by electron diffraction (not shown, the measured *d*-values are consistent with those from the literature).[128] The histogram (**Figure 3.2c**) depicts a narrow particle size distribution with an average diameter of ~ 4 nm. Occasionally, a few bigger nanoparticles were observed (**Supplementary Figure S2**). In addition, the high-resolution TEM images and fast Fourier transformation analysis reconfirms the presence of pure Au (**Figure 3.2d**). The fast Fourier transformation pattern (**Figure 3.2d, inset**) of the square region containing a single Au nanoparticle (*cf*. mark in **Figure 3.2d**) consists of the one expected for zone axis [110]. Scanning TEM–energy-dispersive X-ray (EDX) elemental maps (not shown) recorded on a similar region further support the presence of pure Au nanoparticles. When the experiment with the same reaction composition and conditions was carried out at lower temperature than the Leidenfrost (**Supplementary Figure S3**) or even in a conventional way (using oil bath at 100 °C), no nanoparticles were observed.

Undoubtedly, our results prove that water under Leidenfrost conditions participates in and/or catalyses the chemical reaction, which is also supported analytically (**Supplementary Note 1** and **Supplementary Figure S4**). Once the first clusters are formed, an autocatalytic

pathway could set in where further ions are adsorbed and reduced on the surface of the metal clusters.[129] Nevertheless, our postulation needs further investigations to explore the exact mechanism of the nanosynthesis.

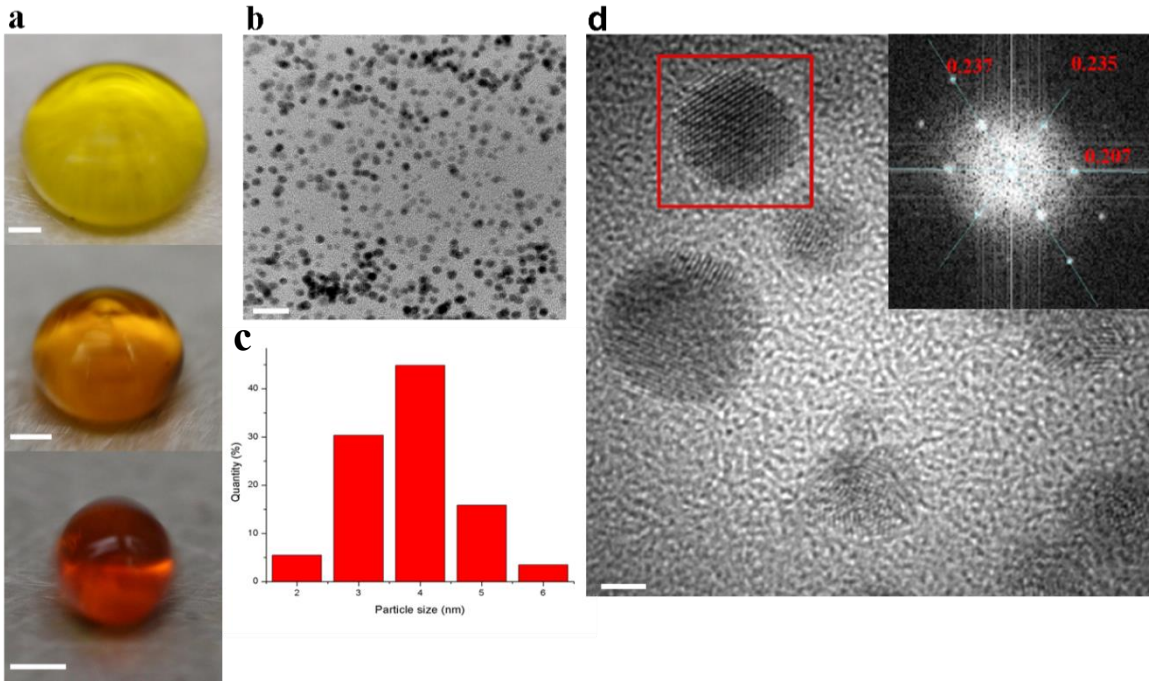


***Figure 3.2: Plasmonic gold nanoparticles using a levitating drop reactor. (a) Gold salts were converted to gold nanoparticles in a levitating drop without additional reducing agent and the drop slowly shrinks from a yellow plate-like disk into a red spherical droplet. Scale bar, 2 mm. (b) Bright field, TEM image recorded on the Au nanoparticles, scale bar, 20 nm and (c) particle-size distribution . (d) High resolution transmission electron microscopy micrograph with inserted Fast Fourier Transformation pattern from marked region showing a single crystalline pattern along the zone axis [110]. Scale bar, 2 nm.***

### 3.3.3 Nanosynthesis and three-dimensional coating in a Leidenfrost reactor

The levitated chemical reactor suggested here can be used to fabricate metal oxide in the same manner. However, the technique is revolutionized when synthesis and coating occur simultaneously. One-pot synthesis and simultaneous coating of 3D objects is still a challenge for the bottom-up technique and is often a problematic task for nanofabrication in general.[130]

Here, we introduce a levitated and rotating drop reactor for one-step synthesis and coating of a 3D object, e.g. TEM grid. As a demonstration, a 300 µl drop of 20 mM zinc acetate precursor solution (pH ~ 6.3) was placed on a TEM grid that was resting on a preheated (250°C) hotplate. **Figure 3.3a** illustrates the drop levitation along with the TEM grid (**Supplementary Movie 5**).

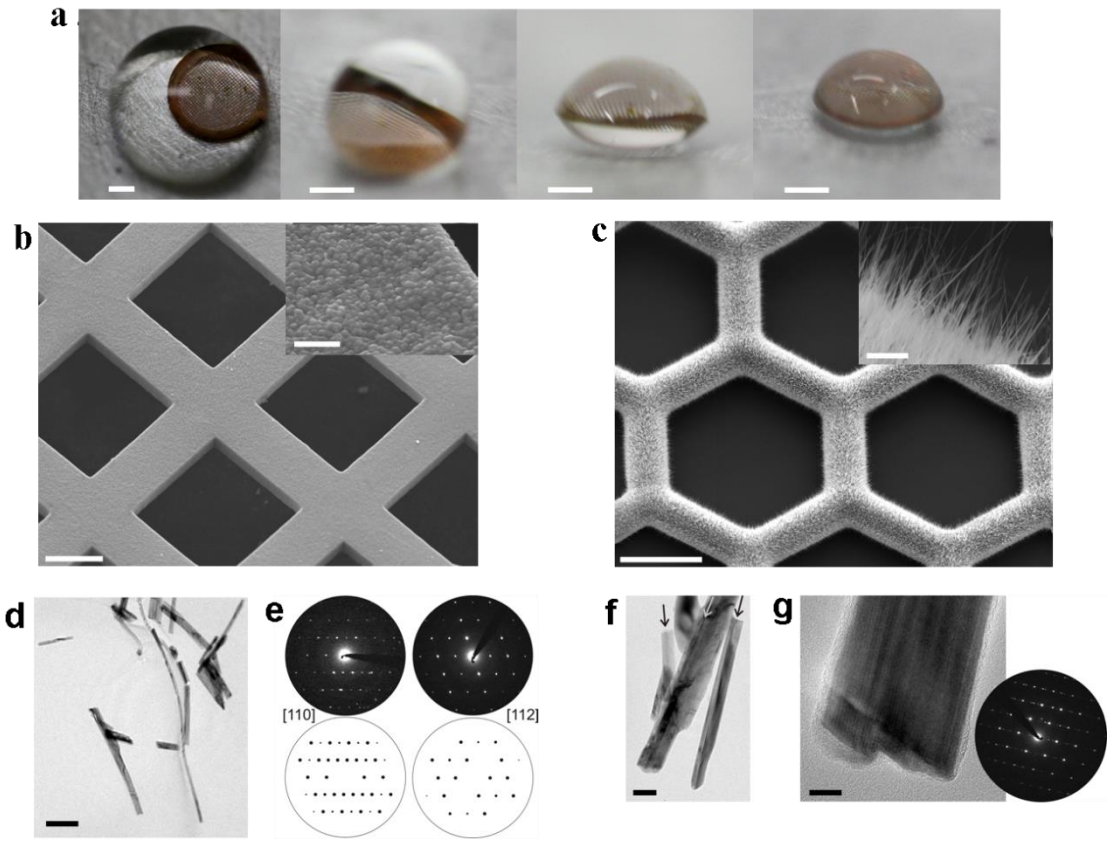


***Figure 3.3: Uniform 3D coating of a complex object with ZnO nanoparticles and CuO nanorods. (a) TEM grid coated through Leidenfrost technique. TEM grid is completely covered by a levitating drop during the 3D coating process. Scale bar, 1 mm. (b) Scanning electron microscopy image of a TEM grid coated with (b) ZnO nanoparticles and (c) CuO nanorods. Inset shows the higher magnification of the coating. Scale bar of the image in b and c, 20 µm and 100 µm, respectively. Scale bar of the inset in b and c, 2 µm. (d) Bright-field image of several CuO nanorods. Scale bar, 200 nm. (e) Precession electron diffraction (PED) and selected area electron diffraction (SAED) patterns recorded on single nanorods with simulated patterns (based on the kinematic approximation). (f) Twinned nanorods with longitudinal twin boundaries, cf. arrows. Scale bar, 50 nm. (g) High-resolution micrograph of a twinned nanorod and SAED pattern. The rotation of the SAED pattern was adjusted according to the Fourier transform of the high-resolution micrograph, zone axis [011]. Scale bar, 10 nm.***

**Figure 3.3b** depicts a scanning electron microscopy (SEM) micrograph of the TEM grid which has been coated three dimensionally with ZnO nanoparticles demonstrating a single one-pot synthesis and coating in a sterile and contamination-free environment using the Leidenfrost technique. EDX analysis at different regions of the sample (**Supplementary Figure S5**) showed that the chemical composition and the intensity ratio—which is very sensitive to any marginal change of the film thickness—are similar in different areas. Thicker coating with ZnO nanoparticles on other grid forms is also possible by increasing the

concentration of the precursor (for example, 40 mM, pH ~ 6.2), (**Supplementary Figure S6a**) or by multiple-steps coating (**Supplementary Note 2** and **Supplementary Figure S6b–f**).

Nanostructured coating of different materials in a rapid, cost-effective manner is routine by using this process. When copper acetate (~ 250 μl, 10 mM, pH ~ 5.5) aqueous solution was used, CuO nanorods were fabricated (**Figure 3.3c**). The number density, length and width of the rods can be manipulated by further heating (heated to 400 °C for 2 h) to produce CuO nanograss with micrometre length and a width in the range of tens of nanometres covering the surface (**Supplementary Figure S6g**). EDX nanoprobe analyses confirmed the presence of Cu and O as the constituting chemical elements of the nanorods. Quantification of the EDX data recorded on several rods was consistent with an equimolar ratio of Cu and O within the experimental errors. The bright-field TEM image (**Figure 3.3d**) shows several nanorods with high aspect ratios, including strongly bent species. The attached experimental and simulated diffraction patterns (**Figure 3.3e**) recorded on single nanorods confirmed the assignment of the structure to the Tenorite-type[131] for the two zone axis (ZA) orientations [110] and [112], respectively. In the case of ZA [110], the precession electron diffraction mode was applied; thus, the dynamical scattering effects were considerably minimized. Many of the analysed crystals contained characteristic twins as recently described for CuO nanowires.[132-133] Twinning is indicated by longitudinal stripes in bright-field contrast microscopy (**Figure 3.3f**), with boundaries running parallel to the (111) layer of the Tenorite-type structure. The twinning produces additional weak intensities between the high-intensity fundamental reflections (**Figure 3.3g**, inset shows the selected area electron diffraction pattern in the ZA [011]) by multiple scattering. Such phenomenon originates from a partial superposition of the twinned domains, and in this case the high-resolution contrasts exhibit clear modulation stripes as can be seen from **Figure 3.3g**.

The Leidenfrost dynamics (for example, large circulation current (**Supplementary Movie 5**)) and the stability of the loaded drop are crucial for a homogenous coating of the object. On the other hand, there are a number of experimental parameters and challenges, which influence the quality of the final structure such as surface roughness, wettability of the hot plate and the substrate to be coated, the geometric parameters of the substrate to be coated (for example, pinning by heterogeneity and defects). In addition, depending on the stability of the droplet, its rotation, deformation, vibration and oscillation, the final product will differ significantly and, consequently, the coating might face lack of uniformity. Moreover, probable sliding of the drop off the plate, the unbalanced substrate and other instability forms (that is,

by bubble generation) could also ruin the feature of final structure (**Supplementary Figure S7**).

### 3.3.4 Plasmonic nanoporous metal in a Leidenfrost pool

Novel fabrication method of nanoparticles, their assembly and integration into practical devices are the main issues in the nanochemistry field. Nanoporous metal as a class of materials with a complex structure and wide variety of potential applications (see review by Bryce *et al*.[86]), along with being outstanding candidates of plasmonic meta-materials with optical response determined by material constituents and porosity,[87] are difficult to be fabricated with traditional nanochemistry techniques.[86]

Although top-down fabrication approaches, such as chemical etching and templating, are recognized as the methods of choice, they have their own disadvantages with respect to cost, yield, materials lost (that is, etching/removing the majority of the materials), requirement of hazardous chemicals, high temperatures and post activation. Wet chemical techniques, which are considered as a simple and low-cost alternative, have also serious drawbacks because of using hazardous chemicals/wastes, several processing steps and time consumption. Although the bottom-up wet chemical design of non-metallic porous structure has made enormous progress, it is still not well suited for metals.[86] In other words, finding a way for high yield of the metallic nanoparticles and their assemblies and agglomeration to form a 3D nanoporous structures is a difficult task, which cannot be performed with the traditional fabrication techniques.

The Leidenfrost reactor is a unique phenomenon whose potential for technological application has not yet been explored. Here the Leidenfrost chemistry and Leidenfrost dynamics are combined and are potentially exploited as a new generator of 3D nanoporous metal.

Achieving the mentioned task requires a production of concentrated aqueous nanoparticles inside the levitated droplet, which cannot simply be achieved by increasing the salt concentration for a good reason. Using only water for production of metallic nanoparticles, the Leidenfrost reactor is facilitated by the hydroxide ions, which promote both basic conditions and electron transfer reactions through discharging. Nevertheless, the yield is low, as the availability of the $OH^-$ ions is governed by the dissociation of water. According to our finding, the yield of the gold nanocrystals should increase, at least for higher concentrations of hydroxide ions. Herein, to meet the need of high concentrations, we further introduced a new type of reducing agent under the Leidenfrost condition, namely NaOH, as a source of hydroxide

ions and enhancer of the basic condition. Indeed, by simply adding 50 µl of NaOH (0.5 M) to a 20 mM aqueous Tetrachloroauric (III) acid solution (pH ~ 6.5) and gently placing a 5-ml drop of the resulting solution on a preheated hot plate (with a constant temperature of 270 °C), a brownish red droplet is formed, containing a dense structure. The structure was collected on a glass plate where a macroscopic spongy system can be seen even by the naked eye (**Figure 3.4a**).

In our opinion, and from technological point of view, the field is revolutionized if 3D nanoporous structures could be fabricated in a suspension form, which would enable a simple casting-based device. To evaluate the potential of this idea, we sought out a way, to design and produce nanoporous metal in a suspension form. For that purpose, sodium citrate was used as a capping agent and simultaneously as a co-reducing agent beside the sodium hydroxide to further enhance the yield. On the basis of the mentioned approach, we demonstrate the first wet chemical synthesis of a suspended nanoporous gold using levitated Leidenfrost pool (1 ml $HAuCl_4$, 20 mM+700 µl sod. citrate 1%+50 µl NaOH 0.5 M, pH ~ 7.3) in a simple, cost-effective and green way (**Figure 3.4b**). At this stage, a portion of the brown suspension was collected to glass bottles and stored for further use (**Figure 3.4c**). Various analytical investigations (ultraviolet–visible spectroscopy for the liquid, as well as SEM and X-ray diffraction (XRD) on dried and rinsed samples) confirmed the formation of suspended plasmonic nanoporous gold (**Supplementary Figure S8**). On the other hand, an orange suspension of a macroscopic 3D network of fused gold particles with different sizes and shapes are formed if only pure sodium citrate is used (**Supplementary Figure S9**).

Gold suspension behaves analogous to polymer chains dispersed in a good solvent and it merely collapses to form a hard sphere upon solvent evaporation. A global evaporation of the levitated suspended gold pool acts very similar; however, it is expected that the gold chains are further fused and welded together to form a 3D nanoporous hard sphere. With that in mind, we further demonstrate an 'all-*in-situ*' fabrication of 3D nanoporous hard sphere in the Leidenfrost drop. A naked eye observation of a levitating drop of the brown gold that converted into 3D nanoporous powder is shown in **Figure 3.4d-h**.

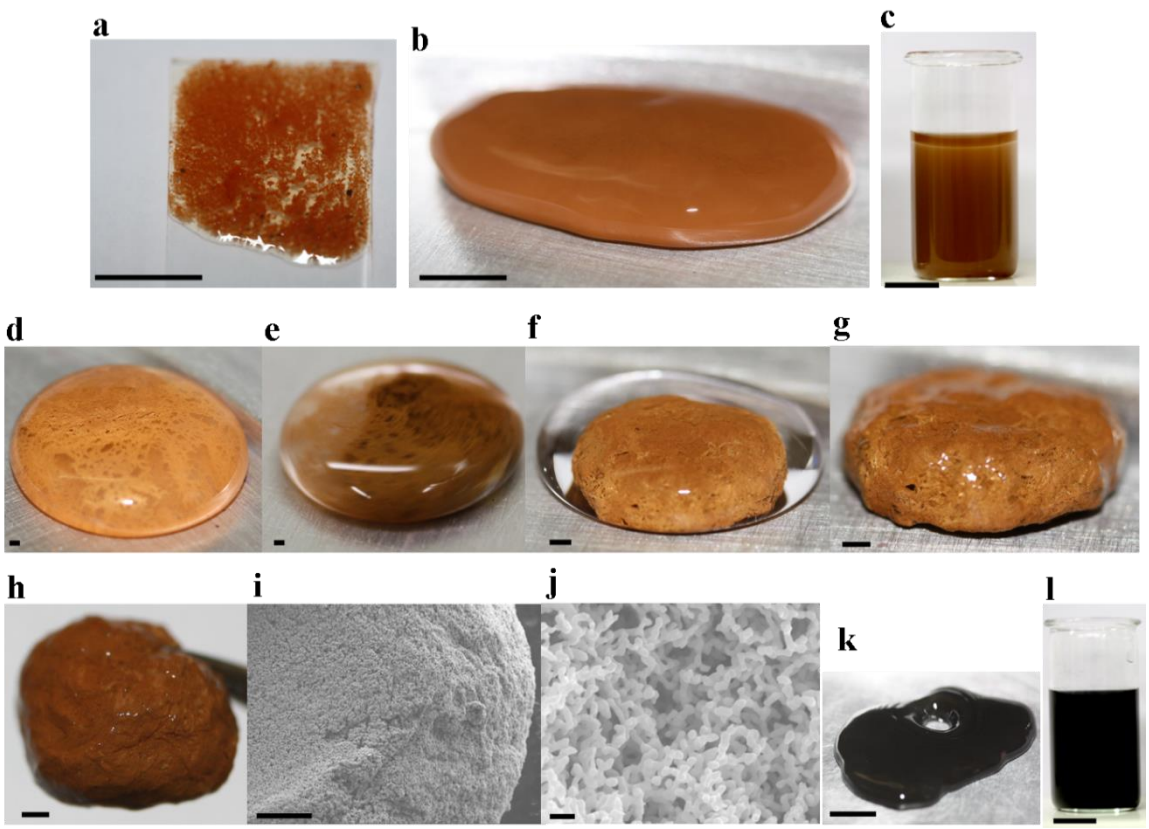


***Figure 3.4: Fabrication steps of nanoporous gold. (a) Photograph of spongy structure collected on a glass substrate using only NaOH. (b) Leidenfrost levitated pool of suspended nanoporous brown gold on hot plate. (c) The same solution as (b) collected inside a glass container. (a–c) Scale bar, 1 cm. Synthesis steps of solid nanoporous gold sphere from initialization (d) to final product as a sponge (e-h). Scale bar, 1 mm. (i) Scanning electron microscopy image of the spongy brown gold. Scale bar, 100 µm. (j) Higher magnification image of the same sample as in i. Scale bar, 300 nm. (k) Leidenfrost levitated pool of suspended nanoporous black gold on hot plate. (l) The same solution as (k) collected inside a glass container. (k,l) Scale bar, 1 cm.***

It is worth mentioning that the nanoparticle synthesis, clustering, assembly and fusion to form an extended 3D network occurred in the levitated drop. Washing, rinsing the sample and removing of residual salt and/or byproduct, or even enlarging the size of the metal spongy can occur 'all-*in-situ*" in the levitated state (**Supplementary Movie 6**). SEM analysis proved the 3D macroporous structure of the gold sphere (**Figure 3.4i,j** and **Supplementary Figure S10**), whereas the XRD pattern indicated the polycrystallinity of the sample (not shown).

Our results demonstrate a new generation of metallic porous materials in a different form fabricated from a levitated drop and manifest the interplay between the Leidenfrost chemistry and Leidenfrost dynamics. To understand the origin of this phenomenon, we investigated the effect of Sod. hydroxide/Sod. citrate ratio as a possible variable on the structure. It is beyond the scope of this article to describe the details of all these experiments. But we can conclude that the shape, size, filling factor (porosity) and the plasmonic colour is

highly affected by the added amount of NaOH and its concentration, whereas the stability of the suspensions is highly altered by the citrate content. Furthermore, our investigations implies the important role of this ratio on the heat transfer in the levitated drop, including the convective heat transfer performance of the nanofluids,[134] the evaporation in the levitated droplet, and the temperature and viscosity field around the particle, which affect its mobility, clustering and networking. Last but not the least, the ratio was found to be a determining factor controlling the place of spongy structure formation. In other words, depending on the ratio of hydroxide and citrate of sodium, the sponge is either likely to be formed mainly inside the droplet or mainly at the liquid–air interface in analogue to levitated liquid marbles.[135-136] We believe that a new multidisciplinary approach needs to be introduced to describe the interdependency between the Leidenfrost chemistry and Leidenfrost dynamics. It would not only enhance our understanding of the heat transfer phenomenon in a levitated droplet but also is essential for a new generation of tunable plasmonic porous materials.

To visualize the role of NaOH mentioned above and to further explore the potential of the mentioned method, we demonstrate the first black gold suspended in a levitated pool (**Figure 3.4k**) and collected in a glass bottle (**Figure 3.4l**). The black gold suspension, which we believe to cause a paradigm shift in the field of plasmonics, has been fabricated by increasing the amount of hydroxide ions, that is, NaOH to 150 µl, while keeping all the other parameters required for the fabrication of the brown gold suspension constant (1 ml $HAuCl_4$, 20 mM+700 µl Sod. citrate 1%+150 µl NaOH 0.5 M, pH ~ 8.5). A full analytical investigation of the resulting black product was performed (see **Supplementary Figures S11 and S12**).

We believe that our black nanoporous suspension fabricated under Leidenfrost condition can turn any substrate to a super absorber by simple casting, and hence enable a new generation of functional plasmonic that can be easily integrated in several energy collecting application, including photovoltaics and thermo-photovoltaics. Although an up-to-date achieving black absorber are mainly based on top-down approaches, such as focused ion beam,[137] lithography[138] and co-sputtering,[84] which are comparably costly and their absorption band limited to the visible spectrum, here we demonstrate the first casting-based wideband superabsorber with almost 100% absorbance covering visible to the telecommunication wavelength. This new type of black coating can be applied onto any kind of substrates, including flexible ones (**Figure 3.5a**) with a thickness of ~ 20 µm (**Figure 3.5b**). As the transmission of such a film is zero, the absorption can be calculated by measuring the reflectance of the samples (absorption=1−reflection). Spectroscopy measurement showed that

the reflectance of the black spongy gold is almost zero in whole, visible up to 2 μm wavelength and, hence, resulting in almost 100% absorbance in that frequency regime (**Figure 3.5c**). We believe that the suppression of light reflection originated through combined effects of strong scattering of the light by the sample roughness, localized and de-localized excitation of plasmon within and on the surface of pores, as well as light trapping inside the gaps. In addition to being a superabsorber, the cast film exhibits a pretty high conductivity of $7.958 \times 10^3$ S $m^{-1}$ and, hence, can function as a new type of window electrode in the photovoltaic device.[139]

### 3.3.5 Hybrid foam in a levitated Leidenfrost drop

The uniqueness and power of Leidenfrost drop as a nanogenerator, nanocoater and nanodesigner of functional porous materials is further revealed by the fabrication of a functional metal–polymer hybrid foam. By introducing a commercial packaging polymer foam in a levitated black pool, a black metal–polymer hybrid foam is generated (**Figure 3.5d (left)**). However, if the polymer foam is immersed onto a glass bottle containing the black suspension for 24 h at room temperature, or even immersed and then followed by evaporation of the solvent, the foam cannot be coated totally to realize a black hybrid foam (**Figure 3.5d (middle)**). Thus, a 3D coating of complex structure can be only performed under the Leidenfrost dynamics, which further shows the uniqueness of this phenomenon for nanocoating processes. However, covering an area larger than the porous template demonstrated in this study is a challenge. In other words, as the deformation and stability threshold of the levitated droplet is size-limited,[110] coating any object bigger than the size of a stable droplet is unattainable.

It is worth mentioning that the fabricated hybrid foam is stable even after repeated washing and air-drying (**Supplementary Figure S13**). In contrast to its neat counterpart, the hybrid foam is superhydrophilic (**Figure 3.5d**), thanks to the high energy porous metal coating. Indeed, the applications of this type of hybrid foam are too numerous to ascertain, one of the most potential uses is in areas where good heat dissipation, low thermal expansion and light weight are needed (for example, electronic packaging and aerospace).

As a proof of concept and only to visualize this effect, placing the foam on the hot plate of 150 °C along with a bare foam showed that stability of the foam is significantly improved because of the metallic coating. **Figure 5e–g** shows the sequence of heating where one can see that the neat foam melted, while the hybrid one maintained its shape due to its metallic-like heat dissipation. Indeed, the black hybrid foam shows a wideband superabsorber behaviour similar to the casted black gold on the polymer foil (not shown).

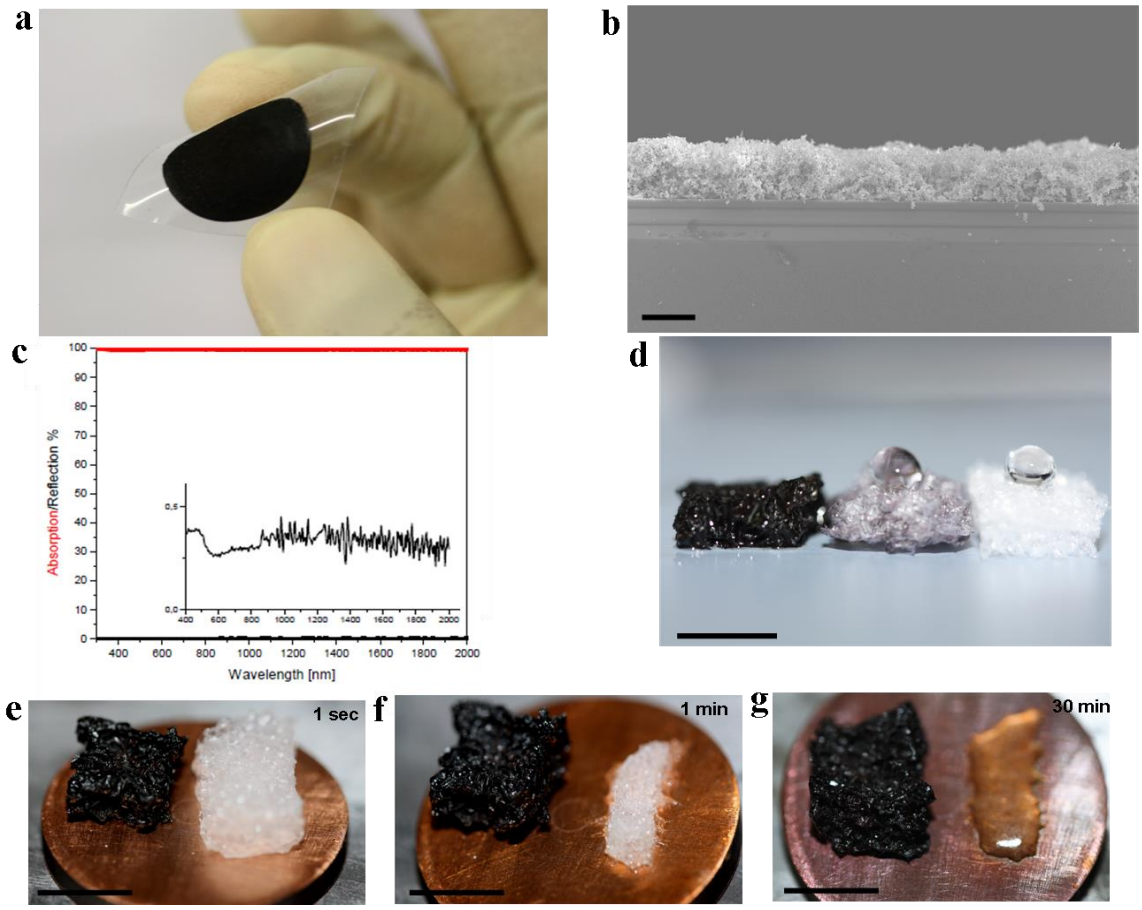


***Figure 3.5: Functions based black nanoporous gold. (a) A flexible polymeric substrate coated with the black spongy gold. (b) Cross sectional scanning electron microscopy image of black spongy gold showing the thickness of film in a. Scale bar, 20 µm. (c) Reflection and absorption spectra of black spongy gold in the visible and near-infrared frequency. Inset shows the magnified reflection spectra in the same frequency. (d, Left of panel) Plastic foam coated with black gold in Leidenfrost levitated drop showing superhydrophilic behavior. (Middle of panel) Plastic foam immersed in black gold solution for 24 h showing hydrophobic behavior. (Right of panel) Neat plastic foam showing hydrophobic behavior. Heating stages of coated (black) and neat foam (white) on a hot plate after (e) 1 s, (f) 1 min and (g) 30 min at 150 °C (d–g). Scale bar, 1 cm.***

As the colour of porous plasmonic meta-materials is dictated by the size of the pores,[140] it is expected that the colour difference of the black (spongy/hybrid) and the brown gold originates from the dissimilarity of the average pore size. BET (Brunauer–Emmett–Teller) analysis of the spongy brown, black and hybrid foam (**Supplementary Figure S14** and **Supplementary Table S1**) proved that the black porous spongy and the black hybrid possessed a nearly similar average pore size of ~ 2.6 and 2.4 nm, respectively, whereas the brown porous gold has an average pore diameter that exceeded 3 nm.

## 3.4 Discussion

All in all, it is possible to say that work has contributed to resolve the 257-year-old Leidenfrost phenomenon, while we prove the electrostatic, thermal gradient and overheated nature of the levitated droplet. The later already manifest our hypothesis of the overheated zones2 and we believe that a new type of charge chemistry has been introduced and the effectiveness of the Leidenfrost drop as a water-based levitated green reactor for nanochemistry along with the extensive usefulness of implementation of its exclusive physiochemical character has been demonstrated. Nevertheless, the exact mechanism of the nanosynthesis, including the role of the fast evaporation and thermocapillary, is still unknown and has to be determined. Lab in a Leidenfrost drop allows the fabrication of nanomaterials and simultaneously implementing it for the designing of functional materials by one fast step, low cost and in an environment-friendly manner, all in a levitated drop. Especially noteworthy is the designing of plasmonic nanoporous gold in suspension form that allow to demonstrate the first bottom-up-based wideband black absorber. The 3D coating of a complex structure performed under the Leidenfrost dynamics further shows the uniqueness of this phenomenon for nanocoating processes. However, although small objects can be coated, covering big object is limited to the biggest droplet that can levitate stably under the Leidenfrost condition. In this context, the uniformity and the quality of the coating is influenced by several parameters, such as surface roughness, wettability of the hot plate and the substrate to be coated, and the geometrical factors, which hinder the movement of the droplet or affect its shape, stability and vibration. Nevertheless, and as was mentioned in previous work,[63] the Leidenfrost drop may be able to maintain a metastable state, although this requires further investigation to be proved. In short, the Leidenfrost reactor has just started and is full of interesting problems that require multidisciplinary investigations to fully understand the phenomenon and to explore the interdependency between the Leidenfrost chemistry, Leidenfrost dynamics and heat transfer phenomenon in a levitated droplet.

## 3.5 Methods

### 3.5.1 TEM and SEM characterizations

TEM measurements were carried out using an FEI/Philips Tecnai F30 G2 TEM (FEG cathode, 300 kV, Cs=1.2 mm) equipped with EDX detector and Gatan imaging filter, and with a Philips CM 30ST microscope (LaB6 cathode, 300 kV, Cs=1.15 mm). A Spinning Star device (Nanomegas) attached to the CM 30 microscope enabled precession electron diffraction. Thin

films were mechanically released to Cu lacey carbon TEM grids by scratching and mixing with Butanol for enhancing adhesion. For the case of CuO nanorods, a Mo TEM grid was used. SEM measurements were carried out using a Phillips XL 30 and a Field Emission SEM ZEISS ULTRA plus equipped with Oxford Instruments INCA-X-act EDS.

### 3.5.2 Ultraviolet–visible/NIR spectroscopic analysis

The reflection and absorbance spectra of black and brown gold nanoparticles (**Figure 5c** and **Supplementary Figure S8b and S11c**) were investigated by Lambda900 UV-Vis-NIR spectrometer (Perkin Elmer). Aluminum mirror were used as a standard for the reflectance measurement, while the standard cuvette was utilized for the solution measurements.

### 3.5.3 Electrical conductivity measurements

The conductivity of black Au film, cast on the plastic substrate, was determined by a Keithley 6517B electrometer and 'National Instruments LabView' software. A constant voltage of 1 V was applied between two Au-wire electrodes located on the film sample (width of electrodes, w=0.3 mm and the distance between the electrodes, d=2 cm).

### 3.5.4 BET, XRD and infrared imaging investigation

Porosity and surface-area characterization for brown, black gold and hybrid foam samples are done by a BELSORPmax machine from Rubotherm. All XRD measurements were carried out by a Seifert XRD 3000 PTS. InfraTec PIR uc 180 with a rate of 24 Hz and a spatial resolution of 40 lm/IR pixel was used for thermographic analysis of the levitated drop.

## 3.6 Contributions

R.A. performed the experiments, electrical measurements, SEM characterization and contributed to the writing. D.D. contributed to the experiments and writing. M.K.H. and J.-H.P. contributed to measurements and writing, and A.U.Z. contributed to SEM characterization and writing. B.E., V.S.K.C., V.D. and L.K. performed the TEM measurements and contributed to the writing. M.E. conceived the concept, designed the experiments, proposed the mechanism, supervised the work and mainly wrote the manuscript.

## 3.7 Acknowledgements

We acknowledge the financial support provided by the German Research Foundation (DFG) through the projects EL554/1-1 and SFB 677 (C01,C09). M.E. thanks the Initiative

Networking Fund of the Helmholtz Association for providing the financial base for the start-up of his research group VH-NG-523. We also thank Professor. Dr. B. Lotsch for enabling the TEM experiments; Professor. Dr E. Quandt and Dr-Ing. C. Bechtold for thermographic measurements by the infrared camera; Dr U. Schürmann for some TEM investigations; Prof. Dr N. Stock, Dipl.-chem, J. Timm and Dipl.-chem and N. Reimer for BET measurements, and Dipl.-Ing. S. Rehders for technical support during the experiments and for drawing the sketches.

## 3.8 Supplementary Information

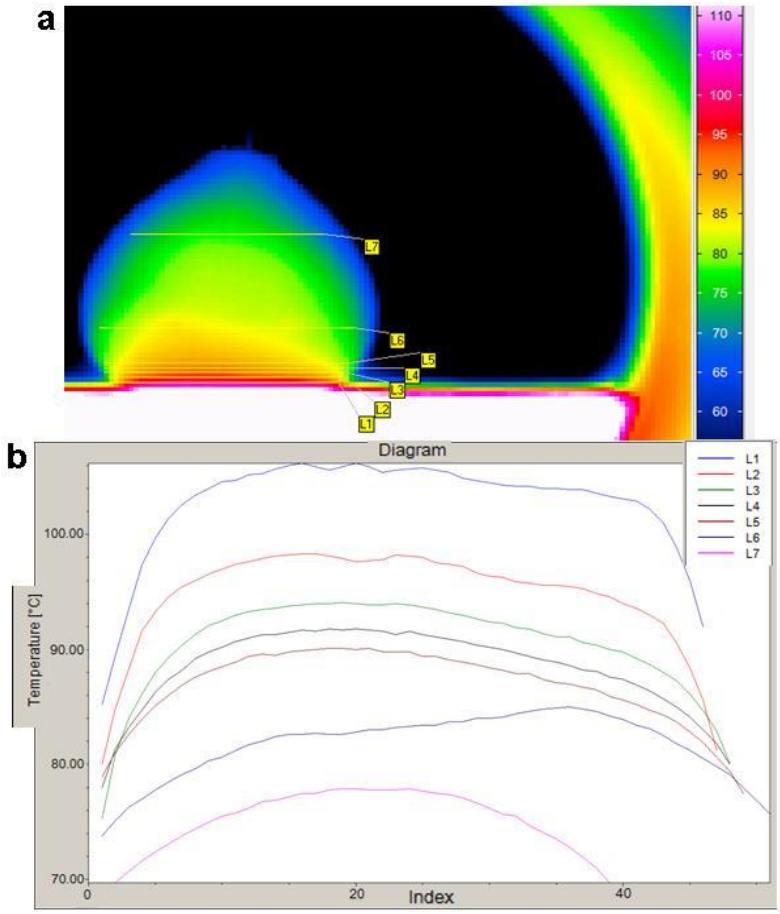


***Supplementary Figure S1: IR-Temperature measurement inside a levitated droplet: a, The cross sectional thermograph view of the levitated drop (~ 400 µL ) on aluminum substrate at 250 °C shows different colors which related to different temperatures. For these measurements, the edge of substrate (which facing toward the camera) were coated with a varnish spray to increase their emissivity (Tetenal camera varnish, emissivity 0.96). There are seven horizontal lines at different levels through the drop, which show the temperature of the different area of drop during levitation where the temperature inside the drop decreases from down to up. b, The graph, which calculated automatically by the software of the camera, shows the temperature gradient corresponding to each line drown in part a. It clearly demonstrate the temperature variation inside and at the edge of the drop.***

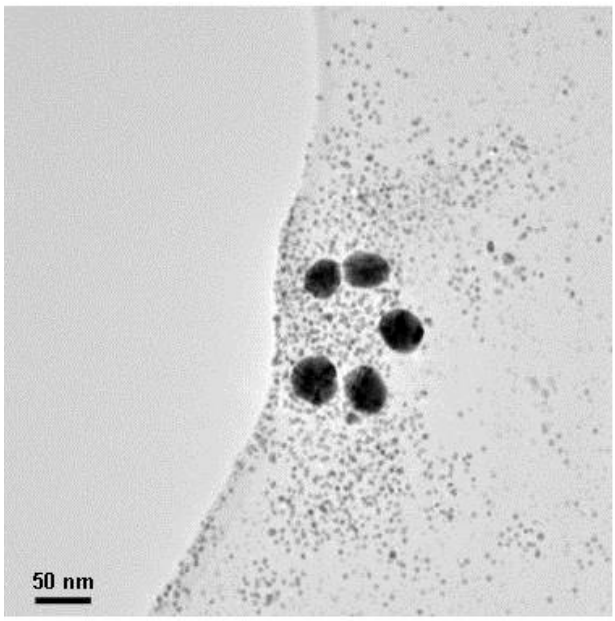


***Supplementary Figure S2: TEM image of bigger gold nanoparticles: Bright field TEM image of few ~ 40 nm gold particles which might be formed due to further growth at the air liquid interface or during drying on the TEM Grid.***

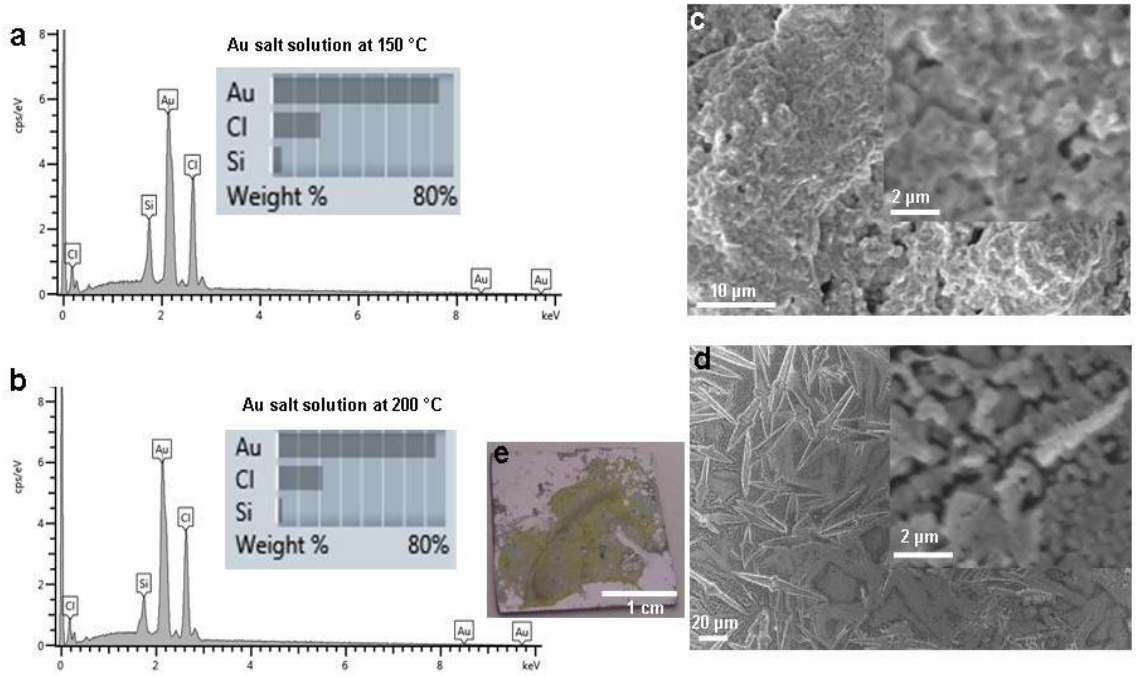


***Supplementary Figure S3: Characterization of gold chloride solution heated at lower temperature than the Leidenfrost: a, EDX spectra of 50 µL droplet of 20 mM solution placed on silicon substrate heated at 150 ˚C. b, at 200 ˚C. Inset in each graph shows the chemical composition in percentage. c & d, SEM images of samples (a) and (b) with 2 magnification, correspondingly. e, The photograph of the analyzed sample at 200°C.***

***Supplementary Figure S4: Detection of chlorine gas in the vapor: Syringaldazine was placed on a glass substrate and the glass substrate was set above a Leidenfrost drop of $AuCl_4^-$ solution. A change in the color of syringaldazine from colorless to red-purple indicates a reaction with chlorine in the vapor.***

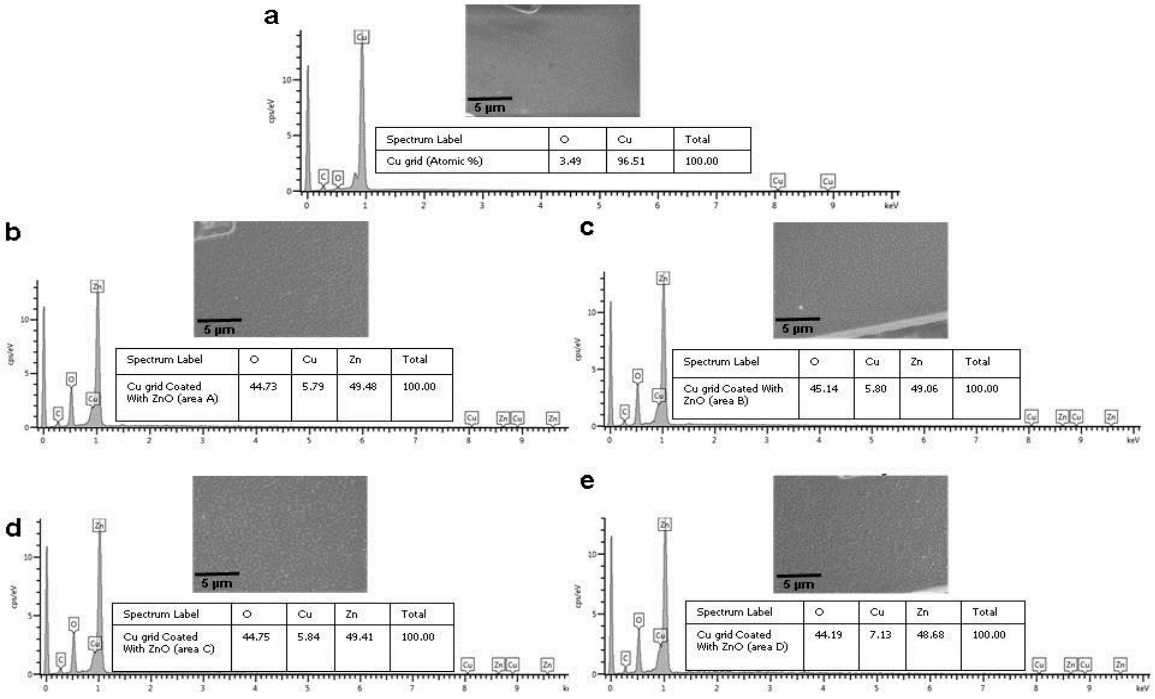


***Supplementary Figure S5: EDX analysis of ZnO coating on the TEM grid: a, uncoated Cu grid. b, c, d & e coated with ZnO, at four different regions. Insets in each graph represents the corresponding SEM image and chemical composition (atomic %) of each area.***

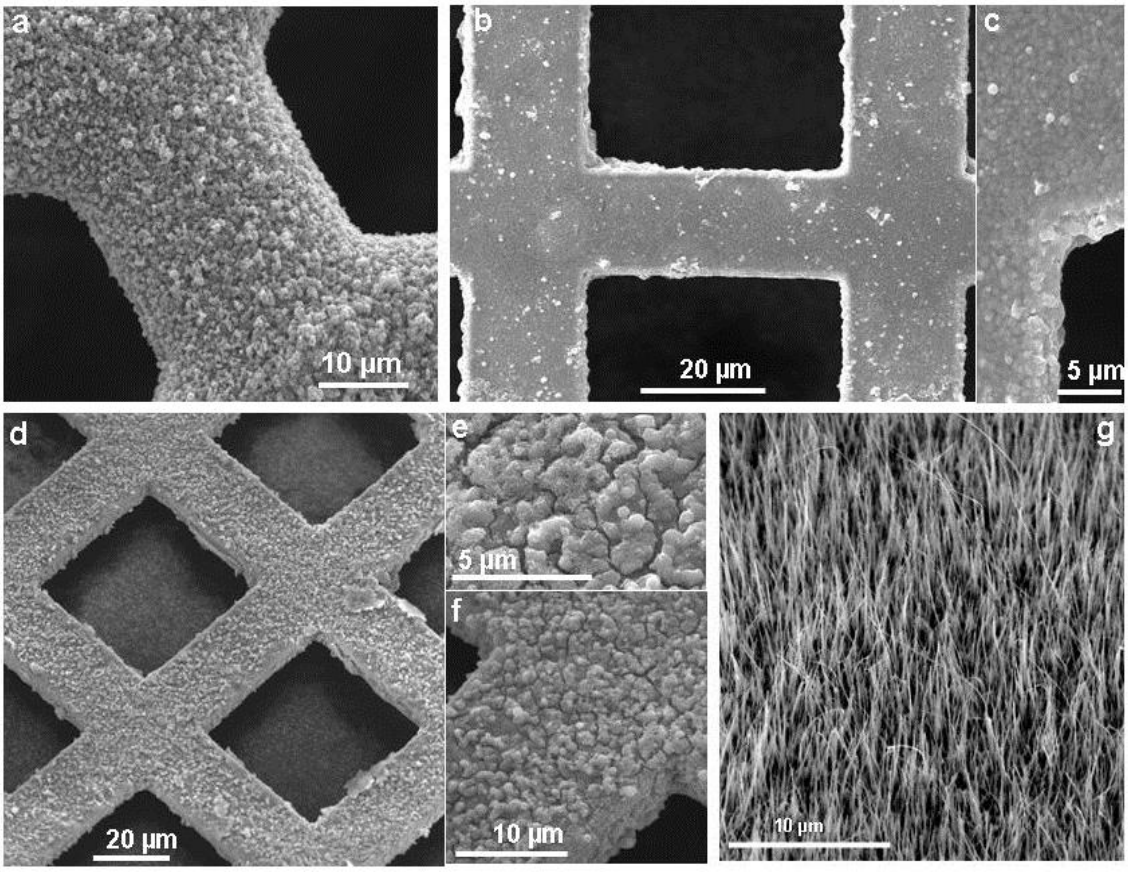


***Supplementary Figure S6: SEM images of ZnO and CuO coating on the TEM grid: a, a thicker coating by using 40 mM zinc acetate aqueous solution. b & c, with 2 times coating by using 20 mM zinc acetate at low and high magnification, respectively. d, e & f, with 5 times coated sample at low and higher magnification. g, The nanograss (CuO) with few micrometer length and few tens of nanometers diameter which covers the surface due to further heat treatment for 2 hours at 400°C.***

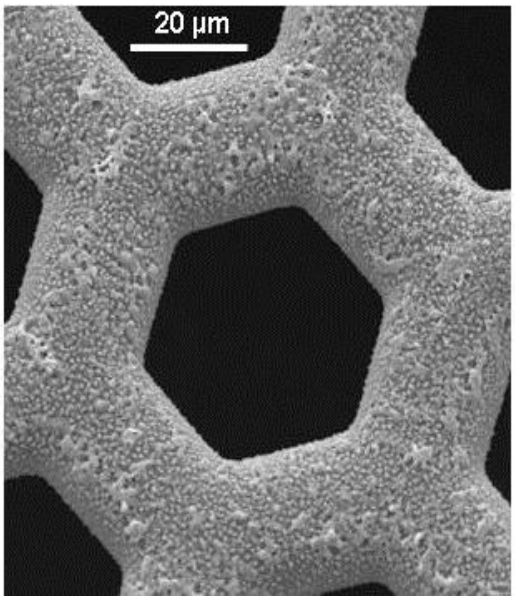


***Supplementary Figure S7: Inhomogeneous ZnO coating: ZnO film coated at the same conditions as of Figure 3b. The non-uniformity of the film is apparent which might have originated from the bubble formation during the process.***

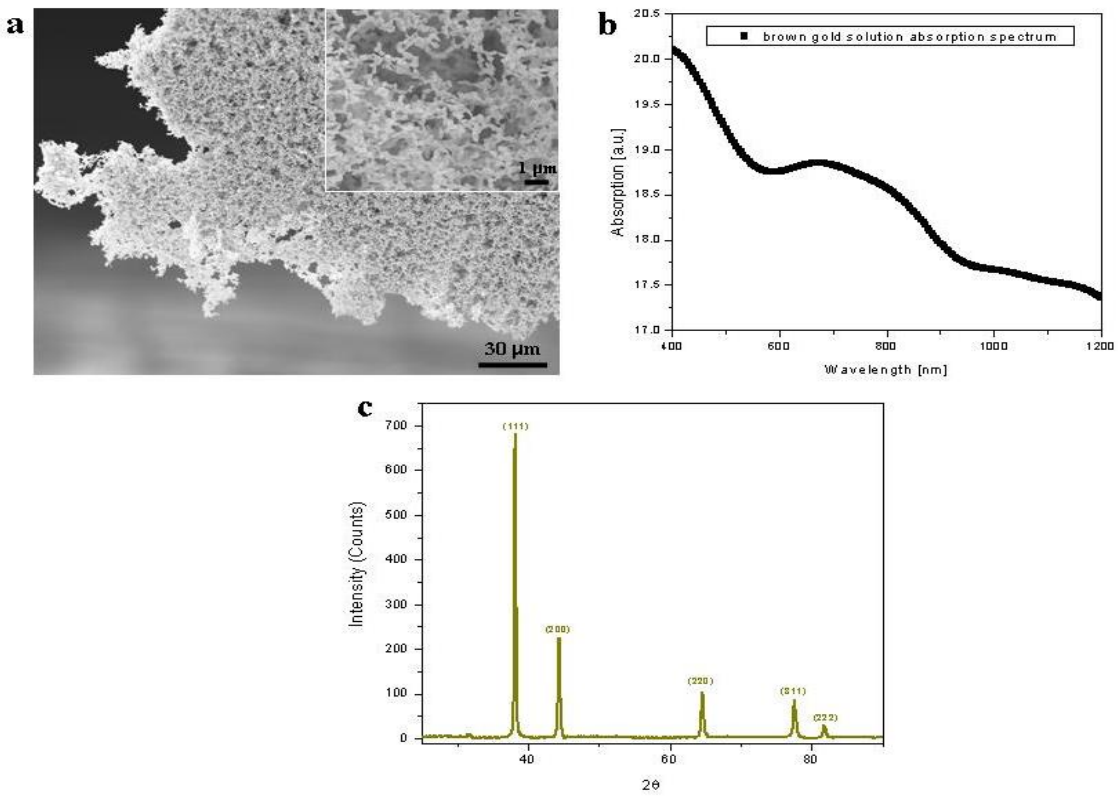


***Supplementary Figure S8: SEM, absorption spectra and XRD pattern of brown spongy gold: a, scanning electron microscopy image of structure of brown spongy gold. b, UV-Vis absorption spectra of brown spongy gold suspension (Figure 4c) in visible and NIR wavelength. c, XRD pattern of brown spongy gold.***

***Diffraction peaks at 2θ = 38.2°, 44.4°, 64.6°, 77.6° and 81.7° corresponds to (111), (200), (220), (311) and (222) planes of pure Gold.***

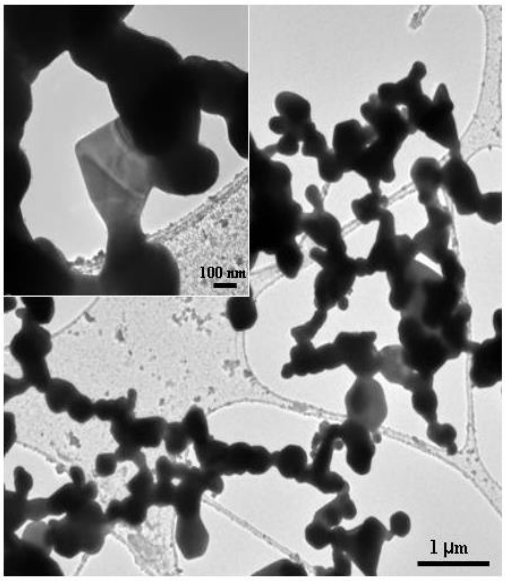


***Supplementary Figure S9: TEM analysis of spongy gold produced by gold salt with sod. citrate only: TEM image of spongy gold showing a porous network formed through fusion of particles by particle impingement and coalescence to some extent.***

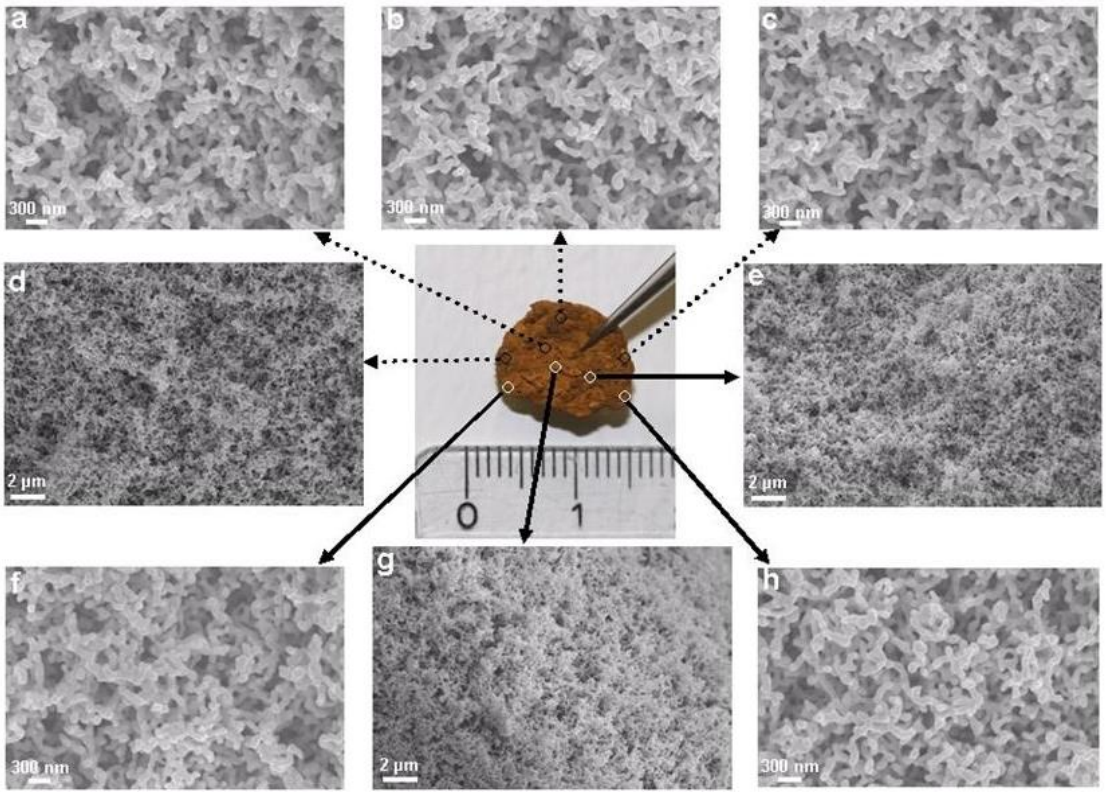


***Supplementary Figure S10: Investigation of the uniformity of the sponge nanoporous gold sample shown in Figure 4i: a, b, c & d, SEM images of the top surface at different places shows the uniformity for the porous structure. e, f, g***

***& h, the backside at different points. The photograph of the analyzed sample is also shown for clarity.***

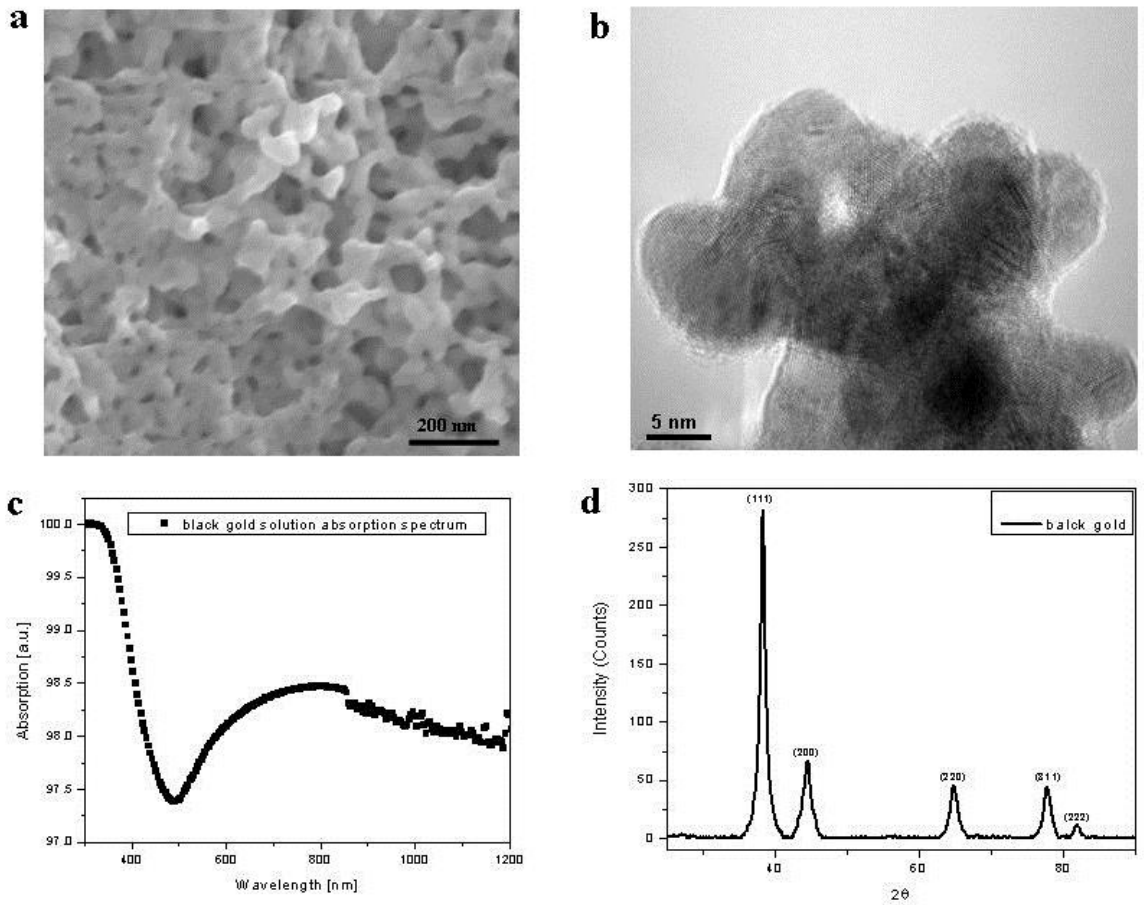


***Supplementary Figure S11: SEM, TEM, absorption spectra and XRD pattern of black spongy gold : a, scanning b, high resolution TEM (HRTEM) images confirms the presence of pure Au and reveals that the nanoparticles have tightly merged together to form interconnected structures. c, absorption spectra of black spongy gold in visible and NIR wavelength. d, XRD pattern of black spongy gold. Diffraction peaks at 2θ = 38.2°, 44.4°, 64.6°, 77.6° and 81.7° corresponds to (111), (200), (220), (311) and (222) planes of pure gold.***

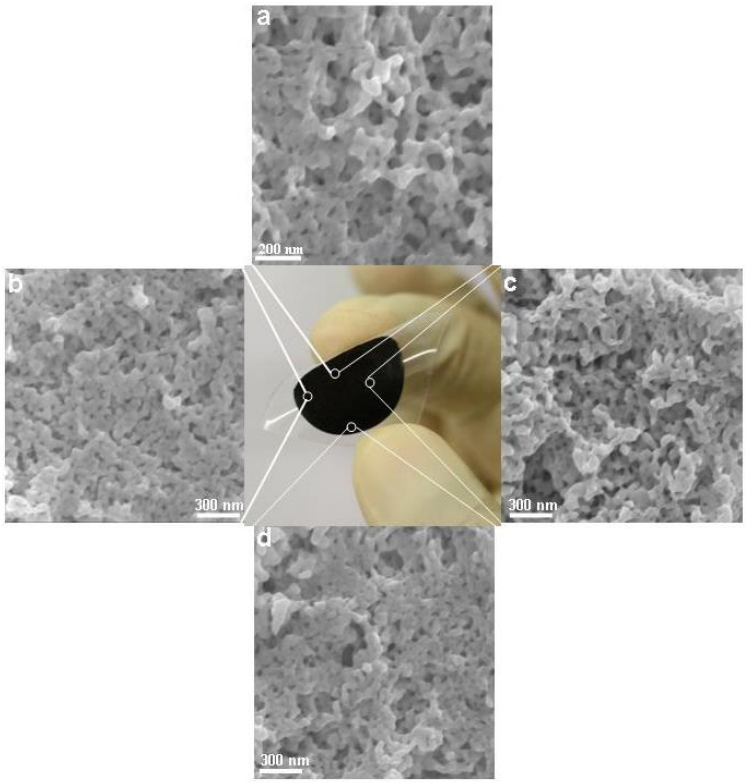


***Supplementary Figure S12: Investigation of the uniformity of the black nanoporous gold sample shown in Figure 5a: a, b, c & d, SEM images of porous film on flexible polymeric substrate at different area show the uniformity of the porous structure of the sample. The photograph of the characterized sample is shown in the middle.***

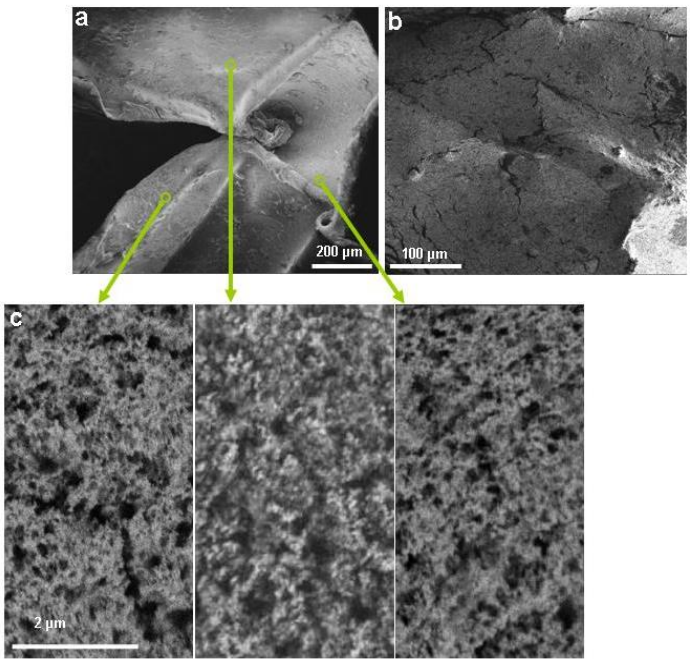

***Supplementary Figure S13: SEM images, of polymer foam coated with black gold, at 3 different magnifications: a, low. b, moderate. c, high magnification of 3 different areas, respectively.***

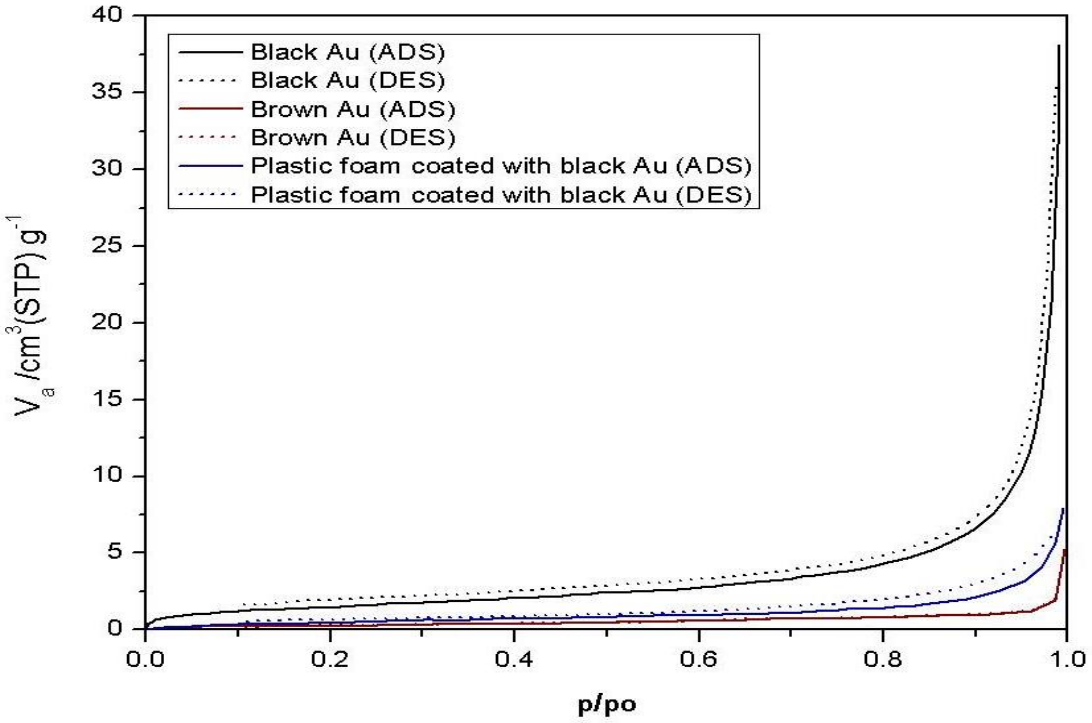


***Supplementary Figure S14: BET analysis: Nitrogen adsorption (ADS)\desorption (DES) curves of the spongy brown, black and hybrid foam gold samples activated at room temperature overnight under vacuum at the same parameters.***

***Supplementary Table S1: BET analysis of spongy brown, black and hybrid gold samples***

| **Parameters [unit]** | **Brown Au** | **Black Au** | **Polymer / black Au** |
|---|---|---|---|
| **$V_m$** [$cm^3$(STP) $g^{-1}$] | 0.2218 | 1.2985 | 0.4713 |
| **$a_{s,BET}$** [$m^2$ $g^{-1}$] | 0.96518 | 5.6516 | 2.0513 |
| **C** | 155.31 | 50.667 | 17.94 |
| **Total pore volume ($p/p_0$=0.500)** [$cm^3$ $g^{-1}$] | 0.000752 | 0.003785 | 0.0012507 |
| **Average pore diameter** [nm] | 3.1175 | 2.6786 | 2.4388 |

Where ($V_m$**)** is monolayer adsorbed gas quantity, ($a_{s,BET}$) is specific surface area and (C**)** is BET constant.

## 3.8.1 Supplementary Note 1: Mechanism of gold reduction

The suggested chemical pathway for the formation of gold nanoparticles follows a multistep reduction mechanism of Au (III) ions into elemental Au through an intermediate state Au(I) ions (i.e. Dichloroaurate) with the release of chlorine/free chlorine gas. This process is facilitated by the Hydroxide ions which promote both basic conditions and electron transfer reactions.[126,141] Thus, the postulated overall reaction can be written as follows:

$$2\ OH^- + AuCl_4^- = \tfrac{1}{2}O_2 + H_2O + Au^o + 2\ Cl_2 \qquad \text{(S1)}$$

Chlorine gas was indicated by using a FACTS method[142-143]. This method is based on the reaction of colorless 3,5-dimethyl-4-hydroxybenzaldazine (syringaldazine) with chlorine /free chlorine (i.e. can be formed if chlorine gas is dissolved in hot water under basic condition) leading to the formation of a red-purple azo-compound. The condensed vapor of the levitated drop was used to prevent any effect from the chloride ions of the salt inside the drop. A positive result was directly registered at the early stage of levitation as shown in **Supplementary Figure S4** (before the plasmonic color change in the drop was observed). Indeed oxidation of chlorine ions to chlorine gas as indicated in the vapor implies the presence of Au (I) ( i.e. $AuCl_2^-$) as a transient in the levitated droplet.

Au (I) ions formed as intermediate are reduced to neutral gold atom either by accepting electrons from the $OH^-$ ions or due to the following disproportionation reaction[144]:

$$3\ AuCl_2^- = AuCl_4^- + 2\ Au^o + 2\ Cl^- \qquad \text{(S2)}$$

The reaction is generally occurred under basic condition which is fulfilled in the Leidenfrost droplet as proved by us.

As recently shown,[145] the association of gold atoms with excess of Au(I) ions is followed by their coalescence into gold clusters, where the further reduction of Au(I) ions is catalyzed by the formed gold nanoclusters in organic solvents (e.g. alcohols). We expect that this process occurs under the Leidenfrost conditions as water at a temperature between 100 and 200 °C behaves like an organic solvent (i.e. water-methanol mixture)[146] owing to the disruption of the hydrogen bond network at the hot interface. Additionally this process is even accelerated and enhanced by the local accumulation of the ions and the increase of diffusion rate owing to the fast phase expansion and global evaporation of the Leidenfrost droplet and thus satisfying a vital condition for the nucleation and growth of the gold clusters.

Finally, it is worth mentioning here that, a titration test with different molarities and volumes, of NaOH solution did not show any trace of HCl neither in the vapor nor in the droplet which agrees well with our suggested reaction pathway.

### 3.8.2 Supplementary Note 2: Coating inside Leidenfrost droplet

Thicker coating achieved by increasing the concentration (**Supplementary Figure S6a**), was also done by multiple steps coating. Two samples were prepared by coating TEM grids with ZnO in multiple steps. SEM images, (**Supplementary Figure S6b, c**), of double coated grid show minor defects in the form of "cluster agglomeration" on the surface of the film. This effect became even worse in case of 5 times deposition, as shown in (**Supplementary Figure S6d**). Higher magnified images (**Supplementary Figure S6e,f**) further showed that, cracks had also been initiated on the film which ruined its quality. It seems that coating of the pre-coated sample does not produce a homogeneous film and the smoothness and uniformity would be sacrificed at the expense of thickness.

### 3.8.3 Supplementary Movie 1: Transitory charges by Leidenfrost droplet

When a 300 µL drop of deionized water was placed on a hot metal surface, heated to 250°C, the drop underwent a fast evaporation followed by levitation. In this process, at the beginning charges were separated due to fast evaporation and transitory positive charges were determined followed by increasing of negative charges during the levitation.

### 3.8.4 Supplementary Movie 2: Positively charged steam during drop levitation

A ceramic substrate was heated above Leidenfrost temperature (280 °C) and by placing the tip above the drop to measure the charge of the vapor phase, only positive charges were registered.

### 3.8.5 Supplementary Movie 3: Levitated negatively charged droplets:

By placing the tip at a distance of 1 mm above an insulating ceramic hot plate, the amount of negative charges increased by adding small droplets of deionized water.

### 3.8.6 Supplementary Movie 4: Gold nanoparticles synthesis in the Leidenfrost drop reactor:

Transformation of Leidenfrost drop from yellow gold salts to plasmonic red color of gold nanoparticles during the levitation.

### 3.8.7 Supplementary Movie 5: 3D synthesis and coating in the Leidenfrost drop

3D coating of TEM grid. A rotary motion of Leidenfrost drop holds the TEM grid inside the drop during the coating.

### 3.8.8 Supplementary Movie 6: 3D nanoporous gold in the Leidenfrost drop

Formation of 3D nanoprous gold hard sphere in the levitated drop followed by rinsing with d $H_2O$ for washing. Further enlarging the size of the metal spongy by adding more precursor (1 ml $HAuCl_4$, 20 mM + 700 µL Sod. Citrate 1% + 50 µL NaOH 0.5 M, pH ~ 7.3) followed by rinsing again with d $H_2O$ and soaking the residual salt and/or byproduct by plastic pipette. Holding the spongy gold by tweezer at the end of the video.

One can watch these movies under the following link

*"http://www.nature.com/ncomms/2013/131029/ncomms3400/full/ncomms3400.html#supplementary-information"*

# Chapter 4

# Nanopowders by water-based Leidenfrost green chemical reactor and their infrared emissivities

## 4.1 Introduction

Recently, metal oxide nanopowders are coming into lime light due to their unique photonic, electronic, catalytic[17,147-148] and various structural properties that make them attractive candidates for different applications like spacecraft thermal control,[149] high emissivity coatings[93] and solar cells.[150] Having considered the general demand, a simple, cost-effective energy, efficient and eco-friendly green method of producing these powders in bulk quantity with a high degree of purity needs to be developed.

The nanopowder is produced in a number of traditional ways. It can be grinding, milling, air micronizing or crushing. However, these forms have their own drawbacks such as the lack of control over dispersity size or incompatibility with the materials which may be sensitive to the temperature and pressure. On the other hand, chemical methods as sol-gel processing, chemical vapor deposition (CVD) and molecular pyrolysis produce nanosized powders but these methods are economically and environmentally useless for being produced on a large scale. For the industrial production of nanopowders, the required equipment generally are expensive owing to high pressure and temperatures involved. These methods, also, are not precise in the control of size, crystallinity and morphology. However, a new method of nanopowder production is proposed to pave a way towards solving these problems.

It has been clear in the previous chapter that when a liquid drop of a precursor solution touches a hot surface, whose temperature is much higher than the boiling point of the liquid, the lower part of the droplet evaporates, an overheated zone generates, charges are separated and hence a new vein of green nanochemistry in a levitated droplet is demonstrated. Thanks to the thermal gradient that governs the rotation, oscillation and convective flow in the levitated drop, one can realize a single step fabrication of nanoscale coatings on complex objects and designing porous metal in suspension and foam form, all in a small drop of maximum 2 mL precursor volume.[3]

But, in this chapter, a further step towards upscaling the Leidenfrost drop method is taken to produce metal oxide nanopowder in different morphologies with high yield. Simply, the metal salt aqueous solution in a large volume, as much as, 50 mL is introduced to a preheated aluminum substrate (300 °C) to form the Leidenfrost puddle. Nanopowder in different morphologies of the same materials can be fabricated in minutes in a single step without the need for special purification methods. Moreover, this one-step approach avoids capping agents, coordination compounds, costly organic surfactants that often contaminate and consequently complicate their successive applications.[151-152] One application of these nanopowders may be in the thermal coatings that can potentially reduce the energy

requirements by effectively improving the radiative heat transfer.[93,153] Infrared high emissivity coating of the inner walls in industrial furnaces has always been playing an important role to increase the thermal efficiency. Recently, a new CuO-ZnO-based coating material sintered at 1600 K has been prepared as an energy-saving coating.[154] The next section shows that Leidenfrost drop cannot only successfully produce such nanostructrued powders but can also control the IR emissivity by tuning the morphology and crystallinity of the particles.

## 4.2 Result and discussion

### 4.2.1 Crystal growth of nanoparticles in solution

The basic model used to explain the mechanism for the formation of colloids or nanocrystals in solution was reported by La Mer and coworkers in 1950. This model can be described by the simple diagram shown in **Figure 4.1a**. The diagram summarizes the suggested mechanism of the synthesis of the colloidal nanocrystals, where the chemical reaction should be designed. It shows that the concentration increases, in a short time, much higher than the saturation concentration. Otherwise, the produced nuclei that grow dominate. Short burst of nucleation leads to the formation of a large number of particles with high rate in a brief period. These particles grow very fast accompanied with decreasing the concentration under the nucleation level. This stage allows further growth of the particles where the rate can be determined by the slowest step during the growth process, and consequently separation between the nucleation and growth with time. In other words, the final slow rate of growth is leading to a very short period of nucleation if compared to the growth period. That is the requirements for monodispersity based on La Mer's diagram.[155-156]

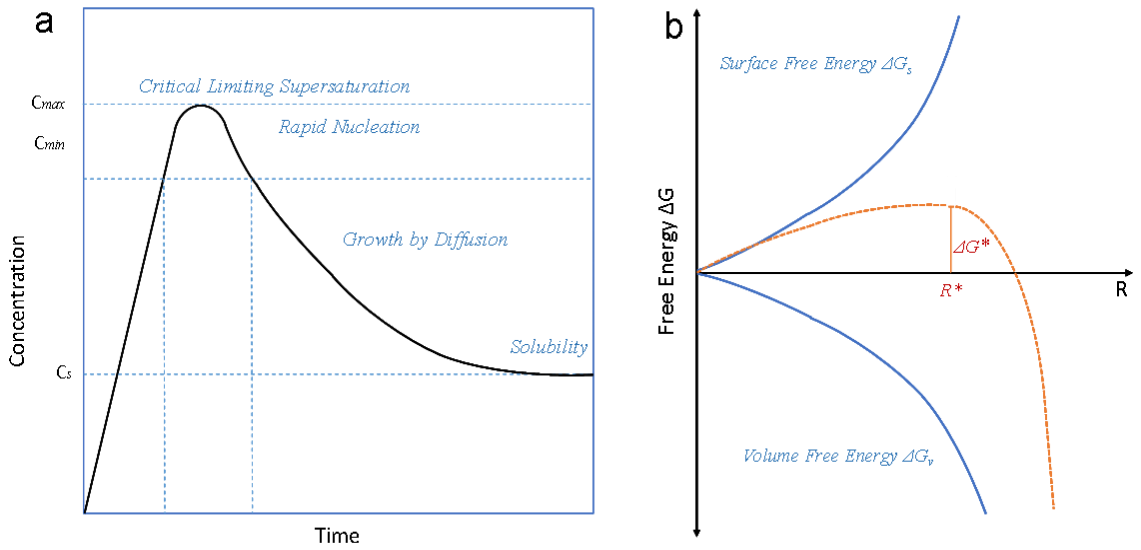


***Figure 4.1: (a) Schematic diagram describing La Mer`s condition for nucleation and growth of nanocrystals as a function of concentration of precursor and the time of reaction. (b) Classical nucleation Schematic model illustrating the free energy diagram of nucleation process.***

One can understand the chemical reaction of the nucleation process from both thermodynamic and kinetic aspects. Based on the classical nucleation theory (**Figure 4.1b**), the exothermicity for the formation of the lattice is the driving force for spontaneous transition phase. The free energy change necessary for the production of nuclei ($\Delta G$) is calculated by the sum of free energy change for both the formation of a solid surface ($\Delta G_s$) and the transformation phase ($\Delta G_v$). As the solvated precursors are less stable than the solid-state crystals, the total Gibbs free energy of the process is decreasing because of negative $\Delta G_v$. On the other hand, the production of nuclei is based on the competition between the decrease in $\Delta G_v$ (favorable condensation of solvated precursors into nuclei) and the increase in $\Delta G_s$ (destabilization of the nuclei toward solvation commensurate with the crystals' surface area). In case of quite small radii ($R$) of the nuclei, $\Delta G_s$ is positive leading to solvation of the small nuclei. The total free energy increases with increasing nuclear size, and reaches a maximum ($\Delta G^*$) at a certain size of the nucleus called the critical nuclear size ($R^*$). With further increase in nuclear size there is a decrease in $\Delta G$ which results in stabilization and growth of the nucleus.[157] According to the Arrhenius reaction rate equation, the kinetics of the nucleation process could be represented by the steady-state rate of nucleation:[158]

$$I = A \exp\left(-\frac{\Delta G^*}{KT}\right) \qquad (4.1)$$

where *I* is homogeneous nucleation rate, *k* is the Boltzmann's constant and *A* is the pre-exponential factor.

Furthermore, there are other proposed models like, LSW (Lifshitz–Slyozov–Wagner) theory and the two-step model to illustrate the mechanism of nucleation process for the production of crystals in solutions.[157,159]

Here in this work, controlling the nucleation and crystal growth of the nanofabricated structure at Leidenfrost condition can be achieved through the optimization of the following conditions:

- The concentration of the precursor
- Leidenfrost temperature values and the hot surface material
- The volume of the drop or puddle
- The pH values of the initial solution
- Time of production

All those parameters are playing very important role to realize the precise control of the rate of formation, the surface free energy on size and morphology of the nanocrystals. The synthesis starts by using 10 mM of zinc acetate (pH ~ 6.5) aqueous solution in a glass burette placed above a preheated aluminum plate (300 °C). By adjusting the feed rate to be 1 mL per 25 s, the solution forms a Leidenfrost puddle which levitates on its own vapor film. The cold salt solution in contact with the hot surface undergoes a fast evaporation and formation of overheated zone at the base of the Leidenfrost puddle. Moreover, it experiences a charge separation and self-ionization to produce metal ions ($M^+$) and hydroxyl ions ($OH^-$).

Due to the loss of hydronium ions ($H_3O^+$) in the vapors, the ideal basic conditions for nanoparticles fabrication inside the puddle is created.[43] The color of the puddle changes from colorless to be milky as shown in **Figure 4.2a**. After complete transformation of the precursor to the oxide form, the ZnO nanopowder coagulates and thus precipitates at the bottom of the Leidenfrost reactor shown in **Figure 4.2b**. Thanks to the highest temperature at the lower part of the droplet,[43] a low density of "alcoholic medium" is formed to ease the precipitation of the metal oxide. Furthermore, since the bottom of the drop has weak convection current,[160] it proves to be the favorable place for the collection of nanoparticles. As shown in the **Figure 4.2a,** the Leidenfrost puddle becomes flattened with increasing volume under the influence of gravity.[161]

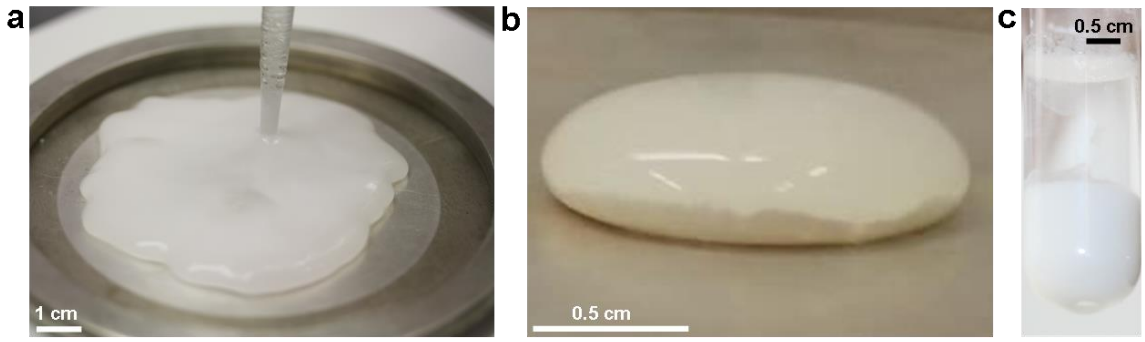


***Figure 4.2: (a) Leidenfrost puddle containing ZnO in white color formed by using 10 mM of zinc acetate aqueous solution. (b) ZnO nanopowder collected at the base of the Leidenfrost drop. (c) The colloidal ZnO nanopowder collected easily in glass tube.***

The colloidal nanopowder can be easily collected in glass tubes (**Figure 4.2c**). In addition, the nanoparticles may be extracted by evaporation of the suspension for further investigations and applications. ZnO nano-tetrapods with average arm diameters vary from 50 to 260 nm, and can successfully be synthesized at pH 6.5, **Figure 4.3a, b**. The synthesis under the Leidenfrost condition would be governed by the following chemical reactions:

$$2H_2O \rightleftharpoons OH^- + H_3O^+ \qquad (4.2)$$

$$M^{+2} + 2OH^- \rightleftharpoons MO + H_2O \qquad (4.3)$$

The ability to produce particles of different shape and organization is a prerequisite to the study of relationship between their morphology and properties. The control over the shape of the nanoparticle leads to manipulation of functionality and selectivity for many applications.[162-163] One of the advantages of Leidenfrost synthesis is that the morphology of the nanoparticles can be easily controlled by adjusting the pH of the precursor solution.

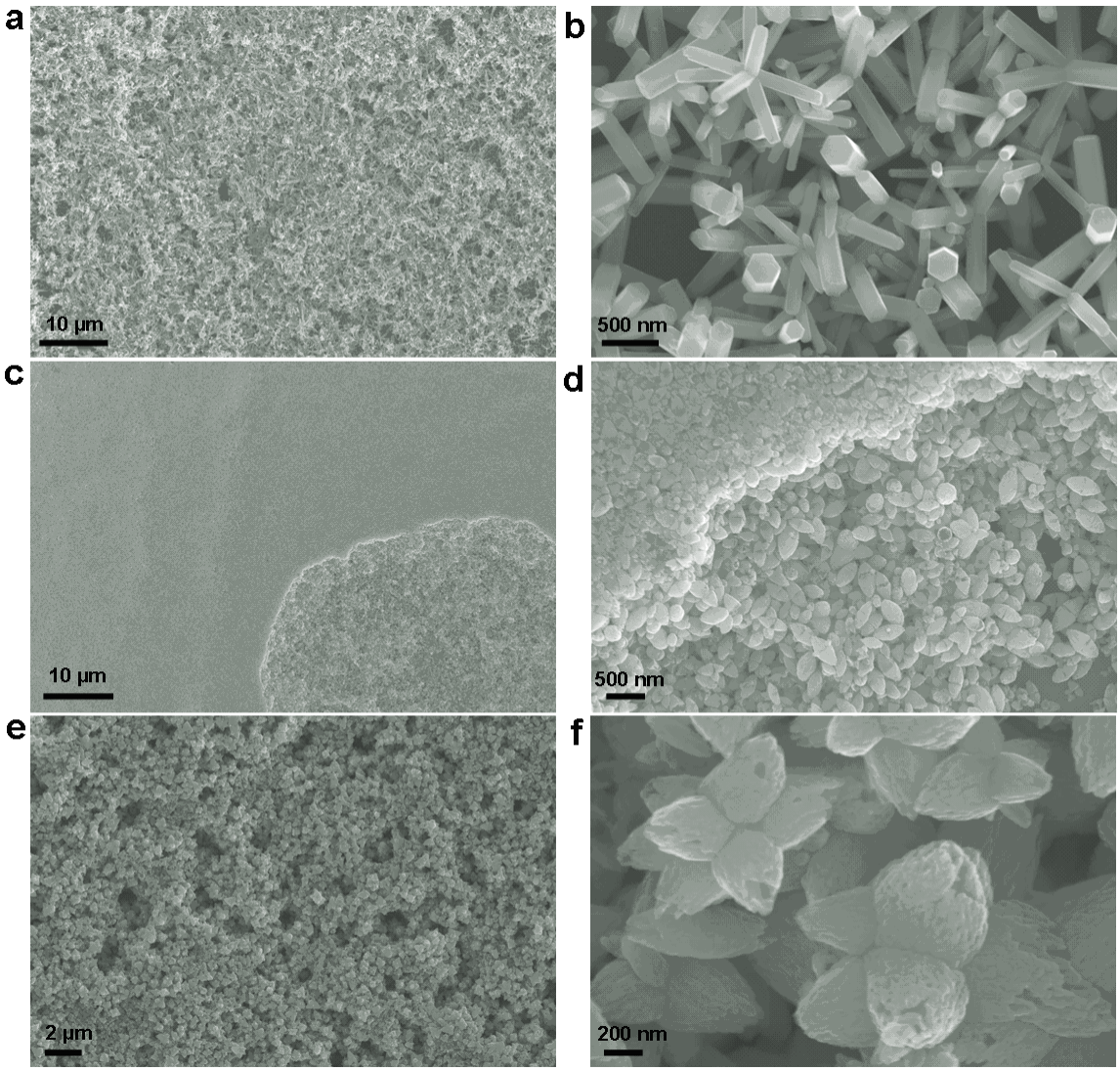


***Figure 4.3: SEM images of ZnO (a) nanotetrapods at low magnification; prepared with pH 6.5 and (b) at high magnification. (c) Rice-like structure at low magnification synthesized with pH 9.6 and (d) at high magnification. (e) Flower-like structures at low magnification obtained with pH 11.3 and (f) at high magnification.***

**Figures 4.3a-f** show different morphologies of ZnO crystals produced at the same precursor concentration (zinc acetate, 10 mM) but at different pH conditions. As seen in **Figures 4.3d,f**, by increasing the pH value from 9.6 to 11.3, ZnO changed from rice-like to flower-like, respectively. The shape changing can be attributed to the fast evaporation at the overheated zone leading to the increased precursor salt concentration. Moreover, the charge separation and loss of hydronium ion to the vapors leads to an increase in hydroxide ion left in the drop that results in local basic pH conditions necessary for the production of nanoparticle.[43]

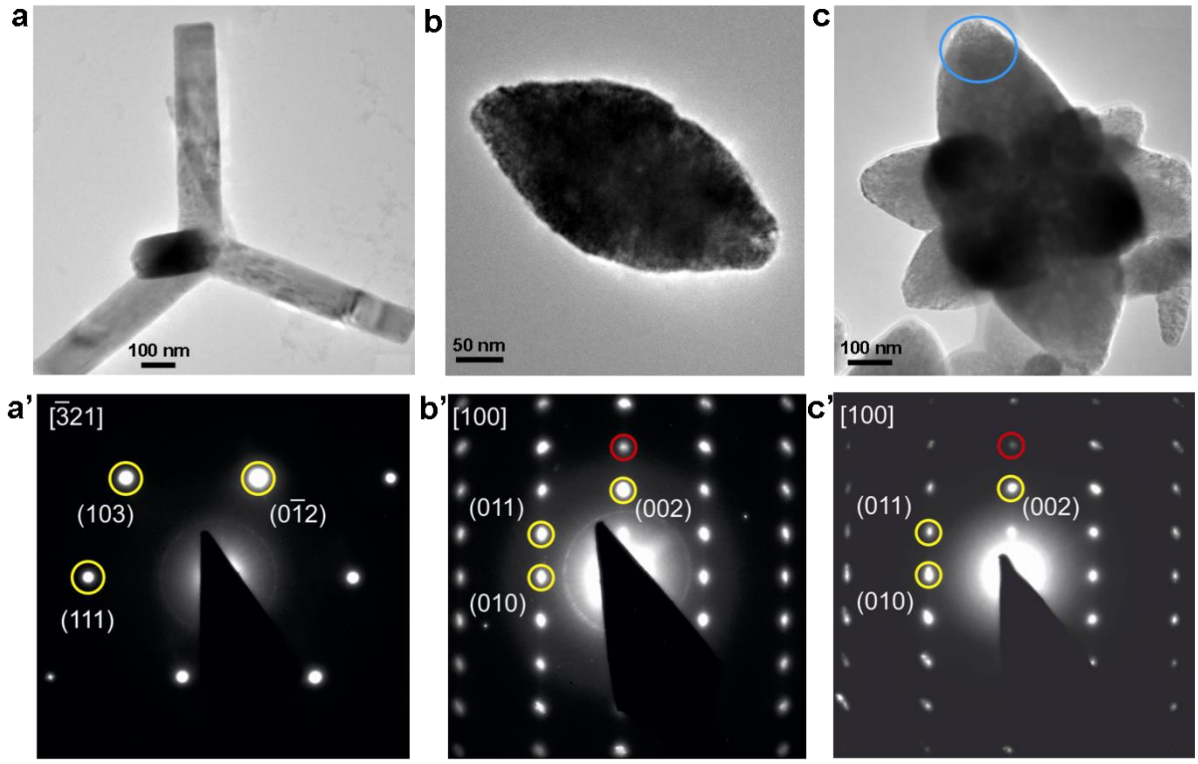


***Figure 4.4: TEM images of ZnO nanostructures and their corresponding SAED patterns (below), (a) tetrapod, (b) rice and (c) Flower-like structure.***

**Figure 4.4a** depicts a bright field image of a typical tetrapod. The tetrapod arms are around 500 nm in length and 110 nm in diameter. Selected area of electron diffraction (SAED) patterns (**Figure 4.4**a') from a tetrapod arm shows single crystalline hexagonal ZnO in [-321] zone axis. **Figure 4.4b** is a bright field image of a rice-like structure. The length and diameter of a typical particle are around 300 nm and 150 nm, respectively. **Figure 4.4**b' represents an SAED pattern of a single particle in[164] zone axis. The yellow circles mark the reflections of the (010) (011) and (002) planes. The red circle marks the (003) diffraction spots which should be extinguished, but they still persist due to dynamical effects. It is confirmed that the rice-like structure is a single crystalline particle with slightly lower crystallinity if compared to the ZnO tetrapod seen by the broadening of the higher order diffraction spots. **Figure 4.4c** represents a bright field image of a typical flower-like structure. The SAED pattern is taken from the blue encircled area. Comparison between the SAED pattern of the rice-like (b') and the flower-like structure (c') shows that the crystallinity of the flower-like structure is further decreased.

The exclusive nature of the Leidenfrost technique is bloomed by the growth of particles with anisotropic shapes. It also yields unity in simple and upscalable manner. According to the TEM observations, oriented attachment seems to be the main driving force of the self-organization. The anisotropic growth is governed by the Leidenfrost dynamics and the Leidenfrost chemistry at the overheated zone.

Despite uncertainty about the origin of the self assembly that necessitates some further investigations, we assume that the thermocapillary driving intensive circulating currents and the associated vortices inside the Leidenfrost drop are responsible for the collision of the formed clusters and self-organization of the nanocrystalline structure. The large swirling motions along with rotation and squeezing at several length scales govern the unique mixing ability of the Leidenfrost reactor.

In addition to the monomer concentration, pH is also a determining factor bringing about an increase in yield. Such an outcome is originated from the rate of reaction which rises with the increase of $OH^-$ concentration in the chemical reactor.[43] Accordingly, the collision of the metal oxide nanocrystals enhances the Leidenfrost mixture and leads to a change in the morphologies and the crystal quality. This behavior i.e. the direct correlation of morphology and the crystal quality to the reaction rate is indeed a well-known fact.[165] However, a precise hydrodynamic study is still needed to be performed. In this regard, multidisciplinary investigations are necessary to fully understand the phenomenon and to explore the interdependency between the Leidenfrost chemistry, Leidenfrost dynamics and heat transfer phenomenon in a levitated reactor.

The ability to produce particles of different shape and organization is a prerequisite to the study of relationship between their morphology and properties. The control over the shape of the nanoparticles leads to manipulation of functionality and selectivity for future applications.[162-163]

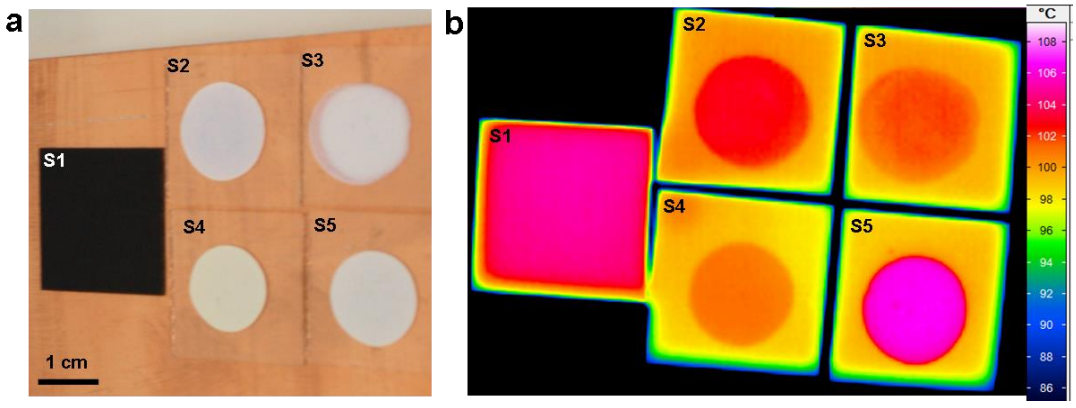


***Figure 4.5: (a) Photograph of different samples placed on copper plate where S1 is glass plate coated with high efficiency black coating, S2 with ZnO rice, S3 spherical (Commercial from Sigma-Aldrich), S4 flower- and S5 tetrapod-like structure. (b) Thermograph view of the same samples as in 'figure. a', heated to 100 °C showing different emissivity depicted by different colors.***

The effect of morphology of nanoparticles on their IR emissivity of ZnO nanocrystals is shown in **Figure 4.5**. It is obvious that tetrapod structure shows the highest emissivity

(Emissivity=0.95) in comparison to rice- (Emissivity=0.91) or flower-like (Emissivity=0.88) structure prepared by Leidenfrost technique. The tetrapod structure prepared by Leidenfrost technique is better than the commercially available ZnO (Emissivity=0.89), and better than the high efficiency black coating (Emissivity=0.93). TEM investigation showed that the tetrapod structure had the highest crystallinity, followed by rice- and flower-like structures in that order. It seems that the morphology and crystallinity are playing a very important role on the IR emissivity property of ZnO nanostructures. More investigations and characterization are still needed to explore the real mechanism behind this effect.

# Chapter 5

# Conclusion and Outlook

## Conclusion and Outlook

In this dissertation, we have tried to resolve the 257-year-old Leidenfrost phenomenon, and to demonstrate the thermal gradient, electrostatic and overheated nature of the levitated Leidenfrost droplet. A new type of charge chemistry has also been presented in this study. In addition, the effectiveness of utilizing the Leidenfrost drop as a water-based green chemical reactor for nanofabrication along with the extensive usefulness of implementation of its exclusive physiochemical character has been explored. We have explored the mechanism of the nanosynthesis such as role of the fast evaporation and charge separation of water at the interface between the hot surface and the levitated droplet as well as an overheated zone within the droplet. The overheated base of the drop acts as a chemical reactor. With the self-ionization of water at the liquid-vapor interface, it leads to a local increase of metal ($M^+$) and hydroxyl ($OH^-$) ion concentrations. The hydroxyl ion increasing is due to the loss of hydronium ions ($H_3O^+$) to the vapor during the fast evaporation. The hydroxide ion facilitates the basic conditions and reduces the effect required for a wide variety of nanofabrication.

Leidenfrost nanochemical reactor allows the fabrication and the simultaneous assembly of nanostructures as well as its implementation for designing functional materials that should be simple to handle, environmental-friendly, energy efficient, low cost and in one fast step.

In this thesis, Au without reducing agent and ZnO in different morphologies have been effectively synthesized by the Leidenfrost green chemical approach. Furthermore, the 3D coating of a complex structure with ZnO, CuO nanoparticles as well as Au in a foam form were performed under the Leidenfrost dynamics showing the uniqueness of this phenomenon for nanocoating processes. A self-organized plasmonic nanoporous material as black Au successfully developed in suspension as well as in powder form. The plasmonic nanoporous black Au can act as a plasmonic wideband superabsorber. The assembled nanoporous foam has been fruitfully used as a coating of plastic foil as superhydrophilic and thermal resistive metal-polymer hybrid foams. The black absorber coating could be promising candidate for harvesting energy and solar cell applications.

In addition, this study demonstrates the applicability of the Leidenfrost reactor to produce nanopowder of ZnO in an upscalable manner. More specifically, the Leidenfrost droplet is introduced as a functional dynamic mixer for a simple fabrication of self-organized nanocrystals with tunable morphology. Tuning anisotropic morphology of the nanocrystals through this approach brings about tailored solar and thermal emissivity. Indeed, our technique offers an inexpensive and sustainable solution for solar energy applications whose performance depends strongly on the morphology of the constituent nanopowders.

Of the strongest points of this work is the simplicity of yield that can be increased in great amounts. It is also easy to wash the product (for example nanoporous gold) during the process to avoid the undesired byproducts. Moreover, the reaction can be stopped at any stage simply by removing the droplet from the hotplate.

There are significant targets to be precisely investigated in the future, for example, the upscaling of the production setup for commercialization of the technique. The upscaling may be achieved by studying the factors that result in enhancement of the charge separation inside the levitated reactor or at the interface. This can be potentially done by adding some other green solvents or using functionalized hot surfaces.

Beside mass production, the perspective of the Leidenfrost synthesis could be oriented towards bionanocomposite fabrication. In this direction, the incorporation of multifunctional reactants derived from natural or biogenic sources to a levitated reactor would act as an additional reducing and capping agent. This may not only increase the efficiency of synthesis but may also act as a driving force for nanoassembly in a biological configuration. Owing to their bio-origin, the synthesized nanomaterials would be nontoxic, biodegradable and utilizable for biomedical applications. The green charge nanochemistry in the levitated reactor would lead to a new breed of nanomaterials with customizable morphologies as well as little or no environmental, health or safety concerns. The ability to tune the shape of the nanoproducts according to the destined function along with the capacity of sustainable mass production with little environmental concerns puts the Leidenfrost reactor at the forefront of functional materials synthesis techniques.

# Acknowledgments

I would like to express my sincere gratitude to **Prof. Dr.-Ing. Mady Elbahri** who has given me the opportunity and honor to work in his group. I honestly state that this thesis would not have been materialized without his continuous encouragement, enthusiasm, and innovative ideas.

I am deeply thankful to Dr. Mehdi Keshavarz Hedayati, M.Sc. Duygu Disci-Zayed, M.Sc. Ahnaf Usman Zillohu, Dr. Shahin Homaeigohar, M.Sc. Moheb abdelaziz and Dipl.-Ing. (FH) Stefan Rehders for contribution, helping and supporting me to finish my PhD research work successfully. I would also like to sincerely thank the following persons for doing characterization and experimental help:

- The group of Synthesis and Real Structure especially Prof. Dr. Lorenz Kienle, Dr. Venkata Sai Kiran Chakravadhanula, Dr. Burak Erkartal, Torben Dankwort Dr. Ulrich Schürmann for TEM investigations.
- The group of Multicomponent Materials, especially Prof. Dr. Franz Faupel
- Prof. Dr. Eckhard Quandt and Dr-Ing. Christoph Bechtold for thermographic measurements by the infrared camera.
- Prof. Dr. Norbert Stock, and Dipl. Chem. Nele Reimer for BET measurements.

Also, my deep gratitude is due to **Dr. Mohamed Adel Mahmoud**, Vice-Dean and Assistant Professor at KKU, KSA, for his tireless efforts in proof reading this thesis.

Special thanks are to Dr. Mehdi Keshavarz Hedayati, Dr. Shahin Homaeigohar and Dr. Ahnaf Usman Zillohu for their kind scientific discussion, performing certain measurements and proof reading of the thesis.

It's my pleasure to thank all my **colleagues and friends in TF** who made these six years of my life special.

I dedicate this thesis to my parents, family, sisters and brother for all the support, prayers and motivation.

**Ramzy Abdelaziz**

# General Declaration

I hereby declare that this dissertation (Green nanofabrication @ Leidenfrost condition) represents my own work except some cited sources.

I declare that this thesis has not been submitted or accepted for the award of any other diploma or degree to any other University or Institution.

Moreover, I declare that this work has not been prepared with any illegal help. I also assert that other authors' contributions used in the thesis or led to some ideas in it are properly cited in written form.

I realize that this PhD thesis is a part of the examination and may not be commercially used or transferred to other party without written permission from my supervising professor

Kiel, date
……
Signature

# List of Figure

# References


1 Bhushan, B. *Springer handbook of nanotechnology*. Springer Science & Business Media (2010).

2 Littau, K., Szajowski, P., Muller, A., Kortan, A. & Brus, L. A luminescent silicon nanocrystal colloid via a high-temperature aerosol reaction. *The Journal of Physical Chemistry* **97**, 1224-1230 (1993).

3 Lovell, A. *Inventory finds increase in consumer products containing nanoscale materials* <http://www.wilsoncenter.org/article/inventory-finds-increase-consumer-products-containing-nanoscale-materials> (2013 ).

4 Khan, F. H. Chemical hazards of nanoparticles to human and environment (a review). *Orient J Chem* **29**, 1399-1408 (2013).

5 *Nanotechnology: A Realistic Market Assessment*, <http://www.bccresearch.com/market-research/nanotechnology/nanotechnology-market-applications-products-nan031e.html> (2012).

6 Chen, H. *et al.* Global nanotechnology development from 1991 to 2012: patents, scientific publications, and effect of NSF funding. *Journal of nanoparticle research* **15**, 1-21 (2013).

7 Masala, O. & Seshadri, R. Synthesis routes for large volumes of nanoparticles. *Annu. Rev. Mater. Res.* **34**, 41-81 (2004).

8 Palui, G., Ray, S. & Banerjee, A. Synthesis of multiple shaped gold nanoparticles using wet chemical method by different dendritic peptides at room temperature. *Journal of materials chemistry* **19**, 3457-3468 (2009).

9 Xu, Z.-C. *et al*. Wet chemical synthesis of gold nanoparticles using silver seeds: a shape control from nanorods to hollow spherical nanoparticles. *Nanotechnology* **18**, 115608 (2007).

10 Wang, Z., Liu, Y., & Zeng, X. One-step synthesis of $\gamma$-$Fe_2O_3$ nanoparticles by laser ablation. *Powder technology* **161**, 65-68 (2006).

11 Athanassiou, E. K., Grass, R. N. & Stark, W. J. Large-scale production of carbon-coated copper nanoparticles for sensor applications. *Nanotechnology* **17**, 1668 (2006).

12 Lung, J.-K. *et al.* Preparation of gold nanoparticles by arc discharge in water. *Journal of alloys and compounds* **434**, 655-658 (2007).

13 Muñoz, J. E., Cervantes, J., Esparza, R. & Rosas, G. Iron nanoparticles produced by high-energy ball milling. *Journal of nanoparticle research* **9**, 945-950 (2007).

14 Torimoto, T. *et al.* Sputter deposition onto ionic liquids: Simple and clean synthesis of highly dispersed ultrafine metal nanoparticles. *Applied Physics Letters* **89**, 243117 (2006).

15 Jiang, Y. *et al.* Hydrogen-assisted thermal evaporation synthesis of ZnS nanoribbons on a large scale. *Advanced Materials* **15**, 323-327 (2003).

16 Thakkar, K. N., Mhatre, S. S. & Parikh, R. Y. Biological synthesis of metallic nanoparticles. *Nanomedicine: Nanotechnology, Biology and Medicine* **6**, 257-262 (2010).

17 Alam, M. N., Roy, N., Mandal, D. & Begum, N. A. Green chemistry for nanochemistry: exploring medicinal plants for the biogenic synthesis of metal NPs with fine-tuned properties. *RSC Advances* **3**, 11935-11956 (2013).

18 Li, Y., Duan, X., Qian, Y., Yang, L. & Liao, H. Nanocrystalline silver particles: synthesis, agglomeration, and sputtering induced by electron beam. *Journal of colloid and interface science* **209**, 347-349 (1999).

19 Chen, X. & Mao, S. S. Titanium dioxide nanomaterials: synthesis, properties, modifications, and applications. *Chemical reviews* **107**, 2891-2959 (2007).

20 Sau, T. K. & Rogach, A. L. Nonspherical noble metal nanoparticles: colloid-chemical synthesis and morphology control. *Advanced Materials* **22**, 1781-1804 (2010).
21 Jun, Y. w., Choi, J. s. & Cheon, J. Shape control of semiconductor and metal oxide nanocrystals through nonhydrolytic colloidal routes. *Angewandte Chemie International Edition* **45**, 3414-3439 (2006).
22 Park, J., Joo, J., Kwon, S. G., Jang, Y. & Hyeon, T. Synthesis of monodisperse spherical nanocrystals. *Angewandte Chemie International Edition* **46**, 4630-4660 (2007).
23 Xiao, L. *Green nanochemistry: synthesis and surface functionalization of tin and iron oxide nanoparticles for gas sensing, imaging (MRI) and cellular uptake applications*. Doctoral dissertation, Universität zu Köln (2012).
24 Ozin, G. A., Arsenault, A. C., & Cademartiri, L. *Nanochemistry: a chemical approach to nanomaterials*. Royal Society of Chemistry (2009).
25 Nune, S. K. *et al.* Green nanotechnology from tea: phytochemicals in tea as building blocks for production of biocompatible gold nanoparticles. *Journal of materials chemistry* **19**, 2912-2920 (2009).
26 Clark, J., Sheldon, R., Raston, C., Poliakoff, M. & Leitner, W. 15 years of Green Chemistry. *Green Chemistry* **16**, 18-23 (2014).
27 Nadagouda, M. N. & Varma, R. S. Green and controlled synthesis of gold and platinum nanomaterials using vitamin B2: density-assisted self-assembly of nanospheres, wires and rods. *Green Chem.* **8**, 516-518 (2006).
28 Anastas, P. T., & Warner, J. C. *Green chemistry: theory and practice*. Oxford university press (2000).
29 Li, C.-J. & Anastas, P. T. Green Chemistry: present and future. *Chemical Society Reviews* **41**, 1413-1414 (2012).
30 Eilks, I. & Rauch, F. Sustainable development and green chemistry in chemistry education. *Chemistry Education Research and Practice* **13**, 57-58 (2012).
31 Ahluwalia, V. K. *Green Chemistry: Environmentally Benign Reactions, Second Edition*. Ane Books (2012).
32 Patel, J. T., Patel, O. B. & Raval, B. P. *Green chemistry: new avenues in chemical research: focus in healthcare*. LAP Lambert Academic Publishing (2012).
33 Kharissova, O. V., Dias, H., Kharisov, B. I., Pérez, B. O. & Pérez, V. M. J. The greener synthesis of nanoparticles. *Trends in biotechnology* **31**, 240-248 (2013).
34 Sanchez-Mendieta, V., & Vilchis-Nestor, A. R. *Green synthesis of noble metal (Au, Ag, Pt) nanoparticles, assisted by plant-extracts*. INTECH Open Access Publisher (2012).
35 Varma, R. S. Greener approach to nanomaterials and their sustainable applications. *Current Opinion in Chemical Engineering* **1**, 123-128 (2012).
36 Tran, Q. H., Nguyen, V. Q. & Le, A.-T. Silver nanoparticles: synthesis, properties, toxicology, applications and perspectives. *Advances in Natural Sciences: Nanoscience and Nanotechnology* **4**, 033001 (2013).
37 Ghorbani, H. R., Safekordi, A. A., Attar, H. & Sorkhabadi, S. Biological and non-biological methods for silver nanoparticles synthesis. *Chemical and Biochemical Engineering Quarterly* **25**, 317-326 (2011).
38 Narayanan, K. B. & Sakthivel, N. Biological synthesis of metal nanoparticles by microbes. *Advances in colloid and interface science* **156**, 1-13 (2010).
39 Dahl, J. A., Maddux, B. L. & Hutchison, J. E. Toward greener nanosynthesis. *Chemical reviews* **107**, 2228-2269 (2007).
40 Walker, J. Boiling and the Leidenfrost effect. *Cleveland State University*, 1 (2010).
41 Leidenfrost, J. G. On the fixation of water in diverse fire. *International Journal of Heat and Mass Transfer* **9**, 1153-1166 (1966).

42 http://fr.wikipedia.org/wiki/Johann_Gottlob_Leidenfrost. Johann Gottlob Leidenfrost.
43 Abdelaziz, R., *et al*. Green chemistry and nanofabrication in a levitated Leidenfrost drop. *Nature communications* 4 (2013).
44 Incropera, F. P. *Introduction to heat transfer*. John Wiley & Sons (2011).
45 https://www.enertron-inc.com/pdf/thermal_design_guildines/Brief-Introduction-to-Heat-Transfer.pdf. *Brief Introduction to Heat Transfer - Enertron Inc*. (2004).
46 Hewitt, G. F., Shires, G. L. & Bott, T. R. *Process heat transfer*. CRC press Boca Raton (1994).
47 Snezhko, A., Jacob, E. B. & Aranson, I. S. Pulsating–gliding transition in the dynamics of levitating liquid nitrogen droplets. *New Journal of Physics* **10**, 043034 (2008).
48 Lisenker, I. Circulation pattern within a drop experiencing Leidenfrost effect.
49 The international association for the properties of water and steam (2007).
50 Release on the ionization constant of $H_2O$. *The International Association for the Properties of Water and Steam*, Lucerne, Switzerland (2007).
51 Bandura, A. V. & Lvov, S. N. The ionization constant of water over wide ranges of temperature and density. *Journal of physical and chemical reference data* **35**, 15-30 (2006).
52 Franks, F. *Water: a matrix of life*. Vol. 22, Royal Society of Chemistry (2000).
53 Bandura, A. V. & Lvov, S. N. The ionization constant of water over wide ranges of temperature and density. *Journal of physical and chemical reference data* **35**, 15-30 (2005).
54 Pitzer, K. S. Self-ionization of water at high temperature and the thermodynamic properties of the ions. *The Journal of Physical Chemistry* **86**, 4704-4708 (1982).
55 Prevenslik, T. in *6th French Electrostatic Society Conference, July*. 7-9.
56 Pounder, C. Electrification from salt water on heated metals. *Journal of Physics D: Applied Physics* **5**, 753 (1972).
57 Prevenslik, T. V. Bubbles and steam electricity. *ESD Journal* (2001).
58 Pounder, C. Charge-carrying particles from Leidenfrost boiling (an aspect of saline contact charging): Part I. Investigation of the Leidenfrost phenomenon and the discovery and examination of particles. *Journal of Electrostatics* **9**, 159-175 (1980).
59 Pounder, C. Charge carrying particles from Leidenfrost boiling (an aspect of saline contact charging): Part II. The electrical properties of Leidenfrost drops and associated particles. *Journal of Electrostatics* **9**, 177-182 (1980).
60 Bernardin, J. & Mudawar, I. The Leidenfrost point: experimental study and assessment of existing models. *Journal of Heat Transfer* **121**, 894-903 (1999).
61 Kenneth J. Bmmeister, R. C. H., and Thomas D. Hamill Metastable leidenfrost states, NASA; United States (1966).
62 Paul, G., Das, P. K., & Manna, I. Droplet oscillation and pattern formation during Leidenfrost phenomenon. *Experimental Thermal and Fluid Science* **60**, 346-353 (2015).
63 Elbahri, M., Paretkar, D., Hirmas, K., Jebril, S. & Adelung, R. Anti-lotus effect for nanostructuring at the Leidenfrost temperature. *Advanced Materials* **19**, 1262-1266 (2007).
64 Berger, M. *Applying a 250-year old discovery to nanotechnology fabrication*, <http://www.nanowerk.com/spotlight/spotid=1907.php> (2007).
65 Bain, C. Nanostructures: Drip painting on a hot canvas. *Nat Nano* **2**, 344-345 (2007).
66 Quéré, D. Leidenfrost dynamics. *Annual Review of Fluid Mechanics* **45**, 197-215 (2013).
67 Hashmi, A. *et al.* Leidenfrost levitation: beyond droplets. *Sci. Rep.* **2** (2012).

68 Lagubeau, G., Le Merrer, M., Clanet, C. & Quere, D. Leidenfrost on a ratchet. *Nat Phys* **7**, 395-398 (2011).
69 Vakarelski, I. U., Patankar, N. A., Marston, J. O., Chan, D. Y. C. & Thoroddsen, S. T. Stabilization of Leidenfrost vapour layer by textured superhydrophobic surfaces. *Nature* **489**, 274-277 (2012).
70 Maquet, L., Colinet, P. & Dorbolo, S. Organization of microbeads in Leidenfrost drops. *Soft Matter* **10**, 4061-4066 (2014).
71 Tsapis, N. *et al.* Onset of buckling in drying droplets of colloidal suspensions. *Physical Review Letters* **94**, 018302 (2005).
72 Lim, C. H., Kang, H. & Kim, S.-H. Colloidal Assembly in Leidenfrost Drops for Noniridescent Structural Color Pigments. *Langmuir* **30**, 8350-8356 (2014).
73 Saha, S., Mandal, M. K., Nonami, H. & Hiraoka, K. Direct analysis of anabolic steroids in urine using Leidenfrost phenomenon assisted thermal desorption-dielectric barrier discharge ionization mass spectrometry. *Analytica chimica acta* **839**, 1-7 (2014).
74 Saha, S., Chen, L. C., Mandal, M. K. & Hiraoka, K. Leidenfrost phenomenon-assisted thermal desorption (LPTD) and its application to open ion sources at atmospheric pressure mass spectrometry. *Journal of The American Society for Mass Spectrometry* **24**, 341-347 (2013).
75 Kelly, K. L., Coronado, E., Zhao, L. L. & Schatz, G. C. The Optical Properties of Metal Nanoparticles: The Influence of Size, Shape, and Dielectric Environment. *The Journal of Physical Chemistry B* **107**, 668-677 (2002).
76 Noguez, C. Surface plasmons on metal nanoparticles: the influence of shape and physical environment. *The Journal of Physical Chemistry C* **111**, 3806-3819 (2007).
77 Zeng, S., Baillargeat, D., Ho, H.-P. & Yong, K.-T. Nanomaterials enhanced surface plasmon resonance for biological and chemical sensing applications. *Chemical Society Reviews* **43**, 3426-3452 (2014).
78 Hou, W. & Cronin, S. B. A review of surface plasmon resonance-enhanced photocatalysis. *Advanced Functional Materials* **23**, 1612-1619 (2013).
79 He, L. *et al.* Colloidal Au-enhanced surface plasmon resonance for ultrasensitive detection of DNA hybridization. *Journal of the American Chemical Society* **122**, 9071-9077 (2000).
80 Nelson, B. P., Grimsrud, T. E., Liles, M. R., Goodman, R. M. & Corn, R. M. Surface plasmon resonance imaging measurements of DNA and RNA hybridization adsorption onto DNA microarrays. *Analytical chemistry* **73**, 1-7 (2001).
81 Hirsch, L. R. *et al.* Nanoshell-mediated near-infrared thermal therapy of tumors under magnetic resonance guidance. *Proceedings of the National Academy of Sciences* **100**, 13549-13554 (2003).
82 Stenzel, O., Stendal, A., Voigtsberger, K. & Von Borczyskowski, C. Enhancement of the photovoltaic conversion efficiency of copper phthalocyanine thin film devices by incorporation of metal clusters. *Solar energy materials and solar cells* **37**, 337-348 (1995).
83 Atwater, H. A. & Polman, A. Plasmonics for improved photovoltaic devices. *Nature materials* **9**, 205-213 (2010).
84 Hedayati, M. K. *et al.* Design of a perfect black absorber at visible frequencies using plasmonic metamaterials. *Advanced Materials* **23**, 5410-5414, doi:10.1002/adma.201102646 (2011).
85 Bhattacharyya, S., Mastai, Y., Panda, R. N., Yeon, S.-H. & Hu, M. Z. Advanced Nanoporous Materials: Synthesis, Properties, and Applications (2014).
86 Tappan, B. C., Steiner, S. A. & Luther, E. P. Nanoporous metal foams. *Angewandte Chemie International Edition* **49**, 4544-4565 (2010).

87 Biener, J. *et al.* Nanoporous plasmonic metamaterials. *Advanced Materials* **20**, 1211-1217 (2008).
88 Seker, E., Reed, M. L. & Begley, M. R. Nanoporous gold: fabrication, characterization, and applications. *Materials* **2**, 2188-2215 (2009).
89 Dixon, M. C. *et al.* Preparation, structure, and optical properties of nanoporous gold thin films. *Langmuir* **23**, 2414-2422 (2007).
90 Maaroof, A. I., Gentle, A., Smith, G. B. & Cortie, M. B. Bulk and surface plasmons in highly nanoporous gold films. *Journal of Physics D: Applied Physics* **40**, 5675 (2007).
91 Nishio, K. & Masuda, H. Anodization of gold in oxalate solution to form a nanoporous black film. *Angewandte Chemie* **123**, 1641-1645 (2011).
92 Jeong, H. & Kim, J. Electrochemical oxidation of glucose at nanoporous black gold surfaces in the presence of high concentration of chloride ions and application to amperometric detection. *Electrochimica Acta* **80**, 383-389 (2012).
93 He, X., Li, Y., Wang, L., Sun, Y. & Zhang, S. High emissivity coatings for high temperature application: progress and prospect. *Thin Solid Films* **517**, 5120-5129 (2009).
94 Cockeram, B., Measures, D. & Mueller, A. The development and testing of emissivity enhancement coatings for themophotovoltaic (TPV) radiator applications. *Thin Solid Films* **355**, 17-25 (1999).
95 LaBel, K. A. *et al. 1997 IEEE Radiation Effects Data Workshop.* 14-21.
96 Yi, J., He, X., Sun, Y. & Li, Y. Electron beam-physical vapor deposition of SiC/SiO.sub.2 high emissivity thin film. *Applied surface science* **253**, 4361-4366 (2007).
97 Bartuli, C., Valente, T. & Tului, M. Plasma spray deposition and high temperature characterization of ZrB 2–SiC protective coatings. *Surface and Coatings Technology* **155**, 260-273 (2002).
98 Elbahri, M., Adelung, R., & Paretkar, D. *U.S. Patent No. 7,914,850*. Washington, DC: U.S. Patent and Trademark Office (2011).
99 http://www.nature.com/ncomms/2013/131029/ncomms3400/metrics. 2013).
100 Schlögl, R. Book Review: Particle Beam Microanalysis. Fundamentals, Methods and Applications. By E. Fuchs, H. Oppholzer, and H. Rehme. *Angewandte Chemie International Edition in English* **31**, 108-109 (1992).
101 Hammond, C. *The basics of crystallography and diffraction*. No. 12, Oxford: Oxford University Press (2009).
102 Pašagić, V., Mužević, M. & Kelenc, D. Infrared thermography in marine applications. *Brodogradnja* **59**, 123-130 (2008).
103 Gaussorgues, G. *Infrared thermography*. Vol. 5, Springer Science & Business Media (1993).
104 Guyer, E. C. *Handbook of applied thermal design*. CRC press (1999).
105 Carey, V. P. Liquid-Vapor Phase-Change Phenomena: An Introduction To The Thermophysics Of Vaporization And Condensation In Heat Transf. (1992).
106 Kim, H., Truong, B., Buongiorno, J. & Hu, L.-W. On the effect of surface roughness height, wettability, and nanoporosity on Leidenfrost phenomena. *Applied Physics Letters* **98**, 083121 (2011).
107 Avedisian, C. T. The homogeneous nucleation limits of liquids. *Journal of physical and chemical reference data* **14**, 695-729 (1985).
108 Rabady, R. I. Modes of Heat Transfer in the Leidenfrost Effect. **41**, 129-135 (2010).
109 Attinger, D. & Poulikakos, D. On quantifying interfacial thermal resistance and surface energy during molten microdroplet surface deposition. **13**, (2003).

110 Biance, A.-L., Clanet, C. & Quéré, D. Leidenfrost drops. *Physics of Fluids (1994-present)* **15**, 1632-1637 (2003).
111 Burton, J. C., Sharpe, A. L., van der Veen, R. C. A., Franco, A. & Nagel, S. R. Geometry of the vapor layer under a Leidenfrost drop. *Physical Review Letters* **109**, 074301 (2012).
112 Stow, C. D. Atmospheric electricity. *Reports on Progress in Physics* **32**, 1-67 (1969).
113 Volta, A. & George, H. Del modo di render sensibilissima la piu debole elettricita sia naturale, sia artificiale. By Mr. Alexander Volta, Professor of Experimental Philosophy in Como, &c. &c.; Communicated by the Right Hon. George Earl Cowper, F. R. S. *Philosophical Transactions of the Royal Society of London* **72**, 237-xxxiii (1782).
114 Faraday, M. Experimental researches in electricity. *Dover: New York*, 21-106 (1965).
115 Lenard, P. Über Wasserfallelektrizität und über die Oberflächenbeschaffenheit der Flüssigkeiten. *Annalen der Physik* **352**, 463-524 (1915).
116 Blanchard, D. C. Positive Space Charge from the Sea. *Journal of the Atmospheric Sciences* **23**, 507-515 (1966).
117 Andreev, S. N. *et al.* Generation of an electrical signal upon the interaction of laser radiation with water surface. *Laser Physics* **17**, 1041-1052 (2007).
118 Anderson, R. *et al.* Electricity in Volcanic Clouds: Investigations show that lightning can result from charge-separation processes in a volcanic crater. *Science* **148**, 1179-1189 (1965).
119 Holmes, A. Principles of physical geology. *GFF* **67**, 115-116 (1945).
120 Gilbert, H. W. Shaw, P. E. Electrical charges arising at a liquid- gas interface. *Proc. Phys. Soc. London* **37**, 195-214 (1925).
121 Leberman, R. & Soper, A. K. Effect of high salt concentrations on water structure. *Nature* **378**, 364-366 (1995).
122 Sue, K., Kimura, K., Yamamoto, M. & Arai, K. Rapid hydrothermal synthesis of ZnO nanorods without organics. *Materials Letters* **58**, 3350-3352 (2004).
123 Kan, C. X., Cai, W. P., Fu, G. H., Li, C. C. & Zhang, L. D. Synthesis and thermal stability of gold nanowires within monolithic mesoporous silica. *Appl Phys A* **78**, 1187-1191 (2004).
124 Liu, B. & Zeng, H. C. Hydrothermal Synthesis of ZnO Nanorods in the Diameter Regime of 50 nm. *Journal of the American Chemical Society* **125**, 4430-4431 (2003).
125 Gitis, D., Mukhopadhyay, S., Rothenberg, G. & Sasson, Y. Solid/Liquid Palladium-Catalyzed Coupling of Haloaryls Using Alcohols as Reducing Agents: Kinetics and Process Optimization. *Organic process research & development* **7**, 109-114 (2002).
126 Sawyer, D. T. & Roberts, J. L. Hydroxide ion: an effective one-electron reducing agent? *Accounts of Chemical Research* **21**, 469-476 (1988).
127 Faraday, M. The Bakerian lecture: experimental relations of gold (and other metals) to light. *Philosophical Transactions of the Royal Society of London*, 145-181 (1857).
128 Swanson, H. E. & Tatge, E. Z. . *Angew. Phys* **8**, 297–299 (1956).
129 Bönnemann, H. & Richards, R. M. Nanoscopic metal particles− synthetic methods and potential applications. *European Journal of Inorganic Chemistry* **2001**, 2455-2480 (2001).
130 Gates, B. D. *et al.* New approaches to nanofabrication molding, printing, and other techniques. *Chemical reviews* **105**, 1171-1196 (2005).
131 Stergiou, A., Kerasiotis, I. & Stergiou, C. Crystallographic study of mixture Ba0. 6Nd0. 4CuOy, in the range of annealing temperatures 860°-910° C. *Journal of optoelectronics and advanced materials* **9**, 2799-2803 (2007).
132 Yang, Q., Yan, P. X., Chang, J. B., Feng, J. J. & Yue, G. H. Growth of bicrystal CuO microsheets from aqueous solution. *Physics Letters A* **361**, 493-496 (2007).

133 Jiang, X., Herricks, T. & Xia, Y. CuO Nanowires Can Be Synthesized by Heating Copper Substrates in Air. *Nano Letters* **2**, 1333-1338 (2002).
134 Wang, X.-Q. & Mujumdar, A. S. Heat transfer characteristics of nanofluids: a review. *International Journal of Thermal Sciences* **46**, 1-19 (2007).
135 Tsapis, N. *et al.* Onset of buckling in drying droplets of colloidal suspensions. *Physical Review Letters* **94**, 018302 (2005).
136 Aberle, C., Lewis, M., Yu, G., Lei, N. & Xu, J. Liquid marbles as thermally robust droplets: coating-assisted Leidenfrost-like effect. *Soft Matter* **7**, 11314-11318 (2011).
137 Søndergaard, T. *et al.* Plasmonic black gold by adiabatic nanofocusing and absorption of light in ultra-sharp convex grooves. *Nature communications* **3**, 969 (2012).
138 Aydin, K., Ferry, V. E., Briggs, R. M. & Atwater, H. A. Broadband polarization-independent resonant light absorption using ultrathin plasmonic super absorbers. *Nature communications* **2**, 517 (2011).
139 Stec, H. M. & Hatton, R. A. Plasmon-active nano-aperture window electrodes for organic photovoltaics. *Advanced Energy Materials* **3**, 193-199 (2013).
140 Lang, X., Qian, L., Guan, P., Zi, J. & Chen, M. Localized surface plasmon resonance of nanoporous gold. *Applied Physics Letters* **98**, 093701 (2011).
141 Gitis, D., Mukhopadhyay, S., Rothenberg, G. & Sasson, Y. Solid/liquid palladium-catalyzed coupling of haloaryls using alcohols as reducing agents: kinetics and process optimization. *Organic process research & development* **7**, 109-114 (2003).
142 Chiswell, B. & O'Halloran, K. R. Acid yellow 17 as a spectrophotometric reagent for the determination of low concentrations of residual free chlorine. *Analytica chimica acta* **249**, 519-524 (1991).
143 Liebermann, J., Roscher, N. M., Meier, E. P. & Cooper, W. J. Development of the FACTS procedure for combined forms of chlorine and ozone in aqueous solutions. *Environmental Science & Technology* **14**, 1395-1400 (1980).
144 Au, L., Lu, X. & Xia, Y. A comparative study of galvanic replacement reactions involving Ag nanocubes and $AuCl2^{-}$ or $AuCl4^{-}$. *Advanced Materials* **20**, 2517-2522 (2008).
145 Dey, G., El Omar, A., Jacob, J., Mostafavi, M. & Belloni, J. Mechanism of trivalent gold reduction and reactivity of transient divalent and monovalent gold ions studied by gamma and pulse radiolysis. *The Journal of Physical Chemistry A* **115**, 383-391 (2010).
146 Afonso, C. A., & Crespo, J. G. (Eds.). *Green separation processes: fundamentals and applications*. Weinheim, Germany: Wiley-VCH (2005).
147 Goesmann, H. & Feldmann, C. Nanoparticulate functional materials. *Angewandte Chemie International Edition* **49**, 1362-1395 (2010).
148 Bell, A. T. The impact of nanoscience on heterogeneous catalysis. *Science* **299**, 1688-1691 (2003).
149 Johnson, J. A., Heidenreich, J. J., Mantz, R. A., Baker, P. M. & Donley, M. S. A multiple-scattering model analysis of zinc oxide pigment for spacecraft thermal control coatings. *Progress in organic coatings* **47**, 432-442 (2003).
150 Lim, Y.-F., Choi, J. J. & Hanrath, T. Facile synthesis of colloidal CuO nanocrystals for light-harvesting applications. *Journal of Nanomaterials* **2012**, 4 (2012).
151 Redel, E. *et al.* Green nanochemistry: metal oxide nanoparticles and porous thin films from bare metal powders. *Small* **8**, 68-72 (2012).
152 Patzke, G. R., Zhou, Y., Kontic, R. & Conrad, F. Oxide nanomaterials: synthetic developments, mechanistic studies, and technological innovations. *Angewandte Chemie International Edition* **50**, 826-859 (2011).

153 Cockeram, B. V., Measures, D. P. & Mueller, A. J. The development and testing of emissivity enhancement coatings for themophotovoltaic (TPV) radiator applications. *Thin Solid Films* **355**, 17-25 (1999).
154 Lian, C., Wei, W., Bai, H. & Li, H. Infrared radiation properties of CuO-ZnO-based sintered material prepared for energy-saving coating. *Energy Technology 2013: Carbon Dioxide Management and Other Technologies*, 47-54 (2013).
155 Rao, C. N. R., Müller, A., & Cheetham, A. K. (Eds.). *Nanomaterials chemistry: recent developments and new directions*. John Wiley & Sons (2007).
156 LaMer, V. K. & Dinegar, R. H. Theory, production and mechanism of formation of monodispersed hydrosols. *Journal of the American Chemical Society* **72**, 4847-4854 (1950).
157 Sun, Y. Controlled synthesis of colloidal silver nanoparticles in organic solutions: empirical rules for nucleation engineering. *Chemical Society Reviews* **42**, 2497-2511 (2013).
158 Fokin, V. M. & Zanotto, E. D. Crystal nucleation in silicate glasses: the temperature and size dependence of crystal/liquid surface energy. *Journal of Non-Crystalline Solids* **265**, 105-112 (2000).
159 Lifshitz, I. M. & Slyozov, V. V. The kinetics of precipitation from supersaturated solid solutions. *Journal of Physics and Chemistry of Solids* **19**, 35-50, (1961).
160 Zhang, N. & Yang, W.-J. Evaporation and explosion of liquid drops on a heated surface. *Experiments in Fluids* **1**, 101-111 (1983).
161 Quéré, D. Leidenfrost Dynamics. *Annual Review of Fluid Mechanics* **45**, 197-215, (2013).
162 Tao, A. R., Habas, S. & Yang, P. Shape control of colloidal metal nanocrystals. *Small* **4**, 310-325 (2008).
163 Wiley, B., Sun, Y., Mayers, B. & Xia, Y. Shape-controlled synthesis of metal nanostructures: the case of silver. *Chemistry – A European Journal* **11**, 454-463, (2005).
164 Shear and compressional dust Alfvén solitons in a magnetized plasma medium of opposite polarity dust. *Astrophysics and Space Science* (2014).
165 Amin, G. *et al.* Influence of pH, precursor concentration, growth time, and temperature on the morphology of ZnO nanostructures grown by the hydrothermal method. *Journal of Nanomaterials* **2011**, 5 (2011).